Mustafa Mengüç Öner

Air Interface Identification for Software Radio Systems

Forschungsberichte aus dem Institut für Nachrichtentechnik der Universität Karlsruhe (TH)

Herausgeber: Prof. Dr. rer. nat. Friedrich Jondral

Vorwort des Herausgebers

Zukünftige Mobilfunkgeräte werden eine wesentlich höhere Flexibilität besitzen als die heute im Betrieb befindlichen. Dazu gehören natürlich die von Software Radios geforderten Multiband- und Multistandardfähigkeiten. Neue Entwicklungen, die in engem Zusammenhang mit veränderten Verfahren der Frequenzvergabe und der Nutzung des elektromagnetischen Spektrums (gemeinsame Nutzung, flexible Ressourcenzuteilung) stehen, zielen unter anderem darauf ab, Endgeräte sensibel für ihre Umgebung zu machen. Dabei stellt das Terminal z.B. fest, wer in seiner Umgebung welche Frequenzen mit welchen Übertragungsverfahren nutzt. In letzter Konsequenz führt das auf die Entwicklung von Cognitive Radios [1] .

Funkübertragungsverfahren werden durch die Definition ihrer Luftschnittstellen, die so genannten Standards, festgelegt. So ist es nur natürlich, dass ein Cognitive Radio die Luftschnittstellen spektral benachbarter Sender bestimmen können sollte. Unter Erkennung einer Luftschnittstelle wird in diesem Zusammenhang immer ihre Wiedererkennung verstanden. D.h. sämtliche Parameter der zu erkennenden Luftschnittstelle sind dem Cognitive Radio bekannt, es führt keine Signalanalysefunktion aus. Seine Aufgabe besteht dann darin, bei vorgegebenem Empfangssignal festzustellen, welcher Standard hinter der Übertragung steht. Da die Erkennung einer Luftschnittstelle Teilaufgaben umfasst, die, wie z.B. die Modulationsartenerkennung oder die Bitstromanalyse, bekanntlich für sich allein genommen schon schwierig sind, sollte in der vorliegenden Arbeit allein die Wiedererkennung von Standards innerhalb der ihnen zugewiesenen Frequenzbereiche untersucht werden. Diese Einschränkung ermöglicht, wie der Autor zeigt, eine Lösung der Aufgabe.

Die vorliegende Dissertation Air Interface Identification for Software Radio Systems von Herrn Mengüç Öner liefert erste Erkenntnisse zur Wiedererkennung von Luftschnittstellen in Software Radios bzw. Cognitive Radios. Der Beitrag der Arbeit liegt in

- der Untersuchung einer Methode zur automatischen Kanalsegmentierung mit Hilfe von Clusteranalyseverfahren und

- dem Nachweis, dass unter den vorgegebenen Randbedingungen (insbesondere die Kenntnis des zu erwartenden Sendeverfahrens) eine Wiedererkennung von Luftschnittstellen über die Analyse zyklostationärer Eigenschaften erfolgen kann.

Karlsruhe, im Dezember 2004

Friedrich Jondral

---

[1] Über eine Definition des Begriffs Cognitive Radio wird derzeit im Software Defined Radio Forum debattiert. Diese Diskussion basiert u.a. auf der Dissertation Cognitive Radio - An Integrated Architecture for Software Defined Radio von Joe Mitola (KTH Stockholm, 2000)

Air Interface Identification
for Software Radio Systems

Zur Erlangung des akademischen Grades eines

DOKTOR-INGENIEURS

von der Fakultät für
Elektrotechnik und Informationstechnik
der Universität Fridericiana Karlsruhe

genehmigte

DISSERTATION

von

Dipl.-Ing. M.Mengüç Öner

aus

Antalya, Türkei

Zusammenfassung

Der Begriff Software Radio (SR) wird um 1990 erstmalig in der Literatur erwähnt. In das Bewusstsein einer breiten Öffentlichkeit wurde er 1995 mit der Veröffentlichung eines Sonderhefts des IEEE Communications Magazine zu diesem Thema gerückt: Ein SR ist ein Transceiver, dessen Funktionen so weit wie möglich als Programme auf einem Rechner laufen. Seine Hardware ist so beschaffen, dass auf ihr unterschiedliche Sende-/Empfangsalgorithmen, die in aller Regel Übertragungsstandards wiedergeben, implementiert werden können. Das Ziel dieser Arbeit ist die Entwicklung eines Verfahrens zur Wiedererkennung des benutzten Übertragungsstandards zur automatischen Einstellung der Basisbandsignalverarbeitung eines SR-Empfängers. Für diesen Zweck sollen die für die Einstellung des Empfängers notwendigen Parameter aus dem Empfangssignal schnell und zuverlässig extrahiert werden.

In dieser Arbeit wird angenommen, dass es keine feste Bindung von Übertragungsstandards zu Frequenzbändern gibt und die Frequenzzuteilung nachfragegesteuert erfolgt. Der Empfänger soll das benutzte Übertragungsverfahren durch das Empfangssignal wiedererkennen und seine Parameter dementsprechend automatisch einstellen. In der Literatur wird dieser Vorgang als Initial Mode Identification (IMI) bezeichnet. Darüber hinaus muß der Empfänger den Kanal ständig überwachen, um alternative Übertragungsmöglichkeiten zu finden, um ein vertikales Handover durchführen zu können, wenn es für den Nutzer vorteilhafter ist, was in der Literatur als Alternative Mode Monitoring (AMM) bezeichnet wird.

In der vorliegenden Arbeit erfolgt die Wiedererkennung in zwei Stufen. In der ersten Stufe werden die Anzahl, die Bandbreiten und die Trägerfrequenzen der sich im Kanal befindenden Signale aus dem digitalisierten Signalgemisch extrahiert. Dieser Vorgang wird als Kanalsegmentierung bezeichnet. In dieser Arbeit wird ein auf Clusteranalyse basierendes automatisches Kanalsegmentierungsverfahren vorgestellt.

Werden die Bandbreiten und Trägerfrequenzen der detektierten Signale richtig geschätzt, kann man davon ausgehen, dass der zweiten Stufe des Erkennungssystems Basisbandsignale zur Verfügung stehen, die zu einem der bekannten Übertragungsstandards zugeordnet, oder als unbekannt abgelehnt werden müssen. In dieser Arbeit wird ein Verfahren zur Wiedererkennung der Luftschnittstellen vorgestellt, das die zyklostationäre Eigenschaften der Empfangssignale ausnutzt, um luftschnittstellenspezifische Merkmale zu erzeugen, die zur Wiedererkennung des Übertragungsstandards benutzt werden können. Dieses Verfahren, im Gegensatz zu den herkömmlichen Modulationsartenerkennungsverfahren, ist robust gegenüber Rauschen und Mehrwegeausbreitung, und in der Lage, Signale mit komplexen Strukturen zu erkennen, zum Beispiel CDMA ond OFDM basierte Signale.

Table of Contents

1 Introduction

Wireless digital communications is experiencing a veritable boom since the beginning of the last decade and has been one of the fastest growing segments in the telecommunications industry. The wireless revolution has started in the nineties, with the introduction of the second generation mobile communications systems, such as GSM and DECT in Europe, IS136 and IS90 in the USA and PDC in Japan. The next generation mobile standards, like UMTS in Europe, are just beginning to enter service. Furthermore, wireless local area network (WLAN) systems are drawing more and more interest. Digital Audio Broadcasting (DAB) and terrestrial Digital Video Broadcasting (DVB-T) systems represent two examples, where digital wireless technology was able to penetrate the area of terrestrial broadcasting, which was traditionally dominated by analog transmission schemes. Works on standardizing the fourth generation of mobile communication systems have already started.

The main disadvantage of this explosion in the number of wireless standards is that the users require different equipment for each of these services. As a consequence, there has been growing interest in terminals, which can use multiple transmission standards (also called air interface standards). Technically, a reconfigurable receiver is required to implement this multi-standard capability.

In nineties, Mitola has introduced the concept of Software Radio, which is a design philosophy for building transceivers, that can accomodate a significant range of radio frequency (RF) bands and air interface standards through software running on general purpose digital signal processors (DSPs) [1]. For the ideal Software Radio, that range includes all the frequency bands and standards required by the user. Although not fully realizable with today's technology, the ideal Software Radio is considered as the ultimate evolutionary stage in wireless communications.

1.1 Software Radio Reconfigurability: Implications

The multi-standard capable Software Radio terminals are expected to provide the users with unprecedented flexibility, since they will make it possible

to choose, among the set of existing air interface standards, the one, which is best suited to the user needs at a given time, in terms of provided service, cost, traffic requirements and quality of service, which is expected to lead to a considerable network indepence. However, in order to fully exploit this flexibility, more intelligence and environmental awareness is required, both from resource management systems, and from user terminals [2].

1.1.1   Spectrum Allocation

One of the most interesting implications of the Software Radio concept affects the area of spectrum management. The reconfigurability and the multi standard capability of the software radio can lead to more flexible, demand oriented dynamic spectrum allocation schemes, that may benefit next generations of wireless communication systems.

The spectrum allocation process aims to distribute the scarce resource of radio spectrum among available services. Today's widely used approach of a fixed and standardized spectrum allocation leads to very well defined frequency channels, which can be only used by specific services. The fixed planning of the spectrum use has the advantage of being easy to manage, encourages strict standardization in user and operator equipments, allows the best choice of technology for a given frequency band, leading to an efficient and robust use of the allocated spectrum.

The main disadvantage of such a conventional approach is the lack of flexibility in ressource allocation. It does not take the user demands and traffic requirements into consideration, which leads to an overall inefficient use of total available spectrum resources. Actually, the main goal of this scheme is rather interference avoidance than capacity maximization

The introduction of reconfigurable Software Radio systems is expected to pave the way to more flexible, demand oriented dynamic spectrum allocation schemes, which will ensure the optimum delivery of the user's wanted service via the most appropriate air interface, while using the available spectrum ressources as efficiently as possible [2].

As the software radio technology progresses, different spectrum allocation schemes with increasing levels of flexibility may be introduced gradually, with the ultimate goal of reaching fully dynamic, demand oriented spectrum allocation.

- **Fixed spectrum allocation with radio ressource sharing.** This is the first logical stage of evolution towards a fully flexible spectrum allocation. In this case, fixed frequency bands are allocated for different wireless air interface standards. Interstandard handovers are

possible to allow radio ressource sharing. This makes it possible to balance the traffic loads between standards and frequency bands. That means, radio ressources are not operated independently of one another, requiring some degree of operator interoperability.

- **Fixed spectrum allocation with spectrum pooling.** Spectrum Pooling is a ressource sharing strategy, which allows a license owner of a spectral band to rent a sporadically used part of it to other users, until he needs it himself [3]. This strategy can be used in combination with fixed spectrum allocation, providing fixed spectrum bands, in time and frequency, for each standard and allowing the sharing of some spectrum bands (the so called spectrum pools) between air interfaces. This scheme allows a dynamic increase or decrease of the spectrum allocated to each air interface according to the traffic needs, leading to a more efficient use of the total available spectral ressources. However, the spectrum sharing between different air interaces of possibly different operators requires new mechanisms for resolving spectrum contention, which will increase the complexity of the ressource management algorithms and signalling requirements.

- **Fully flexible spectrum allocation.** In this scheme, no predefined part of the frequency band is assigned to any of the standards. The spectrum allocation takes place in a totally flexible and demand oriented manner. This strategy requires a very high level of coordination between the operators of the different air interfaces and the user terminals, leading to highly complex ressource management algorithms and signaling requirements.

To be able operate in an environment with dynamic frequency allocation, and make the optimum use of its reconfigurability, a Software Radio terminal needs some kind of environmental awareness. In [4], Mitola has described an "intelligent" agent controlling the software radio user terminal, which is able to adapt itself to the traffic, frequency environment and user needs, which he refers to as the *Cognitive Radio*. The Cognitive Radio has to continuously observe the physical environment, and make decisions about how to use the available ressources in a most efficient manner. One of the most important functions supporting the environmental awareness is the *air interface identification*, which is discussed in the next section.

1.1.2   Air Interface Identification

The multi mode capability of the Software Radio requires that a SR terminal is capable of detecting, identifying and monitoring any of the air interfaces available in its environment. The SR, when it is switched on, has to be able to scan large areas of the spectrum in order to locate, identify and use an air interface, and while connected to a network, it has to be able to monitor alternative air interfaces to be able to perform interstandard handover if necessary.

In the best case, the identification and monitoring takes place in a fixed frequency allocation environment. In this case, the mode identification consists of simple energy detection on a couple of predefined frequency bands: If the software radio detects energy in the 900 MHz band in Europe, it can only be GSM and nothing else.

The worst case scenario occurs, when the identification has to take place in an unknown environment with dynamic frequency allocation, as discussed in the previous section. In this case, the most obvious solution to this problem would be using a global pilot channel, known and accessible to every user, which transmits information about existing air interfaces. The scope of this information could range from the mere existence of the service in a specific frequency band, to more detailed and useful tips like tariff information or the quality of service.

Despite the obvious advantages it offers, the global pilot channel concept is not regarded as a possible future solution. Issues such as the ownership of the channel, the involved costs and revenues and other economical and political problems proved themselves to be insurmountable obstacles for the industry to accept and standardize a global pilot channel [5]. That means that the identification has to take place in a blind manner, i.e. without any help from the network .

In a fully dynamic frequency allocation system, each air interface can be operated at any frequency band. Therefore, prior to identification, the SR has to detect and locate the individual air interface standards in the frequency domain. I.e. it has to determine the number of different available air interfaces in the radio frequency environment, and estimate their carrier frequencies and bandwidths. This process is referred to as the *channel segmentation*.

It is reasonable to assume that, even in an environment with dynamic frequency allocation, there will still be only a limited number of possible well defined air interfaces, whose relevant parameters will be known to the user terminals, or can be downloaded, as new air interface standards emerge.
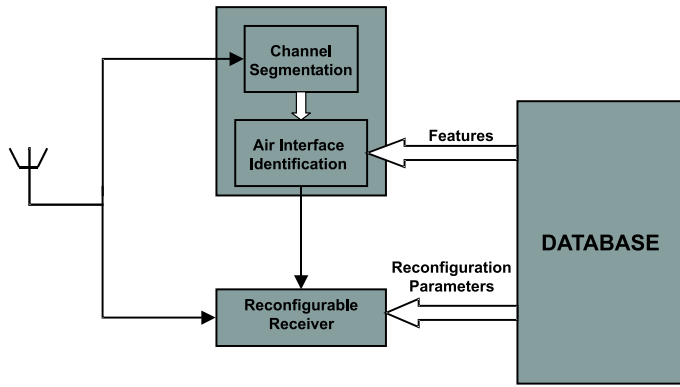
Fig. 1.1 SDR with a Mode Identification Subsystem

This reduces the problem of the air interface identification into a problem of recognition: The air interface identification subsystem classifies the received signal as belonging to one of the known air interfaces, or rejects it as unknown. Fig. 1.1 presents the Software Radio structure proposed in this work, where the air interface identification is performed using the bandwidth and carrier frequency information provided by the channel segmentation stage together with information provided by the air interface database, which includes all the relevant information about the air interfaces to be recognized.

In this work, a novel air interface identification algorithm, along with a channel segmentation step, is investigated, which, unlike many of its counterparts, is fairly robust against multipath fading and AWGN, and is also capable of identifying signals which have a rather complicated structure, such as OFDM and CDMA signals. This work is organized in the following manner: In Chapter 2, an overview of the Software Radio concept is presented, along with the technological aspects regarding its implementation. Chapter 3 provides an overview of the mobile communication environment, where the characteristics of the mobile radio propagation channels are described, and different types of mobile communication signals encountered in today's radio frequency environment are investigated, which give rise to different signal structures. In Chapter 4, a channel segmentation algorithm is presented, which is based on cluster analysis. Chapter 5 provides an air interface identification method based on exploiting the cyclostationary properties of mobile communication signals. And finally, concluding remarks are made in chapter 6.

2 Software Radio Fundamentals

This chapter provides an overview of the Software Radio concept. It begins with a definition of the Software Radio, summarizes the implications of the flexibility which is an inherent property of the Software Radio, and discusses the potential benefits it has to offer. Subsequently, this chapter adresses the technological problems associated with the implementation of the Software Radio, especially analog to digital converters and front end design.

2.1   Software Radio Overview

An exact and standardized definition of Software Radio (SR) does not exist. Some definitions commonly found in the literature are [6]:

- A flexible transmitter/receiver architecture, controlled and programmable by software.

- A transceiver, where the frequency band, radio channel bandwidth, modulation type, coding scheme, radio ressource management and user applications are defined by software.

- Radio equipment, which is dynamically reconfigurable by downloadable software at every protocol layer.

- A transceiver, where digital signal processing takes over as many radio functionalities as possible.

In consideration of all these different points of view, we can come to the following, more general definition: *Software Radio is an emerging design paradigm, geared towards building flexible radio systems, which are multi function, multi mode, multi band as well as reconfigurable and reprogrammable by software.*

The SR is mainly characterized by its flexibility, which is a direct consequence of its reconfigurability. A Software Radio is multi mode capable, which means, its air interface is reconfigurable and reprogrammable by software, leading to a transceiver not only capable of using any existing wireless

Air interface standard	Uplink(MHz)	Downlink(MHz)
GSM 900	890-915	935-960
GSM 1800	1710-1785	1805-1880
GSM 1900	1850-1910	1930-1990
DECT	1881.792-1897.344	1881.792-1897.34
UMTS FDD	1920-1980	2210-2170
UMTS TDD	1900-1920	1900-1920
	2010-2025	2010-2025
Bluetooth	2400-2483.5	2400-2483.5
IEEE 802.11b	2400-2497	2400-2497
HIPERLAN/2	5150-5350	5150-5350
	5470-5725	5470-5725

Tab. 2.1 Operating frequencies of major wireless air interface standards

standard, but also of incorporating any future air interfaces, when they become available, via software downloads or other means. Considering the operating frequencies of today's most important wireless standards given in Tab. 2.1, it becomes quite clear that in the current frequency environment, a multi mode SR transceiver has to be able to cover a wide range of frequency bands, from 890 MHz for GSM to 5725 MHz for Hiperlan/2. This feature is commonly referrered to as the multi band capability.

Another kind of reconfigurability affects the higher layers of the protocol stack. The aim of this kind of reconfiguration may be to improve the performance of those layers in terms of quality, speed and functionality, or to add new features. For example a new encryption algorithm to improve system security, or a new user application.

At the hardware level, achieving a high degree of reconfigurability requires a reduction in the amount of relatively inflexible analog signal processing elements used in the transceiver and the implementation of as many of the radio functionalities as possible in the digital domain. That means the analog to digital conversion in a software radio receiver has to take place very near to the antenna.

From the perspective of digital signal processing hardware, reconfigurabilty means moving from dedicated application specific integrated circuits (ASICs) towards more flexible programmable hardware, such as digital signal processors (DSPs) or field programmable gate arrays (FPGAs) for signal processing. The reprogrammability of the hardware allows the software implementation of radio functionalities such as coding, modulation, demo-

dulation, equalisation etc., which is a fundamental requirement for the multi mode capability.

The software radio concept offers many advantages over the existing conventional systems, which can be mainly attributed to its flexibility. These advantages include:

- The enhanced user roaming provided by the reconfigurable terminals is going to make the users able to roam around the world with the same terminal without worrying about compatibility issues.

- The users will be able to choose the most attractive network, considering cost, quality of service, offered services, etc. from a set of available networks.

- The ability to incorporate new features dynamically, as technology progresses, will lengthen the life spans of the user terminals.

- The radio transmission characteristics of a software radio can be optimized according to the environment, traffic loads and to the service desired, promoting a more spectrally efficient delivery of the service to the user.

2.2   Software Radio Architecture

The simplified structure of an ideal software radio receiver is illustrated in Fig. 2.1. The RF signal from the frequency band of interest, is digitized immediately behind the antenna, without any substantial analog preprocessing steps. All of the signal processing required for the radio functionalities, including downconversion and channelization, is performed by software running on digital signal processing elements. This approach, while allowing a very flexible receiver in terms of reconfigurability, is not practicable with today's technology and will remain so for the forseeable future. Because of the following reasons:

- Analog to digital conversion of the whole frequency band of interest directly after the antenna requires high performance wideband analog to digital converters (ADCs) which are not realizable with today's technology.

- Without the data reduction provided by the analog preprocessing, the amount of data that has to be handled in the digital domain remains
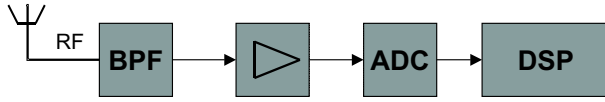
Fig. 2.1 The ideal Software Radio receiver

very high, requiring a very high processing power which in turn leads to very high power consumption.

Hence, the ideal software radio, has to be considered as the ultimate stage of evolution for research and development efforts, which can be hopefully achieved in the future.

As an earlier stage of development towards the ideal Software Radio, the so called Software Defined Radio (sometimes also called the pragmatic software radio) represents a balancing act between full flexibility and technological limitations [1]. In a Software Defined Radio (SDR) the signal has to undergo some analog preprocessing before the transition to the digital domain, reducing the signal bandwidth that the ADC's and the digital processing have to cope with. As the technology progresses in core areas like analog to digital converters, memory chips and signal processors, the transition boundary between the analog and digital domains will shift towards the antenna, approaching the ultimate goal of a fully digital software radio.

In the light of the discussion above, it becomes quite evident that analog to digital converters play a most critical role in the development of the Software Radio technology. The performance of the ADC and its location in the receiver chain affect the whole structure of the device and are key factors determining the extent of the flexibility and the reconfigurability offered by the system. In the following, we are going to have a closer look at the ADCs and discuss their performance issues.

2.2.1   Analog to Digital Conversion

An ideal ADC, as depicted in Fig. 2.2, consists of a sample and hold circuit, which performs the sampling operation, converting the continuous time signal into a discete time signal, a quantizer, and an encoder, which converts the discrete samples into digital words.

For an ideal ADC, the only source of error is the so called quantisation noise $e_n = y_n - x_n$, which is generated in the quantization process. Given an ADC with maximum and minimum quantized values of V and $-V$, a number of of output levels Q_o and a resolution of $N_o = log_2(Q_o)$, the least
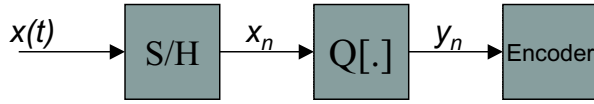
Fig. 2.2 The ideal analog to digital converter

significant bit (LSB) is equivalent to $\Delta = \frac{2V}{Q_o-1}$. Therefore, the quantization error does not exceed half the LSB, i.e. $|e_n| \leq \frac{\Delta}{2}$.

In order to facilitate the analysis, the following assumptions are made about the noise process:

- The quantization noise is a sample sequence of a stationary random process.

- The noise process e_n is uncorrelated with the input sequence x_n.

- The probability density function of the noise process is uniform over $[-\frac{\Delta}{2}; \frac{\Delta}{2}]$.

- The noise process is white.

Under these assumptions, the average power of the noise process is given as:

$$\sigma_e^2 = \frac{\Delta^2}{12} = \frac{1}{12}\left(\frac{2V}{2^{N_o}-1}\right)^2 \approx \frac{1}{12}\left(\frac{4V^2}{2^{2N_o}}\right) \tag{2.1}$$

and the power spectral density of the noise process is given by:

$$S_{EE}(f) = \frac{\Delta^2}{12 f_{sample}}, \qquad |f| \leq f_{sample}/2 \tag{2.2}$$

with the sampling rate f_{sample}

If the signal is a zero mean random process with an average power of σ_x^2, the signal to noise ratio of the ADC due to quantization is given as

$$SNR_Q = 10log(\frac{\sigma_x^2}{\sigma_e^2}) = 10log\frac{\sigma_x^2}{V^2} + 4.77 + 6.02N_o \tag{2.3}$$

It is easily seen that increasing the resolution of the ADC leads to an increase in SNR_Q, about 6dB per extra bit of resolution. Since the total noise

power is independent from the sampling rate, oversampling can be used to spread the noise power over a band greater than the bandwidth of the signal, decreasing the in band noise power. If the input signal is a low pass signal with a bandwidth $2f_{max} \ll f_{sample}$, only a small fraction of the total noise power will fall into the frequency band $[-f_{max}, f_{max}]$. The noise power outside the signal bandwidth can be easily suppressed by a low pass filter after the analog to digital conversion. The in band noise power is calculated as:

$$\sigma^2_{e(ib)} = \sigma^2_e \left(\frac{f_{sample}}{2f_{max}} \right) \tag{2.4}$$

And the signal to noise ratio is then

$$SNR_Q = 10log\frac{\sigma^2_x}{V^2} + 4.77 + 6.02N + 10log\left(\frac{f_{sample}}{2f_{max}} \right) \tag{2.5}$$

An important performance measure of an ADC is its dynamic range. The dynamic range gives the range of input amplitudes, for which the ADC produces a positive SNR [7]. It is defined as the ratio of the power of a sinusoidal signal, which produces the optimum SNR_Q to the power of a sinusoid which results in 0dB SNR_Q. Obviously, the maximum SNR occurs when the signal has the maximum amplitude V, and, accordingly, the power $V^2/2$. The sinusoid with the power $\sigma^2_{e(ib)}$ will produce a SNR_Q of 0 dB. Therefore, the dynamic range of an ADC can be given as:

$$\begin{aligned} D &= 10log\frac{P_{opt}}{P_{min}} = 10log\left(\frac{V^2/2}{\Delta^2/12} \frac{f_{sample}}{2f_{max}} \right) \\ &= 1.76 + 6.02N_o + 10log\left(\frac{f_{sample}}{2f_{max}} \right) \end{aligned} \tag{2.6}$$

In a practical ADC, there exist other error sources than the quantization noise, mainly due to the limitations in the hardware. The most important ones being:

- Aperture jitter

- Thermal Noise

- Intermodulation products due to nonlinearities

- Comparator ambiguities

These errors manifest themselves as additional noise in the ADC output, decreasing the total SNR of the device. This is equivalent to a decrease in the effective resolution for a given output signal to noise ratio, or a decrease in the dynamic range for a given resolution.

The aperture jitter refers to the sample to sample variation in the sampling instant due to the errors in the clock source. In practice, the sampling process can be characterized by a mean and a standard deviation with respect to the sampling time. The mean represents the average delay in the sampling instant, whereas the standard deviation characterizes the variation of the sampling point and is defined as the rms aperture jitter τ_a. The additional noise power due to the aperture jitter errors can be given as

$$\sigma_{aj}^2 = (\pi f_{max} V \tau_a)^2, \tag{2.7}$$

and depends on the bandwith of the input signal. This makes the aperture jitter one of the main factors limiting the bandwidth of an ADC. A detailed analysis of the effects of jitter and other sources of error appearing in practical ADCs is given in [8].

The power consumption is another important performance measure for an ADC, especially in wireless applications, where the battery life is a crucial issue. The power consumption usually increases with increasing resolution and sampling rate, which limits the performance of the ADCs in a mobile terminal.

Over the last two decades, there have been tremendous research efforts in the area of analog to digital conversion, which led to the great amount of different types of ADCs commercially available today. In the following, we are going to have a look at the few core ADC architectures, which most of the converters in the market are based on.

Flash Converters

The flash, or parallel analog to digital converter is one of the oldest and most primitive ADC architectures. It consists of $2^N - 1$ comparators. One input of all of the comparators is connected to the input signal via a sample and hold circuit. The other inputs are connected to successive steps of a resistor ladder, which functions as a voltage divider, as illustrated in Fig. 2.3. The reference voltage connected to the resistor ladder represents the range of the ADC. As the input voltage increases, the comparators, one after another,
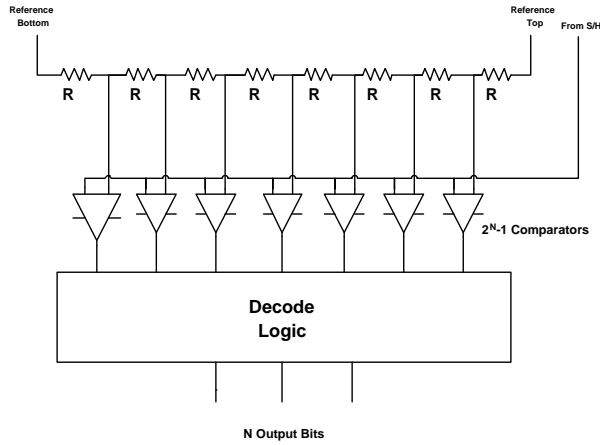
Fig. 2.3 Typical Flash ADC architecture

give 1 as output, which is then encoded into an N-bit word by the encoding logic.

The benefits of this architecture are its straightforward design, high speed, and its low cost at low resolutions. The most important drawback of this design lies in the exponential increase in the number of comparators with increase in resolution, which leads to a very high power consumption, large chip area and high cost at high resolutions. Due to these problems, flash converters are seldomly used for applications requiring more than 10 bits of resolution.

Multistage Converters

A multistage ADC, as shown in Fig. 2.4, consists of a cascade of k stages, each containing a sample and hold circuit, a low resolution m bit analog to digital converter, an m bit digital to analog converter and a gain block between each stage [8]. During the operation, each stage converts the output from the previous stage into a low resolution digital code, and then back to an analog representation. The interstage amplifier is fed with the difference from the held analog signal and the reconstructed analog signal, which turns the residual signal over to the next stage. The residual signal is processed by the next stages in the same manner. After the completion of all k conversion stages, the outputs of the k m bit analog to digital converers are combined to generate the final $k \times m$ bit word.
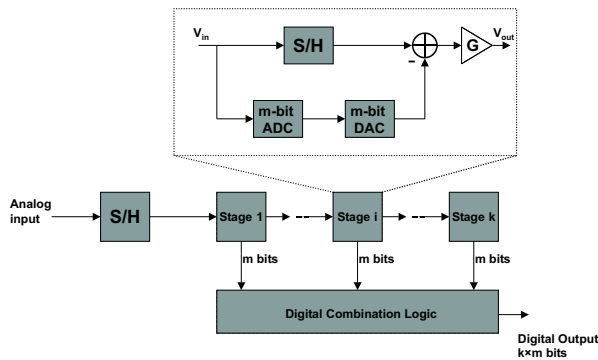
Fig. 2.4 The Multistage ADC

In comparison to the flash converters, the number of comparators required by this design are much less: $k(2^m - 1)$ comparators for $k \times m$ bits of resolution instead of $2^{mk} - 1$, which results in smaller die size, lower power consumption and reduced cost. On the other hand, the speed of conversion is substantially lower, since the conversion takes place in more than one step. With today's technology, multistage ADCs can achieve up to 16 bits of resolution at moderate bandwidths [8].

Sigma-Delta Converters

Sigma-delta (Σ-Δ) analog to digital conversion is a relatively new and promising technology, which uses noise shaping techniques in combination with oversampling to achieve a high resolution. A first order Sigma-Delta Converter is illustrated in Fig. 2.5, where the quantizer has been modeled as an additive noise source with properties described in the previous section. The converter consists of a Σ-Δ modulator subcircuit , a digital low pass filter and a decimator.

If the digital to analog converter is ideal, the output at the quantizer can be given in the time domain as:

$$y_n = x_{n-1} + e_n - e_{n-1} \tag{2.8}$$

and in z-Domain:

$$Y(z) = z^{-1}X(z) + (1 - z^{-1})E(z) \tag{2.9}$$
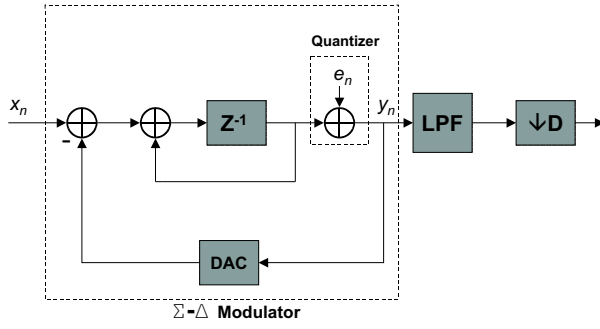
Fig. 2.5 A first order Σ-Δ ADC

The output y_n consists of the sum of the delayed input signal plus the differentiated quantization noise. Since differentiation is a high pass filtering operation, the quantization noise is attenuated at low frequencies and amplified at high frequencies, which is called noise shaping. The out-of-band noise is then removed by the low pass filter and the decimator following the quantization.

The simplest form of Σ-Δ ADC uses 1-bit quantization for the internal DAC and ADCs. This provides sufficient resolution for high oversampling rates. A detailed analysis of such an ADC is given in [9], where it is shown that the output of the 1-bit quantizer is in pulse density modulated format, which is averaged by the digital low pass filter to produce a digital signal closely approximating the analog input signal.

Better noise attenuation can be achieved using a higher order noise transfer function. In such a case, the input-output relationship of the ADC is given as:

$$Y(z) = z^{-1}X(z) + (1 - z^{-1})^L E(z) \qquad (2.10)$$

where L is the order of the ADC.

Due to the noise shaping, the quantization noise analysis for Σ-Δ converters is different. For an L'th order Σ-Δ converter, SNR_Q given as [9]:

$$SNR_Q = 10log\Big(\frac{\sigma_x^2}{\sigma_e^2}\Big) + (2L+1)10log\Big(\frac{f_s}{2f_{max}}\Big) - 10log\Big(\frac{\pi^{2L}}{2L+1}\Big) \quad (2.11)$$

From (2.11), it can be easily seen that increasing the order of the ADC

results in a higher SNR_Q. However, higher order Σ-Δ converters are more complex to design and lead to higher time delays and stability problems.

Another issue associated with the Σ-Δ design is that as a result of noise shaping, high resolution can only be attained for low to medium signal bandwidths. This can be solved by using more complicated conversion architectures with multiple Sigma-Delta converters in parallel, each of them converting different portions of the signal band [8].

In light of the discussion above, the problems associated with the ideal Software Radio approach can be more easily comprehended. In order to digitize the whole frequency band of interest with a bandwidth around 5 GHz, high speed ADCs with very low aperture jitter and very high dynamic range are needed, which cannot be realized with any of the architectures discussed above. This makes the existence of analog preprocessing in the Software Radio receiver indispensable for the time being.

2.2.2   Software Radio Front End

The front end in a conventional wireless receiver performs the following functions:

- Channel selection

- Interference suppression

- Amplification

- Downconversion of the signal from the radio frequency (RF) to base-band.

The front end of a Software Radio has two important differences compared to the conventional receivers:

- Its operating frequency is not predetermined

- Its channel bandwidth is not predetermined

Many different front end architectures are currently in discussion for a SDR. The traditional superheterodyne architecture, which performs the downconversion in multiple steps has the drawback of being highly complex and power hungry. More important than that, it lacks the flexibility, which is crucial for a multi-mode multi-band operation. On the other hand, the zero-IF receivers, which perform the downconversion in a single step, are less complex and provide easier image suppression. The main problem here is
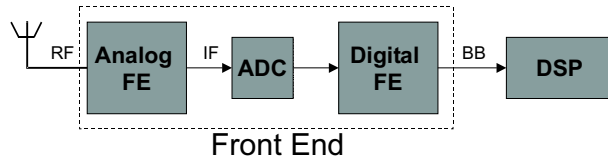
Fig. 2.6 SDR architecture with a digital frontend

the need for phase and amplitude balanced mixers and oscillators over very wide frequency bands [10]

Using a combination of analog mixing and downconversion with digital down conversion and filtering is another approach, which has drawn considerable attention in recent years [10]. In this case, the SDR Frontend consists of an analog and a digital subsystem (see Fig. 2.6). First, in order to match the dynamic range and the bandwidth of the signal to the capabilities of the ADC and the DSPs, a limited band out of the full 5 GHz band is selected and brought to an intermediate frequency (IF) by the analog stage. This wideband signal contains a bundle of different channels, possibly from different wireless standards. The signal is digitized at the IF and further downconversion, filtering and channel selection is performed in the digital domain, by the so called digital front end, which acts as a bridge between the analog (RF and IF) signal processing and the digital baseband (BB) signal processing.

From the Software Radio point of view, transferring a part of the functions of the front end into digital domain makes perfect sense in terms of reconfigurability and reprogrammability, shifting the transition boundary between the digital an analog domains closer to the antenna, thus increasing flexibility.

2.3   Summary

This section presented an overview on the Software Radio concept, along with its strengths and limitations. The technological obstacles in the realization of an ideal Software Radio have been discussed, and an alternative transceiver architecture, the so called Software Defined Radio has been introduced

3 The Mobile Communication Environment

This chapter presents an overview of the mobile communication environment, in which the air interface identification is to be performed. In the first part, the characteristics of the mobile communication channel are described, which is a relatively hostile environment. In the second part, three fundamental transmision schemes encountered in today's radio frequency environment are investigated, which give rise to quite different signal structures.

3.1 The Mobile Radio Propagation Channel

In mobile communications, electromagnetic waves are used to transmit signals from a transmitter to a receiver. The propagation properties of the radiowaves are primarily determined by the carrier frequency of the signal, and the physical environment of the transmitter and the receiver. In terrestrial wireless communications, principally three different types of propagation scenarios are considered [11]

- Picocells, having usually a small radius, up to 100 m, are usually found in indoor areas. Because of the small size of the cell, there usually exists a direct line of sight (LOS) connection between the receiver and the transmitter. The user speeds are usually low, around a couple of kilometers per hour. The picocells are commonly used for wireless LAN (WLAN) and cordless telephony applications.

- Microcells are usually located in urban areas and are characterized by non line of sight (NLOS) conditions. The cell radius may be around 1 km. In this scenario, the user speeds are assumed to be around 50 km/h.

- Macrocells, having radii in the order of tens of kilometers, are usually found in suburban and rural areas. A LOS connection between the receiver and transmitter occurs rarely. The user speeds are assumed to be higher than both of the previous cases, for example on highways or in trains.
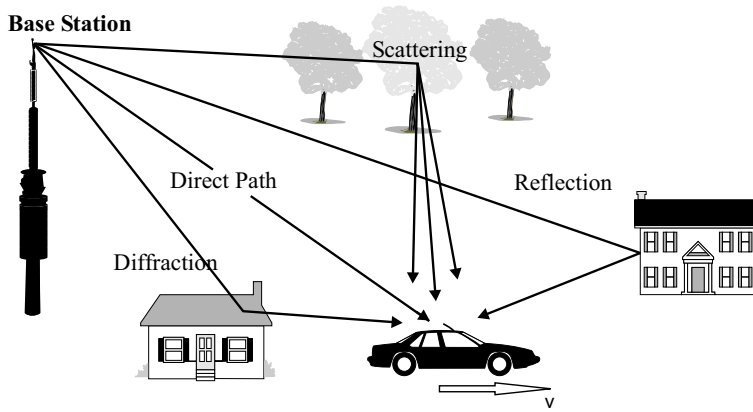
Fig. 3.1 The Multipath Propagation in a Mobile Communications System

The propagation of electromagnetic waves in a mobile communications environment is caracterized by three different effects

- Path loss is the attenuation in signal power due to the distance between the transmitter and receiver. In vacuum, this loss is proportional to the square of the distance. In mobile environments, where no line of sight exists, the path loss may increase with higher exponents of the distance, from 3 to 5, depending on the terrain characteristics. The effect of path loss is a relatively slow long term variation in the mean of the received signal power, which can be corrected using power control schemes.

- Shadowing is the attenuation in signal power due to the physical obstacles on the signal path, i.e. buildings, terrain characteristcs, tunnels, etc. The effects of the shadowing falls into the category of slow fading, and may also be compensated by power control algorithms [12].

- Multipath propagation is caused by the reflection, scattering and diffraction of electromagnetic waves, as illustrated in Fig. 3.1. The signal travels from transmitter to receiver on multiple different paths.The replicas of the signal arrive at different time instants with different phases, different amplitudes, different angles of arrival and different polarisations. The superposition of the signal replicas cause a destructive or constructive interference at the receiver, depending upon the relative phases. Since the variations in the interference pattern take
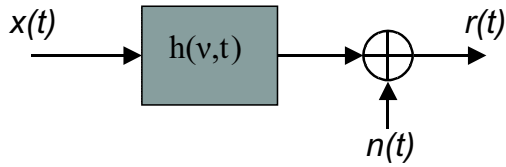
Fig. 3.2 The Mobile Communications Channel

place over distances in the order of the signal wavelength, even small changes in location of either the transmitter or the receiver may cause major changes in the received signal level, giving rise to fast fading.

3.1.1 The Channel Impulse Response

From a system theoretic point of view, mobile communication channels can be characterized as linear time variant systems [12]. Fig. 3.2 illustrates a typical mobile channel, with the time varying impulse response $h(t, \nu)$ and the additive noise component $n(t)$. The received signal in this case can be given as:

$$r(t) = x(t) * h(t, \nu) + n(t) = \int_{-\infty}^{\infty} h(t, \nu) x(t - \nu) d\nu + n(t) \qquad (3.1)$$

The time varying channel impulse response (sometimes also called the delay spread function) is the response of the channel at time t to an impulse at time $t - \nu$. The Fourier Transform of the time varying channel impulse response with respect to ν is called the time varying channel transfer function and is given by:

$$T(t, f) = \int_{-\infty}^{\infty} h(t, \nu) e^{-j2\pi f\nu} d\nu \qquad (3.2)$$

In terms of the time varying channel transfer function, the received signal can be given as:

$$r(t) = \int_{-\infty}^{\infty} \int_{-\infty}^{\infty} T(f, t) x(t - \nu) e^{j2\pi f\nu} df d\nu + n(t) \qquad (3.3)$$

3.1.2   Rice and Rayleigh Fading

A communication channel is called narrowband, when the time delay between the longest and the shortest multipaths $\Delta\tau_0$ is much less then the reciprocal of the signal bandwidth B, i.e.

$$\Delta\tau_0 << \frac{1}{B} \tag{3.4}$$

In such a case, the receiver cannot distinguish between multipath replicas arriving at different times, and cannot resolve the particular paths in time. The channel impulse response in this case can be given as [13].

$$h(t,\nu) = h(t)\delta(\nu) \tag{3.5}$$

and the time varying channel transfer function

$$T(t,f) = \int_{-\infty}^{\infty} h(t)\delta(\nu)e^{-j2\pi f\nu}d\nu = h(t) \tag{3.6}$$

Hence, the received signal is calculated as

$$r(t) = h(t)x(t) + n(t) \tag{3.7}$$

The channel transfer function in this case is a time varying multiplicative attenuation, also called a multiplicative fading coefficient. Since the whole signal spectrum is attenuated with the same fading coefficient, channels of this type are referred to as flat fading channels, or non-frequency selective channels.

Since the wavelengths of the mobile communications systems are usually much smaller than the path differences between multipath replicas of the signal, we can assume that the phases of the multipath components are uncorrelated. This and the assumption of a large number of incident multipath components leads to an analytic description of the probability density function (pdf) of the fading coefficient. Assuming that no single path dominates others, and using the central limit theorem, we get a complex Gaussian density for the fading coefficient, which leads to a uniform distribution in phase over the interval $[0, 2\pi)$ and a Rayleigh distribution in amplitude, which is

defined as [13]

$$f_h(\rho) = \frac{\rho}{\sigma^2} e^{-\rho^2/2\sigma^2}, \qquad 0 \leq \rho < \infty \tag{3.8}$$

where σ^2 is the variance of the underlying Gaussian process and ρ is the amplitude of the process. The Rayleigh density is a useful tool for characterizing narrowband channels with no dominating line of sight component.

If there is a dominant contribution from a line of sight path, the assumptions which have led to the Rayleigh distribution do not hold. It can be shown that in such a case, the fading coefficient follows a Rice distribution

$$f_h(\rho) = \frac{\rho}{\sigma^2} e^{-(\rho^2+\beta^2)/2\sigma^2} I_0\left(\frac{\rho\beta}{\sigma^2}\right), \qquad 0 \leq \rho < \infty \tag{3.9}$$

where β is the amplitude of the dominant path and $I_0(.)$ is the modified Bessel function, first kind, zero order, which is given as

$$I_0\left(\frac{\rho\beta}{\sigma^2}\right) = \frac{1}{2\pi} \int_0^{2\pi} e^{\beta\rho cos(\phi)/\sigma^2} d\phi. \tag{3.10}$$

The Rayleigh distribution can be seen as a special case of the Rice distribution with $\beta = 0$. In Fig. 3.3 Rice pdf's are illustrated for different values of the parameter β.

3.1.3   The Tapped Delay Line Channel Model

Assuming that the transmitted signal $x(t)$ has a two sided bandwith of B, applying the sampling theorem on the low pass equivalent signal $x_l(t)$ results in the following signal representation [14]:

$$x_l(t) = \sum_{n=-\infty}^{\infty} x_l\left(\frac{n}{B}\right) \frac{sin[\pi B(t - n/B)]}{\pi B(t - n/B)} \tag{3.11}$$

The Fourier transform of $x_l(t)$ is

$$X_l(f) = \begin{cases} \frac{1}{B} \sum_{n=-\infty}^{\infty} x_l(n/B) e^{-j2\pi fn/B} & |f| \leq \frac{B}{2} \\ 0 & \text{otherwise} \end{cases} \tag{3.12}$$
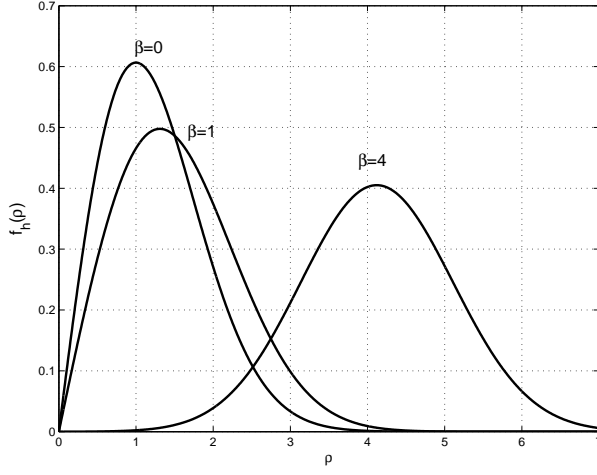
Fig. 3.3 The Rice probability density functions with $\sigma^2 = 1$ for different values of β. For $\beta = 0$, The Rice density reduces to a Rayleigh density.

Using the low pass equivalent of the time variant channel transfer function $T_l(t, f)$ the low pass equivalent of the received signal can be expressed as:

$$r_l(t) = \int_{-\infty}^{\infty} X_l(f) T_l(t, f) e^{j2\pi ft} df + n(t) \tag{3.13}$$

Substituting (3.12) in (3.13) yields

$$r_l(t) = \frac{1}{B} \sum_{n=-\infty}^{\infty} x_l(n/B) \int_{-B/2}^{B/2} T_l(t, f) e^{j2\pi f(t-l/B)} df + n(t). \tag{3.14}$$

Defining the band limited version of the low pass equivalent channel impulse response as

$$h_B(t, \nu) = \int_{-B/2}^{B/2} T_l(t, f) e^{j2\pi f\nu} df = h_l(t, \nu) * \frac{sin(\pi B\nu)}{(\pi\nu)} \tag{3.15}$$

we get

$$r_l(t) = \frac{1}{B} \sum_{n=-\infty}^{\infty} x_l(n/B) h_B(t, t - n/B) + n(t) \qquad (3.16)$$

$$= \frac{1}{B} \sum_{n=-\infty}^{\infty} x_l(t - n/B) h_B(t, n/B) + n(t).$$

Obviously, for large B, $h_B(t, \nu)$ converges to $h_l(t, \nu)$. We can write

$$r_l(t) \approx \frac{1}{B} \sum_{n=-\infty}^{\infty} x_l(t - n/B) h_l(t, n/B) + n(t). \qquad (3.17)$$

Introducing the time varying channel coefficients $h_n(t)$ as

$$h_n(t) = \frac{1}{B} h_l(t, n/B) \qquad (3.18)$$

the output of the channel can be expressed as

$$r_l(t) \approx \frac{1}{B} \sum_{n=-\infty}^{\infty} x_l(t - n/B) h_n(t) + n(t). \qquad (3.19)$$

The form of the received signal in (3.19) implies that the channel can be modeled or represented as a tapped delay line. The time varying impulse response for the channel can be expressed in terms of the channel coefficients as:

$$h_l(t, \nu) = \sum_{n=-\infty}^{\infty} h_n(t) \delta(\nu - n/B) \qquad (3.20)$$

and the time varying channel transfer function is

$$T_l(t, f) = \sum_{n=-\infty}^{\infty} h_n(t) e^{-j2\pi f n/B} \qquad (3.21)$$

In practice, multipath channels can be represented by a finite number of taps. The number of taps M required for a channel depends on the co-
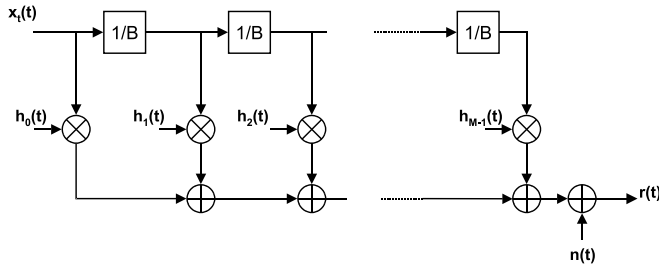
Fig. 3.4 The Tapped Delay Line Channel Model

herence bandwidth of that particular channel, which is defined as the frequency separation, where the correlation of two received signal components becomes less than 0.5 [14]. Fig. 3.4 illustrates a tapped delay line channel with M channel coefficients. The coefficients of the channel impulse response are time varying stochastic processes with complex Gaussian distributions, which give rise to Rice or Rayleigh distributed magnitudes, as discussed in section 3.1.2 .

3.1.4 The WSSUS Assumption

This section describes the simplifying assumptions made in order to model the statistical characteristics of the channel impulse response $h_l(t, \nu)$.

First, the assumption of wide sense stationarity (WSS) shall be examined. A process is called wide sense stationary, if its first two moments, i.e. mean and autocorrelation are independent of absolute time [15]. For a wide sense stationary channel, this means that the autocorrelation function depends only on time difference, and the mean is constant. In the tapped delay line channel, described in the previous section, the WSS assumption leads to random channel coefficients $h_n(t)$ with constant mean values.

The second important assumption is the uncorrelated scattering (US) assumption. In channels with uncorrelated scattering, the statistics describing signal components arriving with different delays are assumed to be uncorrelated with each other. For the tapped delay line channel model, the US assumption leads to channel coefficients which are uncorrelated with each other.

The most useful channel model from the viewpoint of a mobile radio engineer is the hybridization of the above channels, referred to as wide sense stationary uncorrelated scattering (WSSUS) channels. The particular si-
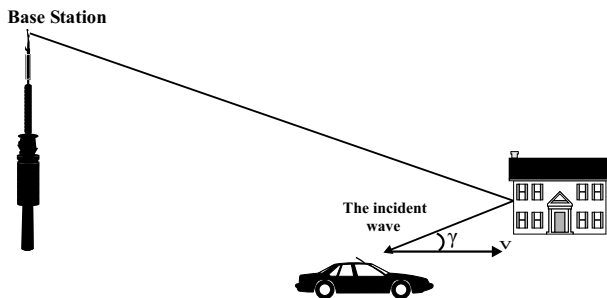
Fig. 3.5 The Doppler effect is caused by the relative movement of the receiver with respect to the transmitter

gnificance of this kind of channels comes from the fact that they are the simplest channels to analyse and model, that exhibit time and frequency selective fading [16].

3.1.5 The Doppler Effect

For an accurate modelling of the mobile communication channels, the effects of the doppler shift have to be also taken into account. The Doppler effect is caused by the relative movement between the receiver and the transmitter, which is illustrated in Fig. 3.5. The relative velocity v of the user causes a shift in the frequency of the incident wave f_C, which can be calculated as

$$f_D = \frac{f_C v}{c} cos(\pi - \gamma) = f_{Dmax} cos(\pi - \gamma) \tag{3.22}$$

whith the Doppler shift f_D, the speed of light $c \approx 3 \times 10^8 m/s$, and the angle of arrival of the wave is $\pi - \gamma$ as shown in Fig. 3.5. The maximum doppler shift $\pm f_{Dmax}$ for a given v and f_C occurs, when the wavefront arrives directly from behind or from ahead (i.e. $cos(\gamma) = \pm 1$).

In an environment with multipath propagation, the signal at the receiver is composed of several multipath components with different angles of arrival and, consequently, different doppler shifts. The superposition of the signals from different multipaths leads to the superposition of their individual Doppler shifts, resulting in a spread of the signal in the frequency domain.

An analytic representation of the effects of the Doppler shift is achieved, using the following simplifying assumptions:
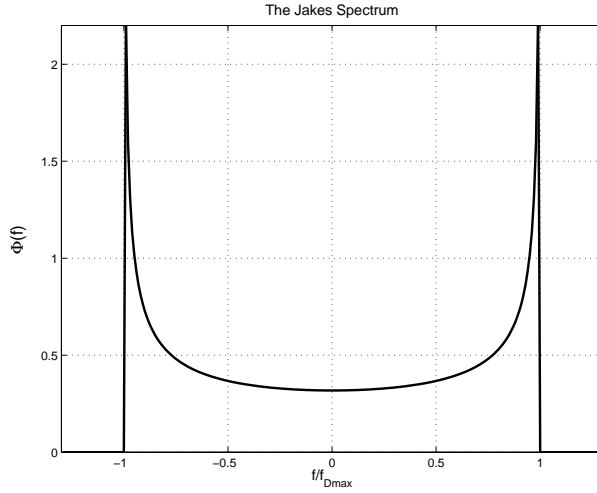
Fig. 3.6 The Jakes Spectrum

- The angle of the arrival of the incident multipath components is uniformly distributed over $[0, 2\pi)$

- The wave propagation takes place on a horizontal plane

- The receiver employs an omnidirectional antenna with a circular pattern

These assumptions result in a Doppler spectrum, which is given as [12]

$$\Phi(f) = \begin{cases} \frac{1}{\sqrt{1-(f/f_{Dmax})^2}} & |f| \leq f_{Dmax} \\ 0 & \text{otherwise} \end{cases} \tag{3.23}$$

and is illustrated in Fig. 3.6. This kind of Doppler spectrum is also called the Jakes Spectrum and represents the spread in the frequency domain of a purely sinusoidal signal under the influence of the Doppler effect in a multipath channel. Due to the time frequency duality, this frequency dispersive phenomenon results in a time selective behaviour of the channel, i.e. higher user velocities result in wider doppler spreads, which lead to faster fluctuations in the channel impulse response.

Taking the WSSUS assumption, Doppler spreading and fading effects into account, an individual channel coefficient of the tapped delay line channel
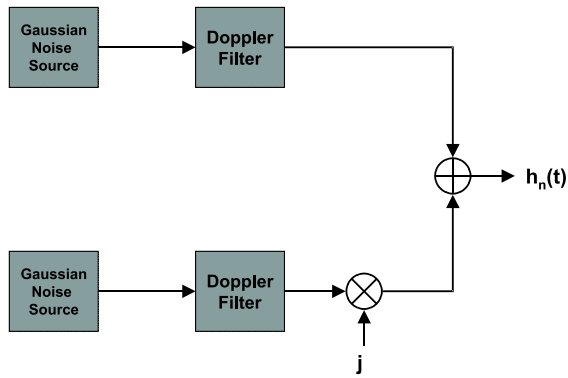
Fig. 3.7 Generation of a channel coefficient

model can be generated numerically as shown in Fig. 3.7. The imaginary and the real parts of the channel coefficient are generated separately by using two uncorrelated white Gaussian processes, giving rise to a Rayleigh distributed amplitude. The effects of the doppler spread are modeled by the filters approximating the Doppler spectrum.

3.2   Mobile Transmission Schemes

According to the transmission scheme used, this chapter divides the mobile communication signals into three categories:

- Single Carrier time division multiple access(TDMA) signals. Most of the second generation mobile telecommunication signals fall into this category. The most prominent examples are GSM, DECT, PDC and IS-136.

- Single carrier code division multiple access (CDMA) signals. The american IS-95 and the 3rd generation UTRA systems are well known examples belonging to this category.

- Orthogonal frequency domain multiplex (OFDM) signals. The wireless LAN standard IEEE 802.11a and the terrestrial digital video broadcasting (DVB-T) systems are air interfaces using this transmission scheme.

Frequency Band	1880-1900 MHz
Carrier Separation	200 KHz
Users/carrier	8
Duplexing Method	FDD
Frame Length	4.616ms
Slot Length	576,9μs
Total Symbol Rate	270,833 Kbit/s
Modulation Type	GMSK with BT=0.3

Tab. 3.1 GSM System Parameters

3.2.1   Single Carrier TDMA Systems

An overwhelming majority of the second generation mobile communication systems currently in operation belongs to the category of single carrier TDMA systems, where each user accesses the full channel bandwidth for a fraction of time on a periodic basis. This means that, at a given time, there is only one signal of one particular user on the channel, which makes the separation of the users relatively less complicated. In the following a brief overview of some air interfaces using this transmission scheme is presented.

GSM

Introduced in early nineties, GSM is one of the most successful mobile communication standards. In Europe, GSM networks are operated on 900 MHz (GSM 900) and 1800 MHz (GSM 1800) bands whereas the GSM variant used in northern America resides on the 1900 MHz band. GSM uses a frequency domain duplex (FDD) scheme, where uplink and downlink signals are transmitted on different frequencies. On 900 MHz band 124 carrier frequencies and on the 1800 MHz band 374 carrier frequencies are allocated for GSM transmission with a carrier separation of 200 MHz. Each carrier is shared by 8 users in a TDMA fashion, with slot lengths of 576,9 μs and frame lengths of 4.616 ms. The total symbol rate on the channel is 270,833 kbit/s resulting in a symbol length T_s of 3.692 μs.

Because of its robustness against signal fading and interference, GSM uses Gaussian minimum shift keying (GMSK) modulation, which is derived from the minimum shift keying (MSK) scheme. The linear phase changes between adjacent bit periods im MSK are smoothed in GMSK using a Gaussian filter, avoiding the discontinuities in the phase derivative that result in a widening of the signal spectrum [16].

GMSK modulation, which is used in GSM, can be interpreted as a 2-level FSK modulation with a modulation index $h = 0.5$. The complex envelope of a GMSK modulated signal is

$$s(t) = exp\Big[j2\pi h \sum_{n=-\infty}^{\infty} d_n \int_{-\infty}^{t} g(\tau - nT_s)d\tau\Big]. \tag{3.24}$$

with the symbol sequence $d_n \in \{-1, 1\}$, the symbol rate $f_s = 1/T_s$ and the frequency impulse $g(t)$ given as

$$g_f(t) = \frac{1}{T_s}rect\Big(\frac{t}{T_s}\Big) * p_{Gauss}(t). \tag{3.25}$$

The gaussian impulse $p_{Gauss}(t)$ has the form

$$p_{Gauss}(t) = \sqrt{\frac{2\pi}{ln2}} \cdot B \cdot exp\Big(-\frac{2(\pi Bt)^2}{ln2}\Big). \tag{3.26}$$

The key parameter of the GMSK modulation is the product of the 3dB bandwidth B and the symbol length T_s, which is also referred to as the normalized badwidth. A low BT_s product results in a broader frequency impulse $g(t)$, leading to a higher ISI, while reducing the bandwidth, whereas for a high BT product, GMSK converges to MSK, decreasing the spectral efficiency. Fig. 3.8 illustrates the frequency impulse $g(t)$ for different values of normalized bandwidths BT_s. For GSM, a BT_s product of 0.3 has been chosen.

In order to compensate for the ISI arising from the low BT product and from the time dispersive nature of the mobile propagation channel, the GSM employs a Viterbi equalizer which performs Maximum Likelihood Sequence Estimation (MLSE).

Originally designed for voice communication, the GSM system has undergone some modifications over the years to allow data communications with moderate symbol rates. The HSCSD (high speed circuit switched data) enhancement is a connection oriented scheme allowing the combination of up to 4 time slots for a single user to achieve net data rates up to 57.4 kbit/s. The GPRS (Global packet radio system) also allows the combination of time slots, however, in a packet oriented manner. Using the GPRS scheme, data rates of 115 kbit/s can be attained. The EDGE (Enhanced Data for Global Evolution) uses a more radical approach to achieve data rates up to 384 kbit/s. It employs a higher level modulation type (8 PSK) instead of GMSK,
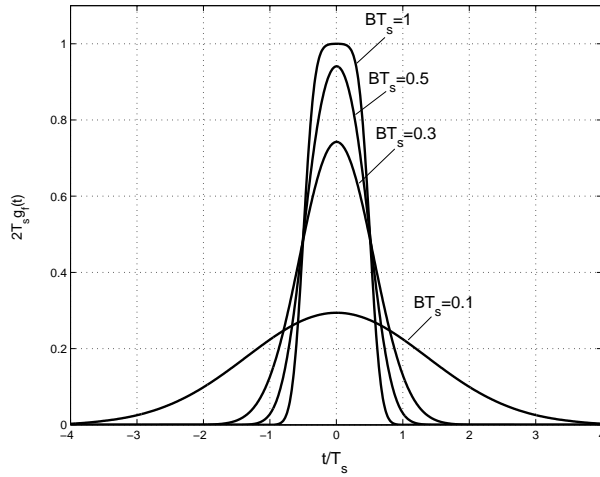
Fig. 3.8 The Frequency pulse $g_f(t)$ for different values of the parameter BT

using a pulse shape designed to maintain the 200 kHz carrier separation.

DECT

The DECT (Digital Enhanced Cordless Telephony) system has been introduced in the early nineties [17]. It has been designed for cordless telephony and data transmission in indoor office environments, for small mobile networks and as a mobile access method to the public telephone network (i.e. local loop).

The air interface of the DECT system is based on TDMA on a frequency band between 1880-1990 MHz. On this band, 10 carriers with a carrier spacing of 1.728 MHz are used. Each carrier is shared by 12 users. The uplink and downlink are separated by using a Time Division Duplex (TDD) scheme. The frame duration is 10 ms, and the slot length 0.417 ms.

The total symbol rate on the channel is 1152 kbit/s, resulting in a symbol length of 0.868 μs. In DECT, like in GSM, the GMSK modulation is employed, however, with a normalized bandwidth of $BT_s = 0.5$. The higher BT_s product compared to GSM results in a simplification on the required clock recovery procedures, and, most importantly, in a reduction in the ISI inherent to the GMSK modulation , while increasing the signal bandwidth (see Fig. 3.8). Since the DECT system has been dimensioned for use in

Frequency Band	1880-1900 MHz
Carrier Separation	1.728 MHz
Users/carrier	10
Duplexing Method	TDD
Frame Length	10ms
Slot Length	0.417ms
Total Symbol Rate	1152 Kbit/s
Modulation Type	GMSK with BT=0.5

Tab. 3.2 DECT System Parameters

picocells with radii in the order of 100 m and with maximum user speeds of 20 km/h, the multipath delays in the order of hundreds of nanoseconds occuring in such indoor environments do not cause any significant intersymbol interference either. Hence, DECT systems do not necessarily use any channel equalization schemes. The flat fading ocurring in the channel is compensated using antenna diversity techniques. Tab. 3.2 summarizes the most important parameters of the DECT system.

IS 136

IS 136 is a mobile communication system primarily used in the USA. It is the succesor of the IS-54 system which was introduced in 1991.

IS 136 uses frequency division duplexing with uplink on the 824-849 MHz band and downlink on the 869-894 MHz band. The carrier separation is 30 kHz, which requires an efficient source coding scheme for voice transmission. 6 Time slots are assigned to each carrier. The total symbol rate is 24.3 kbaud/s, resulting in a symbol duration of 41.15 μs. The IS-136 system employs $\pi/4$-DQPSK modulation using a raised root cosine impulse shaping filter, with the roll-off factor $\rho = 0.35$. The relatively long symbol duration compared to GSM results in a less severe ISI, which requires less complex channel equalisation algorithms. However, unlike in GSM, the channel may change significantly in one burst interval.

3.2.2   Single Carrier CDMA Systems

Most of the 3rd generation mobile communications systems are based on single carrier code division multiple access (CDMA) schemes. In the CDMA scheme, unlike in TDMA, the users are allowed to access the whole available frequency band simultaneously, interfering with each other in time and fre-
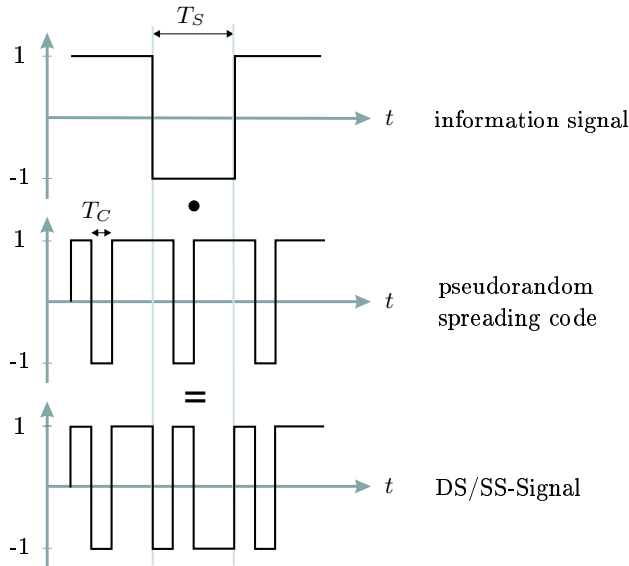
Fig. 3.9 Generation of a DS/SS Signal

quency. The separation of different users is achieved using user specific code signatures. In this section, we shall investigate the principles of the CDMA communications.

CDMA is based on the direct sequence spread spectrum (DS/SS) technique, which was originally conceived to provide covert communications with an inherent robustness to jamming. The Figures 3.9 and 3.10 illustrate the principle of the DS/SS scheme. The information signal with a data rate $1/T_s$ is multiplied with a pseudo random spreading code with a higher rate $1/T_c$. Since multiplication in time domain corresponds to a convolution in the frequency domain, this operation results in a spreading of the information signal in the frequency domain by a factor of T_s/T_c. At the receiver, the signal is recovered by multiplying again with the code sequence.

In a CDMA system, individual users transmit DS/SS signals simultaneously over the whole available channel bandwidth. The separation of the user signals is achieved by using user specific spreading code sequences, which display certain auto- and cross correlation properties.

Considering a synchronous system in an AWGN channel, the CDMA
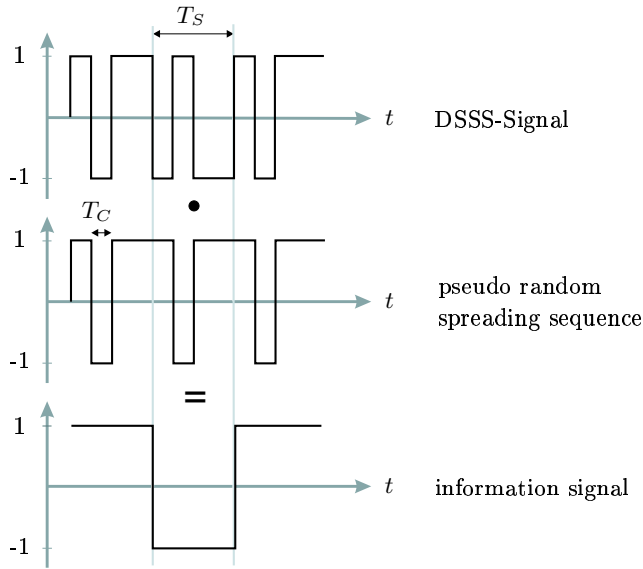
Fig. 3.10 DS/SS signal recovery

signal during the n'th symbol interval can be represented as:

$$r^{(n)}(t) = \sum_{k=1}^{K} d_k c_k(t) + n(t), \qquad (n-1)T_s < t < nT_s \qquad (3.27)$$

with the noise signal $n(t)$, number of users K and the spreading code signal $c_k(t)$ which is defined as follows

$$c_k(t) = \sum_{q=1}^{Q} c_{k,q} g(t - (q-1)T_c) \qquad (3.28)$$

where $g(t)$ is the impulse shaping filter, and $c_{k,q}$ is the code sequence of the k'th user with a code length Q.

In the receiver, the symbol of the j'th user is detected multiplying the received signal with the code sequence of the j'th user and integrating over

a symbol interval, giving

$$\hat{d}_j = \int_0^{T_s} c_j^2(t) d_j dt + \sum_{\substack{k=1 \\ k \neq j}}^{K} \int_0^{T_s} d_k c_j(t) c_k(t) dt + n_j \qquad (3.29)$$

with $n_j = \int_0^{T_s} n(t) c_j(t) dt$. If the codes are normalized, i.e. $\int_0^{T_s} c_k^2(t) dt = 1$, we get

$$\hat{d}_j = d_j + \sum_{\substack{k=1 \\ k \neq j}}^{K} \int_0^{T_s} d_k c_j(t) c_k(t) dt + n_j \qquad (3.30)$$

The middle term in the expression above is called the multiple access interference (MAI), and vanishes if the codes of the different users are orthogonal to each other, i.e.

$$\int_0^{T_s} c_j(t) c_k(t) dt = \delta_{jk} \qquad (3.31)$$

allowing the optimal separation of the individual users. Codes satisfying the ortogonality criterion can be generated using a multitude of different methods.

Under real life conditions with multipath propagation and possibly asynchronous data transmission, where user signals and their multipath replicas arrive at the receiver with different time delays, the orthogonality condition of (3.31) by itself does not suffice to suppress the MAI. In such a case, the cross correlation functions of the codes have to vanish for all possible time delays [18], i.e.

$$\int_{-\infty}^{\infty} c_j(t) c_k(t + \tau) dt = 0 \qquad \forall j \neq k \qquad (3.32)$$

and, additionaly, the autocorrelation functions of the codes must approach the ideal. Since such code sequences are not realizable, this receiver structure is unable to totally eliminate the MAI, however, its effects can be mitigated choosing code sequences with good auto- and crosscorellation characteristics.

The total CDMA signal at the receiver can be expressed as (see Fig.
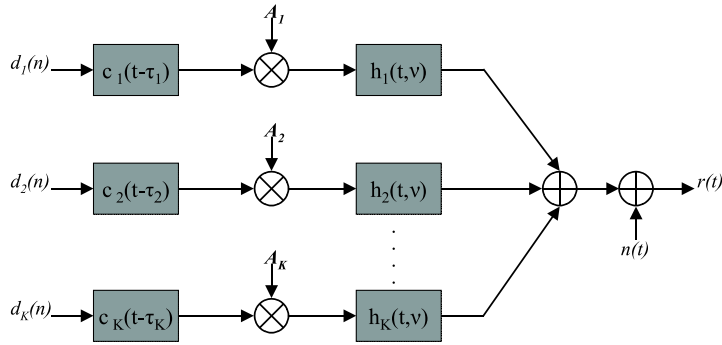
Fig. 3.11 The CDMA signal at the receiver

3.11), [18]:

$$r(t) = \sum_{k=1}^{K} \sum_{-\infty}^{\infty} A_k d_k(n) c_k(t - nT_s - \tau_k) * h_k(t, \nu) + n(t) \qquad (3.33)$$

where

- τ_k is the delay of the k'th user

- A_k is the amplitude of the k'th user

- $h_k(t, \nu)$ is the time variant channel impulse response of the k'th user

As discussed before, one of the most important measures of the performance of a spreading code family are its autocoerrelation and crosscorrelation properties. If the user specific codes do not exhibit appropriate correlation characteristics, additional signal processing may be required. To give an example, the orthogonal variable spreading (OVSF) codes used in the 3rd generation mobile communications system UTRA [19] have the advantage of being very flexible in terms of code selection. The codes from the OVSF family remain orthogonal to each other, even for different spreading factors. This property allows the variation of the symbol rate at a fixed bandwidth according to the user demands. However, the the cross- and autocorelation functions of the codes differ significantly from the ideal, leading to an increased sensitivity against multipath propagation.

In order to improve the correlation characteristics of the user signal, the so called scrambling codes are used [20]. The signal is multiplied with a

scrambling code sequence after the user specific spreading. In UTRA, the scrambling code sequences from the family of Gold codes with a code length of 38400, or from the family of S(2) codes with a code length of 256 are employed. The cell specific scrambling used in UTRA downlink serve also for separating the signals from different cells.

In the following sections, we provide a brief overview of the UTRA and IS-95 air interface standards which are two well known cellular mobile communication systems using CDMA.

UTRA

The 3rd generation mobile communications standard UTRA has two different air interface modi. In UTRA TDD, uplink and downlink are separated using a time division duplexing (TDD) scheme, whereas UTRA FDD uses frequency division duplexing (FDD).

Both air interfaces use a bandwidth of 5 MHz per carrier on the 2 GHz range. A total of 12 carriers are reserved for the UTRA-FDD mode, and 7 carriers for the UTRA-TDD mode. Both modi use QPSK modulation with a root raised cosine impulse shaping filter with roll off factor $\rho = 0.22$ and a chip rate of 3.840 Mchip/s.

The user specific spreading is carried out using orthogonal variable spreading factor (OVSF) codes, which, as pointed out earlier, allow transmitting variable symbol rates over the same 5 MHz channel.

The UTRA FDD signal has a frame length of 10 ms. Each frame consists of 15 timeslots, comprising 2560 chips. The spreading factor may take the values 4, 8, 16, 32, 64, 128 or 256 in uplink, and 4, 8, 16, 32, 64, 128, 256 or 512 in downlink. In the downlink, the user signal undergoes a cell specific scrambling, improving the correlation characteristics of the signal, and providing cell identification. In uplink, the scrambling is done with user specific scrambling codes instead. Since the user separation is provided by a combination of the spreading and the user specific scrambling, this approach allows the reuse of the OVSF codes by other users inside the same UTRA cell. In uplink, each user can transmit over up to 6 data channels in parallel. In such a case, the spreading factor must be chosen as 4.

UTRA-TDD uses time division duplexing to separate the uplink and downlink signals. Like in the FDD mode, each 10 ms frame consists of 15 slots of length 2560 chips. Unlike the FDD, however, these 15 time slots have to be shared between uplink and downlink. It is also allowed to assign the time slots to uplink and downlink in an asymmetric manner, according to the user needs. This flexibility makes the UTRA-TDD mode particularly

Air Interface	UTRA-FDD	UTRA-TDD
Duplexing Method	FDD	TDD
Bandwidth	5MHz	5MHz
Chip rate	3.84 Mchip/s	3.84 Mchip/s
Frame Length	10ms	10ms
Slot per frame	15	15
Modulation Type	QPSK	QPSK
Impulse shaping filter	Root raised cosine roll off: r=0.22	Root raised cosine, roll off: r=0.22
Spreading Codes	OVSF	OVSF
Spreading Factors	4,...,256(Uplink) 4,...,512(Downlink)	1,...,16(Uplink) 1 or 16 (Downlink)
Scrambling code length	256 or 38400	16

Tab. 3.3 UTRA System Parameters

suitable for applications requiring asymmetric data flow, such as internet browsing, where downlink almost always requires higher data rates than uplink.

Again, OVSF codes are used for spreading. In uplink, spreading factors of 1, 2, 4, 8 and 16 are allowed, and each user can transmit over a maximum of 2 parallel channels. The spreading in downlink is carried out with a spreading factor of 16. Tab. 3.3 summarizes the most important system parameters of the UTRA air interface.

IS 95

The mobile standard IS-95 was introduced in the mid nineties in the USA as the first mobile communication system ever based on the CDMA scheme. It operates on the 824-894 MHz band with a bandwidth of 1.25 MHz per channel, leading to a maximum of 20 available carrier frequencies. The chip rate on each channel is 1.2288 Mchip/s with $\pi/4$-DQPSK modulation for the downlink and offset QPSK for the uplink. In downlink, Walsh codes of length 64 are used for user specific spreading in combinalion with long codes, which are used for scrambling. In uplink, the spreading takes place a little differently. Each possible 6 bit combination is assigned to one of the 64 possible Walsh sequences of length 64, which are transmitted in place of the actual bit sequence, which is called an orthogonal modulation. For the user specific spreading, long codes are employed.

3.2.3   OFDM Systems

The main drawback of single carrier transmission is the intersymbol interference (ISI) arising in mobile communication channels, where multipath propagation occurs. This makes the received symbol $\hat{d}_n$ not only dependent of the actual transmitted signal d_n, but also of the previous transmitted symbols d_{n-i}. The ISI increases with decreasing symbol length T_s and increasing delay spread of the channel. Especially for broadband systems with very short symbol time, the removal of ISI requires the use of computationally demanding equalization algorithms, which increase the overall complexity of the systems. The underlying principle of conventional multicarrier transmission is to divide a data stream into lower rate data streams and to transmit them over a number of different subcarriers, well separated in freqency by guard bands to avoid intercarrier interference. This approach allows an increase in symbol duration on each carrier, reducing the time dispersion on each symbol due to the multipath propagation. However, using nonoverlapping carriers separated by guard bands leads to a decrease in the spectral efficiency of the system. OFDM, which is a special case of multicarrier transmission, provides a method for increasing the spectral efficiency by packing the subcarriers more densely, while avoiding intercarrier interference. In an OFDM signal, with the proper choices for the carrier separation Δf and symbol length T_s, it is possible to arrange the the subcarriers so that the signal can be received without interference from neighboring subcarriers.

The OFDM scheme has the following key advantages in comparison to single carrier systems:

- An OFDM system has an inherent robustness against the effects of multipath propagation, reducing, if not eliminating, the computational load required for channel equalization

- An OFDM system is more resistant against narrowband interference, since such interference affects only a small number of subcarriers

- In an OFDM system, it is possible to increase the system capacity by adapting the data rate per subcarrier according to the SNR of that particular subcarrier

- An OFDM system exhibits high spectral efficiency, especially for a high number of subcarriers
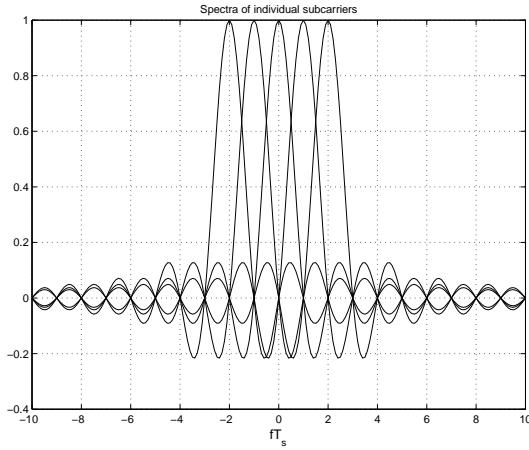
Fig. 3.12 Spectrum of an OFDM signal with 5 carriers

OFDM Transmission

In an OFDM system, the QAM (Quadrature Amplitude Modulation) or PSK (Phase Shift Keying) modulated information symbols are transmitted over multiple carriers in parallel. In contrast to the conventional multicarrier methods, OFDM uses overlapping subcarriers for the transmission. It can be shown that the orthogonality between the subcarriers can be achieved by choosing the subcarrier spacing Δf as an integer multiple of the symbol rate on the individual subcarriers $1/T_s$, and using a rectangular impulse shape of length T_s on each subcarrier. In this case, one single OFDM symbol can be written as:

$$s(t) = \begin{cases} \sum_{i=0}^{N_C-1} d_i exp\left(\frac{j2\pi it}{T_s}\right) & 0 < t < T_s \\ 0 & \text{sonst} \end{cases} \tag{3.34}$$

Where N_C is the number of carriers. The receiver demodulates the OFDM symbol by downconverting each carrier to DC and integrating over a symbol length T_s. I.e. for the l'th carrier we get

$$\hat{d}_l = \int_0^{T_s} exp\left(\frac{-j2\pi tl}{T_s}\right) \sum_{i=0}^{N_C-1} d_i exp(\frac{j2\pi it}{T_s})dt$$
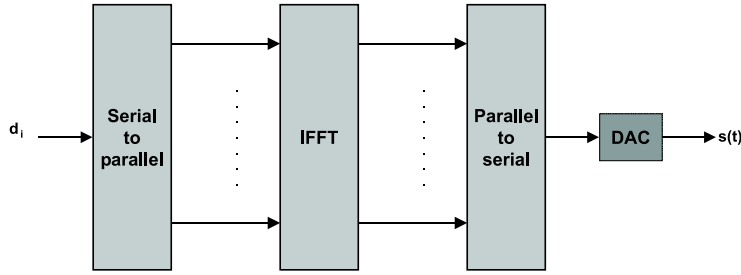
Fig. 3.13 OFDM Modulator

$$= \sum_{i=0}^{N_C-1} d_i T_s \delta[i-l] = d_l T_s. \tag{3.35}$$

Since each of the subcarriers except the desired one exhibit an integer number of periods within the integration interval T_s, they are orthogonal, i.e. their contribution to the demodulation is zero, eliminating the intercarrier interference.

The orthogonality of the carriers can also be observed in the frequency domain. Fig. 3.12 shows the spectra of overlapping carriers in an OFDM system with 5 subcarriers. The use of a rectangular pulse shape of length T_s leads to a $sinc(\pi f T_s)$ type of spectrum for each subcarrier, which has zeros for all f that are integer multiples of $1/T_s$. Since the carrier spacing is also chosen as $\Delta f = 1/T_s$, the maximum of each subcarrier coincides with the zero crossings of all the other subcarriers, which satisfies the orthogonality conditions.

Using a conventional modulator bank to generate the OFDM signal would require a very high number of oscillators and filters, making the implementation of such a system very costly. However, it can be easily shown that the OFDM symbol of (3.35) can be generated by using an inverse discrete Fourier transform (IDFT) on the N_C information symbols [21]. This makes a computationally efficient implementation of the OFDM system possible, using fast and efficientt IFFT algorithms. The OFDM modulation process using IFFT is illustrated in Fig. 3.13. After a serial to parallel conversion, the discrete transmit signal is calculated by using the IFFT. Subsequently, a parallel to serial conversion is carried out and the digital signal is converted to analog. If the number of carriers does not equal the IFFT length, zero padding must be carried out before the IFFT.
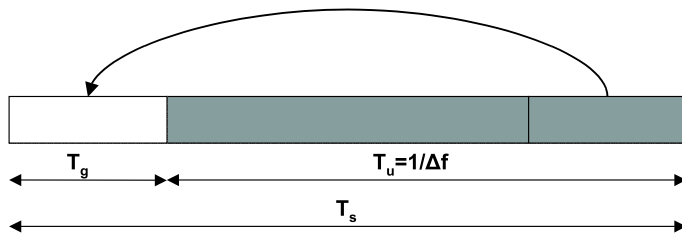
Fig. 3.14 An OFDM Symbol with cylic extension

Guard time and cyclic extension

In practical OFDM systems, the effects of ISI are almost completely eliminated by using so called guard times. The guard time T_g, which is introduced for each OFDM symbol, has to be chosen larger than the expected multipath delays from the channel, so that the signal components from different paths of one symbol do not interfere with the next symbol. At the receiver, the guard interval is removed before the FFT block, restoring the orthogonality, which has been lost by artificially extending the symbol length at a fixed frequency separation.

In order to avoid the intercarrier interference (ICI) under multipath, resulting from the delayed replicas of the OFDM signal, the guard interval has to be designed cleverly. Different subcarriers interfere with each other, if the cycles of the delayed versions of the subcarrier signals in an FFT interval T_u do not have an integer number. To prevent this, the OFDM symbol is cyclically extended in the guard time, as shown in Fig. 3.14. As a result, multipath components, which have delays smaller than the guard interval cannot cause any intercarrier interference.

In the following sections, a brief overview of IEEE 802.11a and DVB-T air interfaces is presented, which are based on OFDM transmission.

IEEE 802.11a

IEEE 802.11a air interface has been developed for wireless local area network (WLAN) applications. In USA, it operates on 5.15-5.25, 5.25-5.35 and 5.725-5.825 MHz bands, with a channel separation of 20 MHz, giving rise to 20 available channels. It uses an OFDM scheme with 52 subcarriers. In each OFDM symbol, four of the subcarriers are dedicated to pilot signals, in order to make the detection robust against frequency offset and phase noise. The symbol duration on each carrier is $T_s = 4\mu s$ with guard interval duration

$T_g = 0.8\mu s$ and the useful signal duration $T_u = 3.2\mu s$, leading to a carrier separation $\Delta f = 312.5$ kHz and a total signal bandwith of 16.6 MHz. As explained above, the OFDM symbols are extended cyclically in the guard interval. The OFDM carriers are modulated with BPSK, QPSK, 16-QAM or 64-QAM modulation depending on the requested net data rate, which can take the values 6, 9, 12, 18, 24, 36, 48 and 54 Mbit/s.

DVB-T

The DVB-T (Digital Video Broadcasting-Terrestrial) is the digital television broadcasting standard developed for use in Europe in the nineties. The DVB-T has two different operation modes, which differ from each other in the length of their FFTs and, consequently, in their carrier separation. The 8k mode, which uses an FFT length of 8192 is primarily conceived for larger single frequency networks, whereas the 2k mode with an FFT length of 2048, which is more robust to multipath propagation, is more suited for single TV stations or smaller networks.

In the DVB-T standard, the subcarriers can be modulated using 4QAM, 16QAM or 64QAM. When transmitting with 16QAM or 64QAM, a so called hierarchical modulation can be used to transmit two different data streams with different priorities. The data stream with the higher priority represents the basic service with a moderate quality of service (i.e. picture or sound quality), requiring lower SNR values, whereas the lower priority signal provides higher picture and sound quality, and possibly other services, requiring higher SNR values for proper demodulation. Depending on the channel state, the user can choose between the both signals. For the details of the hierarchical modulation, see [22].

3.3   Summary

This chapter has provided an overview of the mobile communication environment. In the first part of the chapter, the effects of the multipath propagation on mobile communication signals have been summarized, along with the effects of doppler shift, and the simplifying assumptions, which are made when modeling and analysing the mobile radio channel have been described. An overview of three different transmission schemes has been presented in the second part: single carrier TDMA, single carrier CDMA and OFDM, which give rise to completely different signal structures, making it quite a challenge to devise a single unified method, which can be used to identify

all three of them. Examples are provided in form of actual air interfaces currently in operation.

4 Automatic Channel Segmentation

Prior to identifying an air interface standard, the first thing a Software Radio receiver has to do is to localize its signal in the frequency domain and isolate it. For this reason, the SR has to be capable of analyzing large portions of the electromagnetic spectrum. Using the data from the spectrum analysis, the SR has to automatically detect the number of active emitters in its environment and their respective carrier frequencies and bandwidths, as discussed in chapter 1. In the literature, this problem is referred to as the channel segmentation problem [7].

This chapter provides a brief discussion on different spectrum analysis techniques and introduces an automatic channel segmentation scheme based on applying cluster analysis techniques on the spectrum analysis data.

4.1   Analyzing the Spectrum

In theory, the localization of power in the frequency domain can be performed by passing the signal of interest through a narrow bandpass filter and measuring the average power at the filter output. The spectral band of interest can be partitioned using a bank of narrowband bandpass filters, whose center frequencies are seperated by the filter bandwidths. In the limit, as the filter bandwidths approach zero, the measurements of the average power normalized by the filter bandwidths result in the so called power spectral density (PSD) of the signal. The PSD of a signal $x(t)$ is given as

$$S_{xx}(f) = \lim_{B \to 0} \lim_{T \to \infty} \frac{1}{T} \frac{1}{B} \int_{-T/2}^{T/2} |h_B^f(t) * x(t)|^2 dt \qquad (4.1)$$

where $*$ is the convolution operation and $h_B^f(t)$ is the impulse response of a band pass filter with bandwidth B, center frequency f and a gain of 1 at the center of the pass band.

In practice, two principal methods have emerged for approximating (4.1) over wide frequency ranges, which are used in today's spectrum analyzers
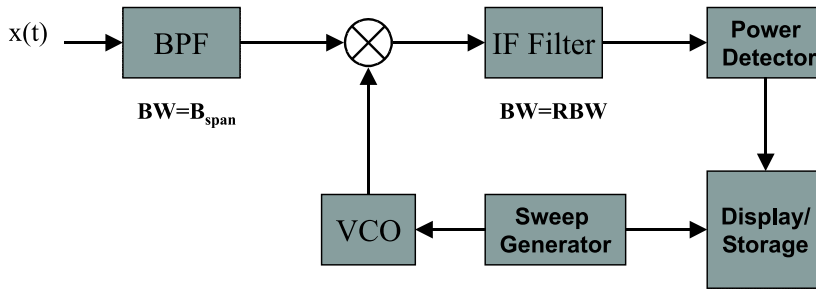
Fig. 4.1 The swept Spectrum Analyzer

1. Swept spectrum analysis

2. FFT analysis

This section briefly presents the basic operation principles of both types of analyzers and discusses the advantages and drawbacks of each method.

4.1.1 Swept Spectrum Analyzers

The swept spectrum analyzer is the most commonly used spectrum analysis technique in practice. Fig 4.1 illustrates the operating principle of such an analyzer. Basically, this type of analyzers attempt to approximate (4.1) by sweeping a narrowband filter across the frequency range of interest B_{span}, measuring the PSD of the signal at each frequency by calculating the average power at the output of the filter. Since bandpass filters tunable over large frequency ranges are very expensive, the input signal $x(t)$ is swept past a fixed narrowband intermediate frequency (IF) bandpass filter instead, mixing the input signal with the output of a voltage controlled oscillator (VCO), which is driven by a sweep generator.

The effects of the parameters of the IF filter on the performance of the analyzer can be summarized as follows:

- Two spectrum components of equal amplitude can be resolved, if their frequency separation is greater than the 3dB bandwidth of the IF filter, which is called the resolution bandwidth (RBW).

- The filter selectivity, which is defined as the ratio of the 3dB bandwidth to 60dB bandwidth determines, as illustrated in Fig 4.2, the resolvability of the spectral components having different amplitudes. Since
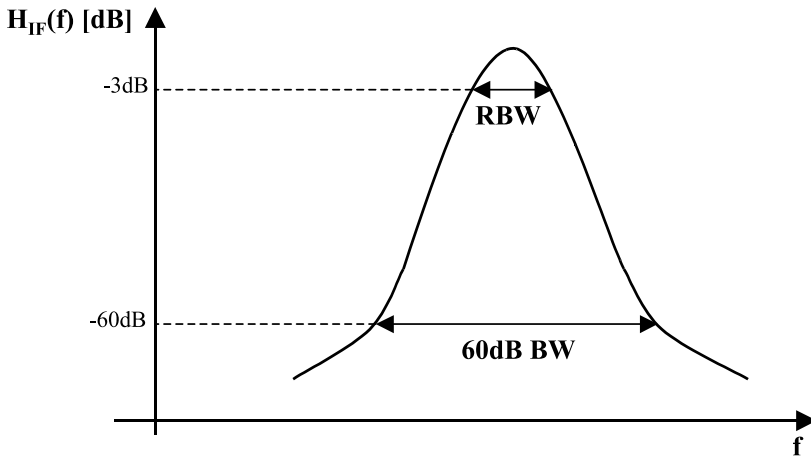
Fig. 4.2 The IF Filter Shape

both signals trace out the same filter response, it is possible for the weaker signal to be buried under the skirt of its stronger neighbour's response, if the selectivity is low.

Thus the IF filter has to be both narrowband and have a good selectivity, approaching the dirac response in the frequency domain, i.e. $\delta(f - f_{IF})$. Because of their good selectivity, filters with approximately Gaussian shape are used in most swept spectrum analyzers. Typical selectivity values which can be realized using analog filters range between 1:15 and 1:11. With digital filters, selectivities in the range of 1:5 to 1:4 are possible [23].

The IF filter requires a certain time period to produce the required output at each frequency, thus, the VCO cannot sweep through the frequency range of interest too fast. This results in long measurement times in measurements requiring a narrow RBW and wide frequency range. The main limiting factor in the measurement speed is the ability of the IF filter to respond to the magnitude variations resulting from the sweep process. This limited response speed leads to errors in amplitude and frequency as the sweep rate increases for a given IF filter. As a rule of thumb, these are proportional to the square of the sweep rate [24]. Conventional swept spectrum analyzers keep these errors within acceptable limits by automatically limiting the sweep rates according to the selected RBW [24].
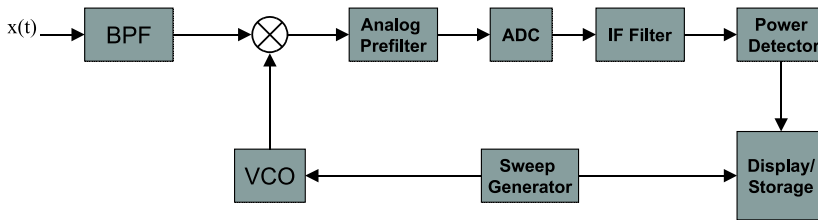
Fig. 4.3 The swept Spectrum Analyzer using a digital IF filter

Swept Spectrum Analysis Using Digital IF Filters

As high performance analog to digital converters and DSP technologies became more and more available and affordable, the transition from analog domain in the spectrum analyzers moved towards the input side of the device, following the general trend observed in all radio receiver architectures. Newer generation swept spectrum analyzers employ digital IF filters instead of analog ones, as illustrated in Fig 4.3, converting the signal into digital right after the mixing process. This approach presents the following advantages over conventional swept spectrum analysis:

- Better filter shapes with higher selectivity can be realized using digital filter design (up to 1:4 vs. a maximum of 1:11 with analog filters)

- Digital filters offer more flexibility in the resolution bandwidth.

- Digital IF filtering allows higher sweep rates, since errors from digital filters can be accurately corrected. This comes from the fact that the dynamic characteristics of digital linear phase IF filters are very predictable and can be therefore corrected to some extent.

4.1.2   FFT Based Spectrum Analyzers

It is well known that the power spectral density of a signal is equal to the Fourier transform of the autocorrelation function of that signal. FFT (Fast Fourier Transform) based spectrum analyzers make use of this fact, which has been established by the Wiener-Khinchine theorem, by converting the whole frequency range of interest into the digital domain and calculating the periodogram of the disrete-time signal, which is the magnitude squared of the Discrete Fourier Transform of the input signal. It can be shown that the periodogram of a signal is equivalent to the Fourier Transform of its
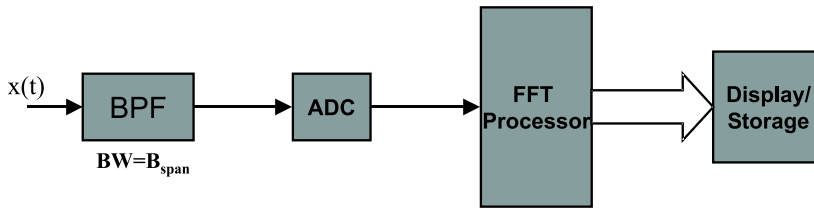
Fig. 4.4 The swept Spectrum Analyzer using a digital IF filter

autocorrelation estimate [25]. The periodogram is calculated using FFT. Fig 4.4 illustrates the basic operating principle of an FFT based analyzer.

In an FFT based spectrum analyzer, the whole spectrum range of interest is analysed simultaneously. Actually, the effect of the periodogram is the same as using a bank of narrow band pass filters in parallel, resulting in a faster measurement speed compared to swept spectrum analyzers, which is the primary advantage of the FFT-based analyzers. The measurement speed is limited solely by the processing power of the DSPs, which perform the FFT operation. Another advantage of the FFT- based analyzers is their snap shot capability. Since the whole frequency range is analyzed simultaneously, phenomena, which occur in a short time interval can be detected by the FFT analyzer, whereas the detection of such an event in a swept spectrum analyzer requires that the analyser was sweeping the particular portion of the frequency range of interest, where the event took place, at the precise moment in which the event took place, which is unlikely if the sweep time of the analyzer is much higher than the duration of the event.

The major problem in FFT based spectrum analyzers is that the whole frequency range of interest has to be converted from analog to digital at the same time. However, as discussed in chapter 2, errors in ADCs resulting from the jitter effects increase with increasing signal bandwidth, which adversely affects the dynamic range of the converter. From that reason, the dynamic range of analog to digital converters become an issue, if the frequency span to be analysed is large. Note that the swept spectrum analyzers using digital IF filters also require high speed analog to digital converters, however, in this case, only a narrow frequency segment in the same order of magnitude as the resolution bandwidth is converted into digital, avoiding the dynamic range problems.

If the frequency span to be analysed exceeds the bandwidth specifications of the ADCs, multiple FFT's computed over narrower bandwidths can be concatenated to cover the required frequency range. This approach can be

interpreted as a combination of the swept spectrum analysis with the FFT analysis, since a frequency window is swept over the frequency span to be covered, albeit in discrete steps. Obviously, the measurement speed of this approach is less than the single FFT case, nevertheless, it is still faster than the swept spectrum analysis, limited solely by the processing power of the DSPs and the hopping time of the oscillators and represents a reasonable trade-off.

The variance of the PSD estimate in both swept spectrum and FFT based analyzers can be reduced employing time averaging: Averaging the results from multiple sweeps at each frequency bin in the former, and averaging multiple periodograms in the latter [25].

From an engineering point of view, using FFT based spectrum analysis techniques in a Software Radio terminal seems more reasonable, since the SR already requires high performance wide band analog to digital converters, as discussed in chapter 2 in order to perform as many of the radio functionalities as possible in the digital domain and furhermore, it requires FFT capability as an integral part for OFDM communication, as discussed in chapter 3. Thus, FFT based spectrum analysis can be performed using capabilities, which are already integrated into the SR architecture, even if it may require improved performance from the correponding modules, such as longer FFT length etc. Using swept spectrum analysis in a SR would require the integration of a different receiver structure completely dedicated to spectrum analysis into the Software Radio, which would be undesirable.

4.2   Automatic Channel Segmentation

Fig 4.5 exhibits the spectrum analysis data from a spectral band which is occupied by 4 different radio emitters with different transmit powers and spectral shapes, which has been estimated using an FFT based approach with an FFT length of 4096. The task of the automatic channel segmentation subsystem is to detect the presence of these 4 different sources and to estimate the bandwiths and carrier frequencies of every one of them, so that they can be isolated and brought to the base-band one by one for further analysis and processing.

This problem pretty much resembles the so called *image segmentation* problem encountered in computer vision. Image segmentation is used in many applications of image processing. Its aim is to extract useful information from a digital image [26], such as detection of objects or structures and estimating their parameters, such as area or center of weight, by either iden-
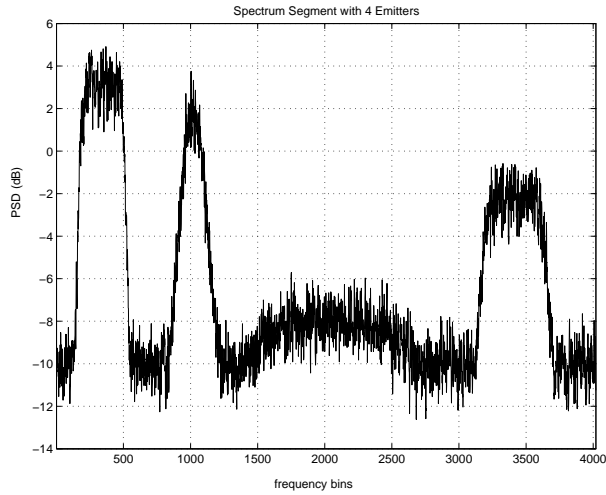
Fig. 4.5 A channel segment with 4 sources

tifying homogenous regions in the image (i.e. region based segmentation), or by detecting the contours of the regions (i.e.boundary based segmentation).

Channel segmentation can essentially be interpreted as an image segmentation problem [27] where the output of the spectrum analyser represents a one dimensional image, the "pixels" are the frequency bins and the "pixel intensities" are the values of the PSD estimates at each frequency bin. The regions to be detected are the contributions from the individual emitters, and the parameters to be estimated are the bandwidths and carrier frequencies. In this section, a region based automatic channel segmentation method is presented, which treats the spectrum data as a one dimensional digital image and makes use of image processing techniques like smoothing, morphological operations such as erosion and dilatation and image segmentation methods based on cluster analysis. The proposed algorithm consists of three main stages:

1. Preprocessing

2. Cluster analysis

3. Postprocessing and parameter extraction.
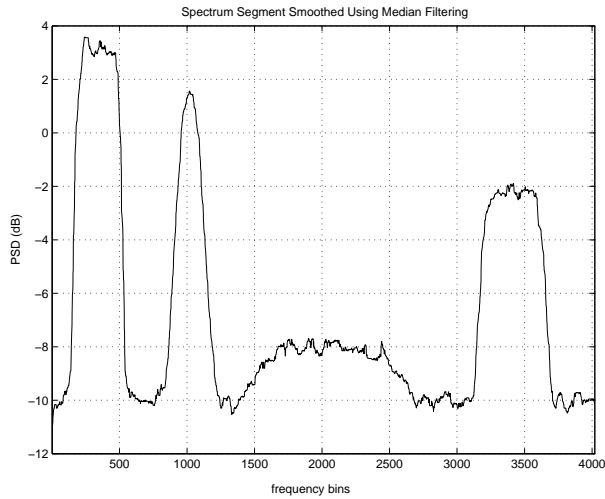
Fig. 4.6 A channel segment with 4 sources smoothed by a median filter

4.2.1   Preprocessing

The key functionality of preprocessing is to improve the spectrum analysis data in a way to increase the chance of succes of the following processing stages. In this case, preprocessing involves the smoothing of the spectrum, which facilitates the convergence of the cluster analysis algorithm employed in the succeeding stages. The two most commonly used smoothing methods in the image processing are averaging, which is essentially a low pass filtering operation, and median filtering, which is a nonlinear filtering operation. Since median filtering is known to preserve the edge information [26], as opposed to averaging, which smears the edges, widening the spectra of the individual signals, the proposed algorithm employs median filtering to reduce the amplitude variations in the spectrum data due to AWGN, measurement noise, multipath fading, etc., producing a relatively smooth spectrum. Care should be taken that the filter window does not exceed about 20 % of the bandwidth of the signal with the narrowest bandwidth expected, so that no oversmoothing takes place, and all the spectral features are preserved. Fig 4.6 exhibits the result of such a smoothing operation on the spectrum data from Fig 4.5, using a filter window of 53 frequency bins.

4.2.2   Cluster Analysis

Clustering is a popular method employed in image segmentation. The aim of cluster analysis is to partition a set of objects into homogenous groups, so called clusters. The partitioning should be performed in such a way that:

- The objects belonging to the same cluster are as similar to each other as possible, i.e. inside a cluster, homogeneity is required.

- The objects belonging to different clusters are as different from each other as possible, i.e. between clusters, heterogeneity is required [28].

Clustering can be considered as an unsupervised learning process, which aims at discovering and detecting hidden structural relationships between the data points in a data set [29], which makes them particularly interesting for segmentation problems. Usually, pixel intensities are used as features in clustering based segmentation techniques in gray value images, which gives rise to a one dimensional feature space, or RGB values in color images, which leads to a 3-D feature space. This kind of segmentation can be viewed as an adaptive quantization of the image, where the discrete quantization levels are determined by the clustering algorithm. The same principle can be applied to the channel segmentation problem, adaptively quantizing the spectrum analysis data in such a way that the contributions from individual sources can be distinguished from the background noise.

The most popular clustering techniques found in literature belong to the family of competitive learning algorithms, where randomly initialized cluster centers, also called cluster prototypes compete with each other based on some optimality criterion in the feature space as the algorithm progresses. This competitive step is usually followed by a learning step, where the parameters of the cluster prototypes are updated. These steps are repeated until some convergence criterion is met or the number of iterations exceeds some predetermined maximum value. The simplest competitive learning (CL) algorithms are based on the hard competitive learning principle [29], where the adaptation of the prototype of a particular cluster is performed using solely those data points, for which this particular prototype has won the competitive stage. For example the well known K-means algorithm belongs to this group. Soft competitive learning algorithms, such as the fuzzy c-means algorithm, however, treat more than one prototype as the winner to some extent, and the adaptation is performed accordingly. Since the channel segmentation problem, by its very nature, requires unambiguous region borders, hard competitive learning algorithms are more suited for this purpose. In the next section, starting with the much popular K-means algorithm,
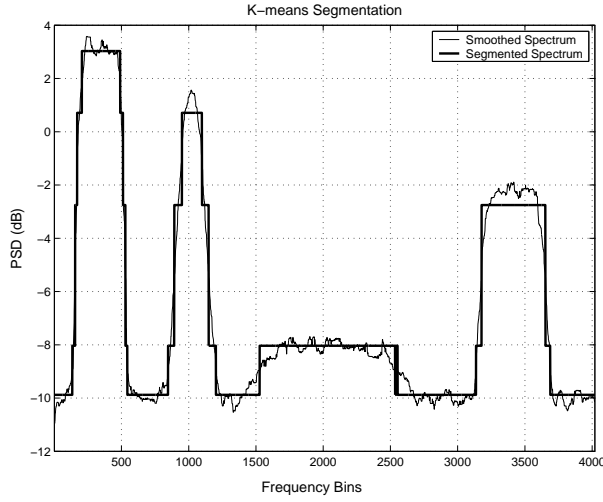
Fig. 4.7 Channel Segmentation with K-means Algorithm; K=5

cluster analysis methods based on hard competitive learning principle are investigated for use in the proposed channel segmentation algorithm.

K-means

The K-means algorithm has its roots in the works of Gauss [30], where he proposed using the method of minimum mean squared error for parameter estimation problems. The K-means clustering algorithm is explicitly described for the first time in the works of Hart and Duda [31]. K-means partitions the data into K clusters in such a way that the mean squared error cost function

$$J_{K-means} = \sum_{j \in \Omega} \| \vec{X}_j - \sum_{k=1}^{K} z_{jk} \vec{P}_k \|^2 \tag{4.2}$$

is minimized,where $\vec{X}_j$ is the feature vector for the j'th sample in the data domain Ω, (which is the smoothed PSD estimate at the j'th frequency bin in our case), $\vec{P}_k$ is the cluster prototype of the k'th cluster and z_{jk} is the membership indicator function, which is equal to unity, if the vector $\vec{X}_j$ belongs to the cluster k and zero otherwise. The K-means clustering problem

can be stated as:

$$[z_{jk}, \vec{P}_k] = \underset{z_{jk}, \vec{P}_k}{\operatorname{argmin}} \, (J_{K-means}), j \in \Omega, k = 1 \ldots K \qquad (4.3)$$

(4.3) can be solved iteratively by alternating between a competitive step, where the assignment is carried out given the current estimate of the cluster prototypes, and a learning step, where the cluster centers are updated given the current clustering. The entire procedure is repeated until the clusters no longer change. The cluster assignment of an input sample is determined by selecting the cluster that minimizes the cost function, i.e. using the nearest neighbor criterion. The cluster prototypes are determined by solving for the zero gradient condition on $J_{K-means}$ with respect to the cluster prototypes. The algorithm can be summarized as follows:

1. Choose the number of clusters K

2. initialize K cluster prototypes randomly

3. For each $j \in \Omega$, select z_{jk} such that

$$z_{jk} = \underset{z_{jk}}{\operatorname{argmin}} \, (J_{K-means}), j \in \Omega, k = 1 \ldots K$$

4. For $k = 1 \ldots K$

$$\vec{P}_k = \frac{\sum_{j \in \Omega} z_{jk} \vec{X}_j}{\sum_{j \in \Omega} z_{jk}}$$

5. Repeat steps 3 and 4 until z_{jk} no longer changes.

Fig. 4.7 displays the K-means clustering results with K=5 on the smoothed spectrum from Fig. 4.6. Note that all four sources are detected fairly well, however, the bandwidth of the weakest source is somewhat underestimated, since it is only 2 dB above the noise level.

Edge Adaptive Competitive learning

A problem associated with the K-means algorithm is that the contextual information which is contained in the data set is completely disregarded, that is all data points are evaluated by themselves, and their neighborhood relationships are completely ignored during the clustering process. In [32]

Pham has proposed an image segmentation algorithm, which incorporates the edge information already present in the image in the cost function. This algorithm is referred to as the edge adaptive K-means algorithm and can be considered as a generalisation of the K-means clustering. The cost function of the edge adaptive clustering algorithm is given as:

$$J_{EA} = \sum_{j \in \Omega} |X_j - \sum_{k=1}^{K} z_{jk} P_k|^2 + \lambda \sum_{j \in \Omega} \|\nabla X_j - \nabla \sum_{k=1}^{K} z_{jk} P_k\|^2 \qquad (4.4)$$

Note that the vector signs on P_k and X_j have been dropped, since this algorithm is specifically designed for a 1-dimensional feature space. ∇ is the gradient operator which in our case is a simple differentiation, since the image is one dimensional and can be approximated by using finite differences. The first term in (4.4) is the cost function of the K-means algorithm, which penalizes the difference between the original image and the segmented image. The second term is the so called edge penalty, which requires that the gradients of the original and segmented images to be as close as possible to each other. Hence the segmentation is carried out based on both the spectrum intensity and the edge information, and the balance between the both terms is controlled by the parameter λ. For $\lambda = 0$ this algorithm converges to the ordinary K-means algorithm, whereas when λ is large, the influence of the edge information on the segmentation becomes more predominant. Since the scales of the amplitude feature space and gradient feature space are different, it is more convenient to introduce a normalized balance factor λ_0 which is defined as

$$\lambda_0 = \lambda \frac{scale(\nabla X_j)}{scale(X_j)} \qquad (4.5)$$

As in the previous case, the competitive and learning stages are carried out alternatingly, and the cluster prototypes are determined by solving for the zero gradient condition on J_{EA} with respect to the cluster prototypes. The algorithm can be summarized as follows:

1. Compute the gradient of the spectrum data

2. Choose the number of clusters K

3. Initialize K cluster prototypes randomly
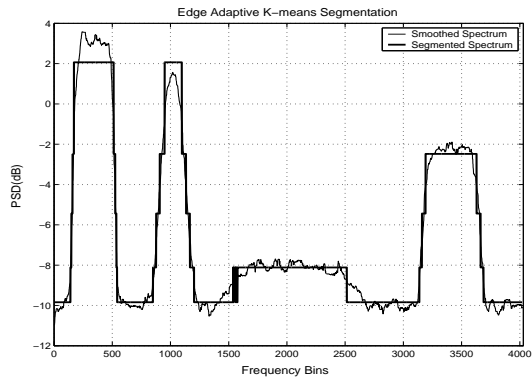
(a)
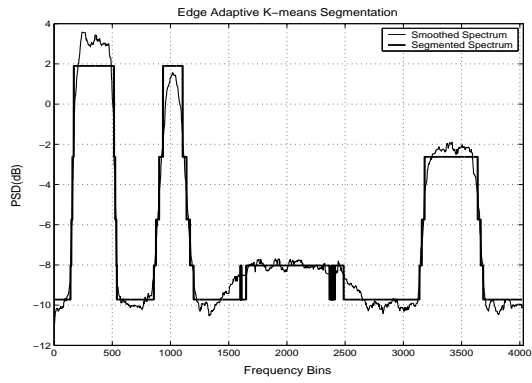
(b)

Fig. 4.8 Edge Adaptive K-means segmentation with (a)$\lambda_0 = 1$ (b)$\lambda_0 = 5$.

4. For each $j \in \Omega$, select z_{jk} such that

$$z_{jk} = \underset{z_{jk}}{\operatorname{argmin}} \ (J_{EA}), j \in \Omega, k = 1 \ldots K$$

5. For $k = 1 \ldots K$

$$P_k = \frac{\sum_{j \in \Omega} \left(z_{jk} X_j + \lambda \nabla (X_j - \sum_{l \neq k} z_{jl} P_l) \nabla z_{jk} \right)}{\sum_{j \in \Omega} z_{jk} + \lambda ||\nabla z_{jk}||^2}$$

6. Repeat steps 4 and 5 until z_{jk} no longer changes.

Figs 4.8(a) and 4.8(b) display the results of an edge adaptive K-means segmentation on the spectrum data from Fig. 4.5, $\lambda_0 = 1$ and $\lambda_0 = 5$ respectively. As λ_0 increases, the edge information becomes more influential on the learning process, i.e. the algorithm tries to place the cluster borders at the extrema of the gradient of the smoothed spectrum, which may result in misclassifications, if there are any sharp local peaks in the spectrum due to noise or multipath fading, etc. which could not be smoothed out and give rise to sharp maxima and minima in the gradient data. This phenomenon can be observed in Fig. 4.8(b) where frequency bins belonging to the weakest emitter have been misclassified because of the presence of a local maximum in the smoothed spectrum.

Determining the Number of Clusters

Although both the K-means and the Edge Adaptive K-means are unsupervised learning algorithms, they require that the number of clusters K is predetermined. However, the number of the natural clusters in the input data set is usually not known prior to the cluster analysis. If K is chosen too low, this may lead to the so called one-prototype-takes-multiple-clusters (OPTMC) phenomenon, which means that some of the natural clusters in the input data set may be merged into one single cluster, and the corresponding cluster prototype moves into the center of weight of these clusters. This phenomenon is illustrated in Fig 4.11(a) in a two dimensional feature space with three natural clusters and $K = 1$. If the K-means algorithm is used, the cluster prototype $\vec{P}_1$ obviously moves into the center of the clusters and starts to oscillate as input patterns are presented to the algorithm. In the context of channel segmentation, this means that the segmentation algorithm may fail to detect emitters with low SNR values, as illustrated
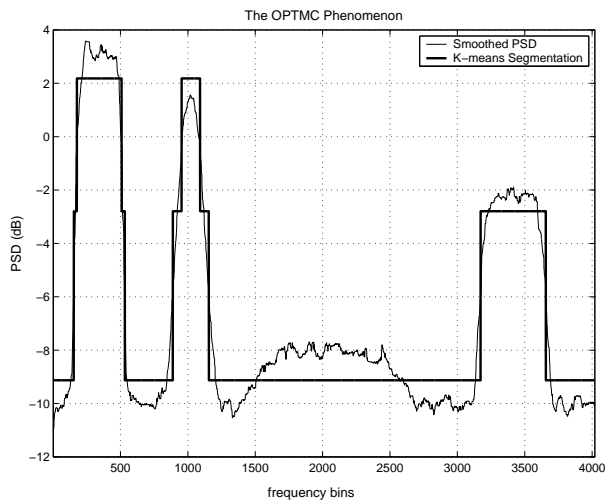
Fig. 4.9 The OPTMC problem in Channel Segmentation

in Fig. 4.9 with $K = 3$, where the noise level and the level of the weakest emitter a have been merged into one single cluster.

If K is chosen too large, this may lead to the so called *shared cluster* problem, where one single natural cluster is unnecessarily partitioned into multiple clusters, as displayed in Fig. 4.10 leading to an ambiguous segmentation of the channel.

The usual approach for determining the optimum number of clusters is to repeat the clustering for different values of K, incrementing it after each clustering. The clustering result is evaluated using the corresponding cost function at the end of each pass (i.e. $J_{K-means}$ or J_{EA} in our case). The loop is terminated, if the gain resulting from further incrementing K (i.e the reduction in the cost function) drops below a predetermined threshold. However, this approach not always yields good results, if the abovementioned threshold is chosen arbitrarily, without taking into account the distribution of the input data, which requires a further analysis of the feature space.

The Self Splitting Competitive Learning (SSCL) algorithm, which is investigated in the following section presents a viable alternative to the approach described above, automatically finding the optimal number of clusters in a data set, leading to good segmentation results.
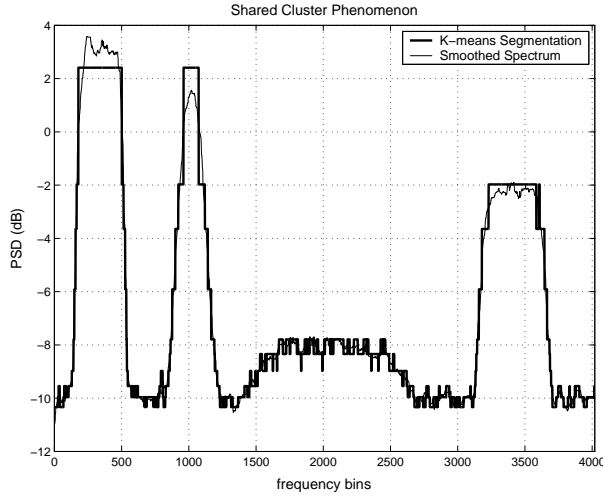
Fig. 4.10 The Shared Cluster Phenomenon in Channel Segmentation

Self Splitting Competitive Learning

The Self Splitting Competitive Learning (SSCL) algorithm, which has been proposed by Zhang and Liu in [29] is based on the so called OPTOC (one prototype tales one cluster) paradigm. The SSCL starts with one single prototype randomly initialized in the feature space. During the learning process, this prototype splits into two prototypes, based on a so called split validity criterion. As the algorithm progresses, other prototypes are chosen to split, if they meet the necessary criterion. The splitting terminates, if no more prototype is found suitable for splitting. The membership function z_{jk} is determined using the nearest neighbor criterion as before.

In the core of the SSCL algorithm lies the OPTOC idea. In conventional CL schemes, choosing the number of prototypes K less than the number of the actual natural clusters in the data set leads to the OPTMC phenomenon, as discussed previously where two or more natural clusters are merged into one single cluster, and the corresponding cluster prototype moves into the center of mass of these clusters. The OPTOC principle, however, ensures that this cluster prototype is biased towards only one of these clusters and ignores the others, as illustrated in 4.11(b)

This behaviour is achieved by assigning an auxilliary vector for each cluster prototype, called the asymptotic property vector (APV) $\vec{A}_k$, which

(a)   (b)
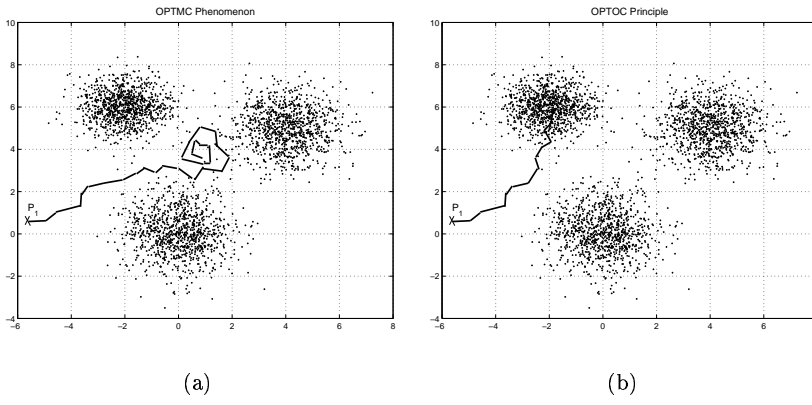
Fig. 4.11 Trajectory of a cluster prototype (a) In the case of OPTMC (b) using OPTOC paradigm

is initialized at a random location far away from the corresponding prototype $\vec{P}_k$. With the help of the asymptotic property vector, the so called dynamic neighborhood of $\vec{P}_k$ is defined as the set of input patterns $\vec{X}_j$ for which

$$\|\vec{P}_k - \vec{X}_j\| \leq \|\vec{P}_k - \vec{A}_k\|. \tag{4.6}$$

The OPTOC scheme is devised in such a way that the data points inside this neighborhood will contribute much more to the learning process of $\vec{P}_k$ than those outside. At the beginning of the algorithm, $\vec{A}_k$ is far away from $\vec{P}_k$, hence the neighborhood of $\vec{P}_k$ is large, containing patterns from all of the natural clusters, i.e. there is no bias towards any of the clusters. As the input patterns are randomly presented to the algorithm, $\vec{P}_k$ and $\vec{A}_k$ are updated in such a way that they choose a natural cluster and converge to its center, progressively reducing the size of the neighborhood. The patterns $\vec{X}_j$ are presented to the algorithm one by one in a random fashion. Each time a pattern is presented to the algorithm, the winning prototype is determined using the nearest neighbor criterion. Assuming that $\vec{P}_k$ is the winning prototype for $\vec{X}_j$, the update equation for the corresponding APV is given as:

$$\vec{A'}_k = \vec{A}_k + \frac{\delta_k}{n_{\vec{A}_k}}(\vec{X}_j - \vec{A}_k)\Theta(\vec{P}_k, \vec{A}_k, \vec{X}_j) \tag{4.7}$$

Where $\vec{A'}_k$ is the APV update and $\Theta(\vec{P}_k, \vec{A}_k, \vec{X}_j)$ is an indicator function given as

$$\Theta(\vec{P}_k, \vec{A}_k, \vec{X}_j) = \begin{cases} 1, & \|\vec{P}_k - \vec{A}_k\| \geq \|\vec{P}_k - \vec{X}_j\| \\ 0, & \text{otherwise} \end{cases} \tag{4.8}$$

$0 < \delta_k \leq 1$ is the learning rate of $\vec{P}_k$, which may be constant or adaptive, and $n_{\vec{A}_k}$ is the so called winning counter of $\vec{A}_k$ which is updated as

$$n'_{\vec{A}_k} = n_{\vec{A}_k} + \delta_k \Theta(\vec{P}_k, \vec{A}_k, \vec{X}_j) \tag{4.9}$$

Thus, $\vec{A}_k$ will shift towards the presented sample, if it lies in the neighborhood of $\vec{P}_k$, otherwise it will not be updated at all. OPTOC is achieved by letting $\vec{A}_k$ guide the learning process of $\vec{P}_k$. Consider the update equation:

$$\vec{P'}_k = \vec{P}_k + \eta_k(\vec{X}_j - \vec{P}_k) \tag{4.10}$$

with

$$\eta_k = \left(\frac{\|\vec{P}_k - \vec{A}_k\|}{\|\vec{P}_k - \vec{X}_j\| + \|\vec{P}_k - \vec{A}_k\|} \right)^2 \tag{4.11}$$

For $\|\vec{P}_k - \vec{X}_j\| \gg \|\vec{P}_k - \vec{A}_k\|$, the learning rate η_k approaches 0, hence the patterns outside the neighborhood do have only a small amount of influence on the learning process of $\vec{P}_k$, whereas for $\|\vec{P}_k - \vec{X}_j\| \ll \|\vec{P}_k - \vec{A}_k\|$, $\eta_k \to 1$, which means patterns inside this neighborhood have a very large influence on the learning stage. It can be shown that ultimately, $\vec{A}_k$ and $\vec{P}_k$ converge to the same natural cluster, ignoring the others. $\vec{P}_k$ is considered to have converged, if the distance between $\vec{A}_k$ and $\vec{P}_k$ is smaller than a predefined threshold $\zeta^{(1)}$, i.e.

$$\|\vec{P}_k - \vec{A}_k\| < \zeta^{(1)} \tag{4.12}$$

OPTOC by itself is not enough for a successful clustering, since it enables each prototype to find one natural cluster, but does not adress the issue of finding the optimum number of clusters K, which is especially crucial in OPTOC, since choosing K too low will cause some of the clusters to be ignored. In [29], a so called split validity criterion is introduced to judge if

all the natural clusters have been classified after an OPTOC stage. If this is not the case, one of the prototypes is chosen to split into two, incrementing the number of clusters, and the OPTOC stage starts over from the begining. This procedure is repeated until no further prototype satisfies the splitting criterion. The overall clustering algorithm starts with one single prototype, randomly initalized, and a new ptototype is spawned after each OPTOC iteration, until all the natural clusters are found.

To calculate the split validity criterion, another auxilliary vector, the so called center property vector $\vec{C}_k$ is assigned to each prototype. During the learning process for $\vec{P}_k$, $\vec{C}_k$ is updated according to K-means learning rules using the input patterns, for which $\vec{P}_k$ has been the winner. Obviously, if the discrepancy between $\vec{P}_k$ and $\vec{C}_k$ is too large at the end of the OPTOC stage, this means that this prototype does not accurately represent all the patterns in the cluster k, and there must exist at least one natural cluster which has been ignored by the OPTOC stage. The split validity criterion is fulfilled,if

$$\|\vec{P}_k - \vec{C}_k\| > \zeta^{(2)} \tag{4.13}$$

where $\zeta^{(2)}$ is a preset threshold. To simplify the algorithm, $\zeta^{(1)} = \zeta^{(2)} = \zeta$ may be chosen. The parameter ζ controls the accuracy of the clustering. Choosing a too large threshold may lead to larger clusters and OPTMC phenomenon, whereas a too small threshold leads to an unnecessarily large number of clusters, leading to shared clusters and increasing the convergence time of the algorithm. Determining ζ adaptively from the analysis of the feature space usually gives good results. In our case, choosing ζ as 5% of the maximum scale of the input feature space has provided a robust segmentation of the channel.

After splitting, the mother prototype stays in its location, whereas the daughter prototype has to be initialized at a location far away from the mother prototype, in order to ensure that it does not compete with its pre-cursor for the same cluster in the next OPTOC iteration. This is achieved by employing a third auxilliary vector, a so called distant property vector $\vec{R}_k$, which is initialized at the same location as $\vec{P}_k$, an progressively moves away from it, as the OPTOC stage progresses. The update equation for $\vec{R}_k$ is given as

$$\vec{R'}_k = \vec{R}_k + \frac{\kappa_k}{n_{\vec{R}_k}}(\vec{X}_j - \vec{R}_k)\Theta(\vec{P}_k, \vec{X}_j, \vec{R}_k) \tag{4.14}$$
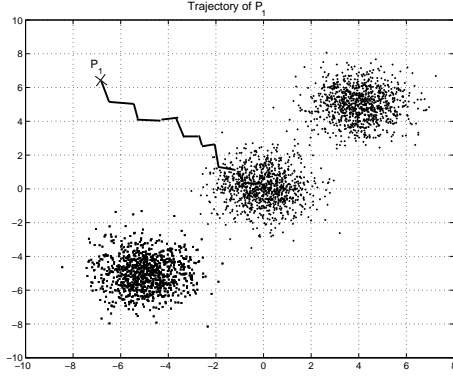
Fig. 4.12 $\vec{P}_1$ moving towards the centroid of a cluster coinciding with the global centroid

$0 \leq \kappa_k \leq 1$ is the learning rate, which may be constant or adaptive, and $n_{\vec{R}_k}$ is the winning counter of $\vec{R}_k$ which is updated as

$$n'_{\vec{R}_k} = n_{\vec{A}_k} + \kappa_k \Theta(\vec{P}_k, \vec{X}_j, \vec{R}_k). \tag{4.15}$$

If $\vec{P}_k$ is found to be suitable for spliting, the daughter prototype is initialized at the location of $\vec{R}_k$.

It may sometimes occur that $\vec{P}_k$ moves to a cluster whose centroid coincides with the global centroid of the feature space. In this case, $\vec{P}_k$ will not fulfill the split validity criterion, and the algorithm terminates, failing to find the other clusters. This phenomenon is illustrated in Fig. 4.12. To prevent this from happening, an additional bias factor is introduced to the update equation of $\vec{P}_k$, which is guided by $\vec{R}_k$. The overall update equation $\vec{P}_k$ can be given as:

$$\vec{P'}_k = \vec{P}_k + \xi_k \eta_k (\vec{X}_j - \vec{P}_k) \tag{4.16}$$

where the bias factor ξ_k is given as

$$\xi_k = \left(\frac{\|\vec{P}_k - \vec{R}_k\|}{\|\vec{P}_k - \vec{X}_j\| + \|\vec{P}_k - \vec{R}_k\|} \right)^2 \tag{4.17}$$

as a result, data samples closer to $\vec{P}_k$ will attract $\vec{P}_k$ more than those closer to $\vec{R}_k$, leading to a bias effect. The interested reader is referred to [29] for more details on the SSCL algorithm. The overall clustering algorithm can be summarized as follows:

- Initialization

  - Set $K = 1$;
  - Initialize $\vec{R}_1 = \vec{P}_1$ randomly;
  - Initialize $\vec{A}_1 = \vec{C}_1$ randomly, but far from $\vec{P}_1$;
  - Determine ζ;

- Clustering

  1. Repeat until $\|\vec{P}_l - \vec{A}_l\| < \zeta$ for $l = 1, \dots, K$ or a maximum number of iterations is reached:
     - Present a randomly chosen data point, find the winner prototype using the nearest neighbour criterion, label it with index k,
     - Update $\vec{A}_k$, $\vec{C}_k$, $\vec{R}_k$ and $\vec{P}_k$ accordingly.

  2. Splitting:
     - $\|\vec{P}_m - \vec{C}_m\| = \max_l \|\vec{P}_l - \vec{C}_l\|$ for $l = 1, \dots, K$
     - if $\|\vec{P}_m - \vec{C}_m\| > \zeta$, split $\vec{P}_m$, increment K;
     - $\vec{P}_K = \vec{R}_m$;
     - assign $\vec{C}_K, \vec{R}_K$ and $\vec{A}_K$;
     - goto 3
     - else goto 4

  3. Reset:
     - for l=1,...,K do:
     - $\vec{R}_l = \vec{P}_l$;
     - $\vec{A}_l = \vec{C}_l$;
     - set all the winning counters to zero
     - goto 1

  4. Find K clusters, terminate.
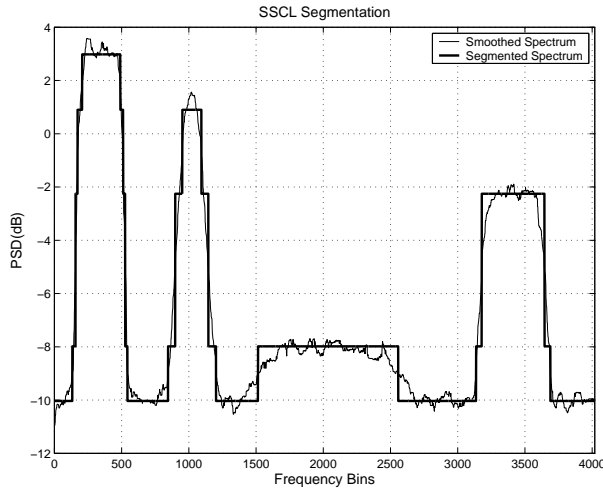
Fig. 4.13 Segmentation using the SSCL Algorithm

Fig. 4.13 displays the results of an SSCL segmentation. The algorithm has determined $K = 5$ as the optimal number of clusters. Comparing Fig. 4.13 to Fig. 4.7 and 4.8(a), the SSCL segmentation traces out the spectral shape of the individual emitters and background noise much better than the K-means and Edge Adaptive K-means algorithms, which is mainly due to the progressively decreasing neighborhood size in the OPTOC paradigm, which allows the input patterns concentrated in the close proximity of the natural cluster centers to have more influence on the learning of cluster prototypes than the ones farther away. Interestingly, the results provided by the SSCL algorithm are better than the ones provided by the Edge Adaptive K-means algorithm, although the latter makes use of the edge information, whereas the former ignores it. Even though the SSCL algorithm can be modified to incorporate the edge information, or some other type of contextual information, it increases the computational complexity of the algorithm, which is already considerably higher than the conventional clustering algorithms, resulting in very little, if any, performance increase in return. Because of the aforementioned advantages, the SSCL algorithm has been chosen to be the core piece of the overall channel segmentation algorithm presented in this work.

4.2.3   Post Processing and Parameter Estimation

After the cluster analysis, the quantized spectrum data has to be processed in such a way to detect the individual emitters and estimate their parameters. The post processing stage can be summarized as follows:

1. Binarize the quantized spectrum by determining the noise level from the clustering results.

2. Remove small artefacts or spikes which may arise at cluster boundaries causing ambiguities using morphological operations, such as erosion and dilation.

3. Detect the regions belonging to each emitter.

4. For each detected emitter, do the following:

    (a) Focus on each emitter by extracting the corresponding frequency bins from the smoothed spectrum, allowing for some offset from the neighboring noise regions.

    (b) Use SSCL clustering once more, this time only on the extracted spectrum segment.

    (c) Binarize the result.

    (d) Remove the artifacts using morphological operations

    (e) Estimate the bandwidth and carrier frequency of the emmiter using the binarized spectrum.

Step 4 is an optional step, which focuses on the emitter segments one by one, that have been detected in the initial clustering of the whole spectrum range, in order to increase the accuracy of the parameter estimation, which increases the computational complexity of the algorithm, since the clustering has to be repeated for each detected signal source.

The noise-level threshold used in binarizing the quantized spectrum in step 1 and step 4(c) is determined using by analyzing the two lowest quantization levels, making, to some extent, allowances for the shared cluster phenomenon, which may arise if the fluctuations due to measurement noise, fading and AWGN could not be smoothed adequately in the preprocessing stage. The lowest quantization level is chosen as the binarization threshold, if the difference between the two lowest levels does exceed a predetermined value ς, otherwise, the average of the two lowest quantization levels are taken as the binarization threshold. ς is chosen as 15% of the scale of the input data segment for the step 4(c), and as $\varsigma = 0.5$dB for the step 1.

The morphological operations used on the binarized spectrum in steps 2 and 4(d), the dilation and erosion operators are well known basic operators in image processing employed on binary images [26]. The so called opening operator, which is an erosion operation followed by a dilation, is known to remove artefacts like spikes, which may arise at the region boundaries due to ambiguities in the segmentation, while preserving the region shapes exceeding the dimensions of the analysis window. Care sould be taken that the window size of the opening operation does not exceed the smallest bandwidth the segmentation algorithm is required to detect, so that its contribution is not totally removed from the binary image.

4.2.4   Simulation Results

This section provides simulation results for the segmentation algorithm described in the previous section. Three different scenarios are considered in the simulations, which are displayed in Figs. 4.14(a), 4.14(b) and 4.14(c) respectively.

Scenario 1

This scenario represents a crowded spectrum segment with 6 different sources which have different bandwidths, different spectral shapes and considerably different SNR. Tab 4.1 summarizes the parameters of the emitters for this scenario. The SNR values for each source is given in terms of the background noise level, NL, which is , for example, -15 dB in Fig 4.14(a).

S_{ij} represents the j'th emitter (from left) in the i'th scenario. Tables 4.2 to 4.4 present the channel segmentation results for NL=-10dB,-15dB and -20 dB respectively, where

- the mean value of the carrier frequency estimates $\overline{\hat{f}_C}$

- the standard deviation of the carrier frequency estimates σ_{f_C}

- the mean value of the bandwidth estimates $\overline{\hat{B}}$

- the ratio of the standard deviation in the bandwidth estimate normalized by the mean value of the bandwidth estimate $\sigma_B/\hat{B}$

are used to evaluate the segmentation of the channel. 1000 different realizations of the same channel are used for the segmentation algorithm for each value of NL. In these three cases, the FFT resolution is 2 kHz/bin, and an FFT length of 4096 is used to cover the 8MHz band. The segmentation
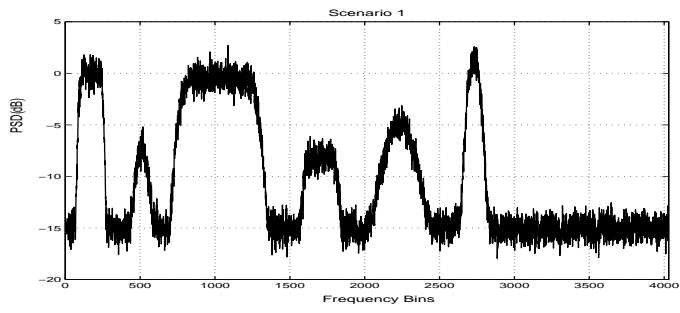
(a)
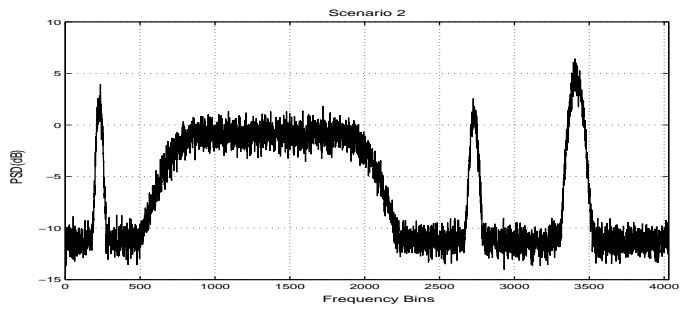
(b)
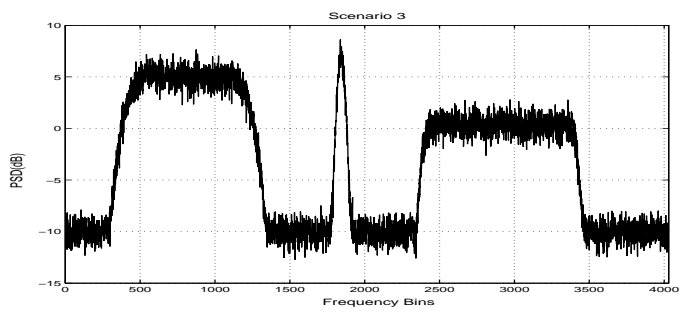
(c)

Fig. 4.14 The channels to be segmented (a)Scenario 1 (b) Scenario 2 (c) Scenario 3

results indicate that both the carrier frequency and the bandwidth estimates are pretty accurate, and the standard deviations of the estimates increase as the SNR decreases. Obviously, the emitters with lowest SNR values have the highest standard deviations.

Tables 4.4 to 4.7 display the segmentation results for the same scenario, but this time, the FFT resolution is twice as fine as the previous case i.e. 1kHz per frequency bin. Decreasing the resolution bandwidth results in a reduction in the standard deviations of the estimates and leads to an increase in the in the accuracy of the measurements, at the expense of an increase in the computational burden, both on the clustering stages on the spectral analysis stage.

Scenario 2

The second scenario represents a case, where a wide band and three comparatively narrowband signals occupy the frequency band of interest, as shown in Fig. 4.14(b). Table 4.8 summarizes the parameters of the four sources to be detected. The ratios of the bandwiths of the narrowest emitter to the wideband emitter is approximately 1:20. Note that all the emitters are accurately detected, even though the emitter with the narrowest bandwith occupies only about 2% of the spectrum range to be detected. Similar to the previous scenario, three simulation runs have been performed using a resolution of 2 kHz per frequency bin, which are displayed in Tables 4.9, 4.10 and 4.11 (with NL=-5dB,-10dB and -15dB respectively), and another three simulations are carried out with a resolution bandwidth of 1kHz/frequency bin, which are shown in Tables 4.12 to 4.14.

Scenario 3

The third and final scenario describes a case, where two wide band and one narrowband signals occupy the frequency range of interest, as illustrated in Fig. 4.14(c). The parameters of the three emitters have been summarized in Table 4.16. Tables 4.17 to 4.19 display the segmentation results for a resolution bandwith of 2kHz with NL=-5dB,-10dB and -15dB respectively, whereas in Tables 4.20 to 4.22, the results for 1kHz/frequency bin case are shown.

The simulation results provided in this section allow the following conclusions:

- The presented channel segmentation algorithm is capable of detecting the signals and accurately estimating their bandwidths and carrier fre-

quencies, even under low SNR conditions, and even if the bandwiths, magnitudes and spectral shapes of the individual signals differ significantly.

- The variance of the estimates increase as the SNR decreases, since the fluctuations in the signal spectra increase and the distance to the background noise level decrease with decreasing SNR.

- As expected, the variance of the estimates decreases and the measurement accuracy increases with increasing FFT resolution.

- The mean of the bandwidth estimates increase with increasing SNR, since a larger portion of the signals remain above the background noise level.

4.2.5 Summary

Starting with a brief overview on spectral analysis methods, this chapter presented a channel segmentation method based on cluster analysis of the spectrum data. Several clustering algorithms have been investigated, and among them, the SSCL has been found the most suitable for channel segmentation purposes. The performance of the algorithm is shown by means of simulation results.

The main problem associated with the proposed channel segmentation approach is the bandwidth of the frequency range to be covered. If the whole 890MHz-5.8 GHz range has to be segmented, the amount of processing power, storage and time required for spectrum analysis and segmentation would be enormous. The choice of the FFT resolution is also of considerable relevance to this problem, which is dictated by the smallest signal bandwidth to be detected: For an UTRA-FDD signal with 5 MHz bandwidth, a 40 kHz/bin FFT resolution may be more than sufficient for an accurate estimation of the parameters, whereas for a 200kHz GSM signal, it is obviously insufficient. However, using, for instance, a 2kHz/bin resolution, which would be adequate for the GSM Signal would obviously generate a 20 times more spectrum samples to be analysed.

Actually this is the same question, which was adressed in chapter 2. If the segmentation is to be implemented in an ideal Software Radio application, this would require the segmentation of the whole 5 GHz frequency range, leading to a very high computational complexity, but ensuring a very high flexibility.

If however, we are talking about a Software Defined Radio, which digitizes a limited band out of the full 5 GHz band, the computational burden

required by the segmentation algorithm could be brought to menagable levels. However, this approach would require a-priori information in some form about where, in the frequency domain, to look (or where not to look) for a specific type of service, or that only a limited number of spectrum bands out of the whole 5Ghz band are reserved for dynamic ressource allocation (e.g. so called spectrum pools), which is a reasonable assumption for the forseeable future.

If the spectrum range of interest is still too large, an iterative channel segmentation may be the best way to go, performing the segmentation with a low resolution at the beginning of the analysis, and filtering out and analysing interesting segments with higher resolution.

Source	f_C	B	SNR
S_{11}	342.33kHz	414kHz	-NL(dB)
S_{12}	1024kHz	341.3kHz	-NL-12dB
S_{13}	2048kHz	1331.2kHz	-NL-0.5dB
S_{14}	3413.33kHz	591.6kHzkHz	-NL-9dB
S_{15}	4468.3kHz	682.6kHz	-NL-8dB
S_{16}	5461.33kHz	341.3kHz	-NL-2dB

Tab. 4.1 Channel segmetation Scenario 1

Source	$\overline{\hat{f}_C}$	$\sigma_{\hat{f}_C}$	$\overline{\hat{B}}$	$\sigma_B/\overline{\hat{B}}$
S_{11}	340.4kHz	3.87kHz	395.82kHz	0.048
S_{12}	1016kHzz	45.3kHz	256.6kHz	0.2537
S_{13}	2047kHz	5kHz	1251kHz	0.022
S_{14}	3414.6kHz	44.71kHz	518.5kHz	0.12
S_{15}	4468kHz	13.8kHz	663kHz	0.1
S_{16}	5460kHz	5.25kHz	334.6	0.08

Tab. 4.2 Scenario 1, FFT resolution= 2kHz/bin, NL=-10 dB

Source	$\overline{\hat{f}_C}$	$\sigma_{\hat{f}_C}$	$\overline{\hat{B}}$	$\sigma_B/\overline{\hat{B}}$
S_{11}	340.4kHz	3.26kHz	405.32kHz	0.04
S_{12}	1022.4kHz	16.7kHz	301.4kHz	0.12
S_{13}	2046.8kHz	3.76kHz	1274.7kHz	0.018
S_{14}	3412.6kHz	7.07kHz	548.6kHz	0.051
S_{15}	4466.8kHz	9.61kHz	743.8kHz	0.06
S_{16}	5460.2kHz	3.86kHz	363.76kHz	0.0721

Tab. 4.3 Scenario 1, FFT resolution= 2kHz/bin, NL=-15dB

Source	$\overline{\hat{f}_C}$	$\sigma_{\hat{f}_C}$	$\overline{\hat{B}}$	$\sigma_B/\overline{\hat{B}}$
S_{11}	340.7kHz	3.01kHz	418.72kHz	0.038
S_{12}	1023.6kHz	5.29kHz	329.24kHz	0.077
S_{13}	2046.8kHz	2.52kHz	1293.62kHz	0.014
S_{14}	3412.8kHz	3.06kHz	556.6kHz	0.036
S_{15}	4466.5kHz	6.10kHz	806.28kHz	0.046
S_{16}	5460.1kHz	3.51kHz	394.12kHz	0.073

Tab. 4.4 Scenario 1, FFT resolution= 2kHz/bin, NL=-20 dB

Source	$\overline{\hat{f}_C}$	$\sigma_{\hat{f_C}}$	$\overline{\hat{B}}$	$\sigma_B/\overline{\hat{B}}$
S_{11}	340.9kHz	2.55kHz	394.4kHz	0.043
S_{12}	1023.1kHz	23.39kHz	282.75kHz	0.152
S_{13}	2047.5kHz	3.45kHz	1254.2kHz	0.020
S_{14}	3412.5kHz	6.50kHz	532.8kHz	0.048
S_{15}	4467.5kHz	10.1kHz	683.19kHz	0.085
S_{16}	5461kHz	3.1kHz	332.801kHz	0.072

Tab. 4.5 Scenario 1, FFT resolution= 1kHz/bin, NL=-10 dB

Source	$\overline{\hat{f}_C}$	$\sigma_{\hat{f_C}}$	$\overline{\hat{B}}$	$\sigma_B/\overline{\hat{B}}$
S_{11}	341.06kHz	1.55kHz	397.35kHz	0.034
S_{12}	1024.1kHz	5.07kHz	313.31kHz	0.085
S_{13}	2047.5kHz	2.28kHz	1275.1kHz	0.015
S_{14}	3412.9kHz	3.50kHz	547kHz	0.040
S_{15}	4467.5kHz	6.31kHz	753.94kHz	0.056
S_{16}	5461.1kHz	2.89kHz	359.03kHz	0.062

Tab. 4.6 Scenario 1, FFT resolution= 1kHz/bin, NL=-15 dB

Source	$\overline{\hat{f}_C}$	$\sigma_{\hat{f_C}}$	$\overline{\hat{B}}$	$\sigma_B/\overline{\hat{B}}$
S_{11}	340.81kHz	1.6kHz	408.03kHz	0.043
S_{12}	1023.8kHz	3.3571kHz	340.24kHz	0.061
S_{13}	2047.4kHz	1.69kHz	1292.2kHz	0.011
S_{14}	3412.9kHz	2.03kHz	553.53kHz	0.0314
S_{15}	4467.9kHz	4.28kHz	814.89kHz	0.039
S_{16}	5461.2kHz	2.12kHz	385.02kHz	0.054

Tab. 4.7 Scenario 1, FFT resolution= 1kHz/bin, NL=-20dB

Source	f_C	B	SNR
S_{21}	455kHz	170.6kHz	-NL(dB)
S_{22}	2730kHz	3550kHz	-NL(dB)
S_{23}	5461kHz	227.5kHz	-NL(dB)-1
S_{24}	6824.6kHz	341.2kHz	-NL+3dB

Tab. 4.8 Channel Segmentation Scenario 2

Source	$\overline{\hat{f}_C}$	$\sigma_{\hat{f}_C}$	$\overline{\hat{B}}$	$\sigma_B/\overline{\hat{B}}$
S_{21}	452.91kHz	3.4kHz	170.12kHz	0.14
S_{22}	2729.6kHz	18.3kHz	3240.6kHz	0.026
S_{23}	5460kHz	5.6kHz	212.22kHz	0.106
S_{24}	6827.2kHz	6.735kHz	383.7kHz	0.084

Tab. 4.9 Scenario 2, FFT Resolution=2kHz/bin, NL=-5dB

Source	$\overline{\hat{f}_C}$	$\sigma_{\hat{f}_C}$	$\overline{\hat{B}}$	$\sigma_B/\overline{\hat{B}}$
S_{21}	452.94kHz	2.71kHz	179.7kHz	0.107
S_{22}	2728.6kHz	9.90kHz	3335.2kHz	0.017
S_{23}	5460kHz	3.86kHz	227.56kHz	0.088
S_{24}	6827kHz	4.1085kHz	406.276kHz	0.064501

Tab. 4.10 Scenario 2, FFT Resolution=2kHz/bin, NL=-10dB

Source	$\overline{\hat{f}_C}$	$\sigma_{\hat{f}_C}$	$\overline{\hat{B}}$	$\sigma_B/\overline{\hat{B}}$
S_{21}	453.64kHz	2.68kHz	195.42kHz	0.099
S_{22}	2729.2kHz	5.9303kHz	3394.4kHz	0.013351
S_{23}	5460.2kHz	3.3208kHz	250.276kHz	0.079
S_{24}	6826.4kHz	5.4015kHz	431.88kHz	0.06972

Tab. 4.11 Scenario 2, FFT Resolution=2kHz/bin, NL=-15dB

Source	$\overline{\hat{f}_C}$	$\sigma_{\hat{f}_C}$	$\overline{\hat{B}}$	$\sigma_B/\overline{\hat{B}}$
S_{21}	453.56kHz	2.69kHz	161.38kHz	0.093
S_{22}	2730.8kHz	12.68kHz	3195.2kHz	0.0269
S_{23}	5461.9kHz	3.72kHz	202.74kHz	0.087
S_{24}	6828.1kHz	4.29kHz	363.25kHz	0.067

Tab. 4.12 Scenario 2, FFT Resolution=1kHz/bin, NL=-5dB

Source	$\overline{\hat{f}_C}$	$\sigma_{\hat{f}_C}$	$\overline{\hat{B}}$	$\sigma_B/\overline{\hat{B}}$
S_{21}	454kHz	1.65kHz	172.44kHz	0.067
S_{22}	2730.2kHz	8.55kHz	3326.4kHz	0.018
S_{23}	5460.7kHz	2.7kHz	221kHz	0.0674
S_{24}	6827.2kHz	2.4kHz	395.3kHz	0.053

Tab. 4.13 Scenario 2, FFT Resolution=1kHz/bin, NL=-10dB

Source	$\overline{\hat{f}_C}$	$\sigma_{\hat{f}_C}$	$\overline{\hat{B}}$	$\sigma_B/\overline{\hat{B}}$
S_{21}	454.1kHz	1.47kHz	186.2kHz	0.065
S_{22}	2730.2kHz	4.75kHz	3393.8kHz	0.0122
S_{23}	5460.7kHz	2.2kHz	239.98kHz	0.066
S_{24}	6826.7kHz	1.7kHz	416.72kHz	0.044

Tab. 4.14 Scenario 2, FFT Resolution=1kHz/bin, NL=-15dB

Source	f_C	B	SNR
S_{31}	1638.4kHz	2130kHz	-NL+5dB
S_{32}	3686.4kHz	227.5	-NL+3.5dB
S_{32}	5800.6kHz	2250.6kHz	-NL(dB)

Tab. 4.15 Channel Segmentation Scenario 3

Source	$\overline{\hat{f}_C}$	$\sigma_{\hat{f}_C}$	$\overline{\hat{B}}$	$\sigma_B/\overline{\hat{B}}$
S_{31}	1637.1kHz	6.50kHz	1992kHz	0.021
S_{32}	3684.8kHz	5.15kHz	229.04kHz	0.104
S_{33}	5801.6kHz	6.9685kHz	2173.8kHz	0.015

Tab. 4.16 Scenario 3, FFT resolution=2kHz/bin, NL=-5dB

Source	$\overline{\hat{f}_C}$	$\sigma_{\hat{f}_C}$	$\overline{\hat{B}}$	$\sigma_B/\overline{\hat{B}}$
S_{31}	1637.44kHz	3.91kHz	2030kHz	0.017
S_{32}	3685kHz	3.52kHz	249.62kHz	0.093
S_{33}	5801.4kHz	4kHz	2201.8kHz	0.010

Tab. 4.17 Scenario 3, FFT resolution=2kHz/bin, NL=-10dB

Source	$\overline{\hat{f}_C}$	$\sigma_{\hat{f}_C}$	$\overline{\hat{B}}$	$\sigma_B/\overline{\hat{B}}$
S_{31}	1637.38kHz	2.64kHz	2055.2kHz	0.014
S_{32}	3685kHz	3.42kHz	272.48kHz	0.092
S_{33}	5801.4kHz	2.72kHz	2216.4kHz	0.008

Tab. 4.18 Scenario 3, FFT resolution=2kHz/bin, NL=-15dB

Source	$\overline{\hat{f}_C}$	$\sigma_{\hat{f}_C}$	$\overline{\hat{B}}$	$\sigma_B/\overline{\hat{B}}$
S_{31}	1637.9kHz	4.44kHz	1995.3kHz	0.020
S_{32}	3685.6kHz	3.39kHz	227.66kHz	0.088
S_{33}	5801.6kHz	5.19kHz	2181kHz	0.0130

Tab. 4.19 Scenario 3, FFT resolution=1kHz/bin, NL=-5dB

Source	$\overline{\hat{f}_C}$	$\sigma_{\hat{f}_C}$	$\overline{\hat{B}}$	$\sigma_B/\overline{\hat{B}}$
S_{31}	1638.1kHz	2.85Hz	2033kHz	0.015
S_{32}	3685.8kHz	2.42kHz	245.5kHz	0.073
S_{33}	5801.4kHz	2.99kHz	2197.6kHz	0.010

Tab. 4.20 Scenario 3, FFT resolution=1kHz/bin, NL=-10dB

Source	$\overline{\hat{f}_C}$	$\sigma_{\hat{f}_C}$	$\overline{\hat{B}}$	$\sigma_B/\overline{\hat{B}}$
S_{31}	1638kHz	1.95kHz	2052.4kHz	0.014
S_{32}	3685.9kHz	1.83kHz	263.6kHz	0.0623
S_{33}	5801.4kHz	2.03kHz	2212.7kHz	0.008

Tab. 4.21 Scenario 3, FFT resolution=1kHz/bin, NL=-15dB

5 Air Interface Identification Exploiting Cyclostationarity

5.1 Introduction

This chapter presents a method for identifying the air interface signals of interest, that have been isolated and brought to the baseband after the channel segmentation stage, which has been investigated in the previous chapter. We limit the analysis of the signal of interest to the physical layer, which is the easiest to access. As a matter of fact, the parameters from higher protocol layers are only accessible after the demodulation of the signal, which requires actually knowing the air interface standard.

In the literature, most commonly, modulation type recognition algorithms are proposed for the purpose of air interface identification. Algorithms of this kind usually include a feature extraction subsystem and a classification subsystem. The feature extraction subsystem maps the received signal into a feature vector, which is used by the classification subsystem to assign the signal to a modulation class. The modulation type classification algorithms found in the literature most commonly use the phase, amplitude and instantaneous frequency information from the received signal to recover the modulation type specific features required for the classification. The generation of features is performed using well known tools of statistical signal processing, such as histograms, statistical moments of second or higher order, linear or nonlinear transformations (such as DFT, Wavelet Tansform, quadratic or higher order nonlinearities) on the phase, amplitude or instantaneous frequency information (see [33], [34], [35], [36], [37] and [38]). The classification of the modulation type is usually performed using a pattern recognition or decision theoretic approach, employing standard techniques of pattern recognition (such as polynomial classifiers, nearest neighbor classifiers) in the former, and multiple hypothesis testing methods in the latter.

There are three practical problems that makes this approach unsuitable for air interface identification in a Software Radio system

- The recognition of the particular modulation type employed in the received signal may not be sufficient for a non-ambiguous identification

of an air interface standard. As a matter of fact, there exist air interface standards which use the same modulation scheme (such as PDC and IS 136, both of which use $\pi/4$ DQPSK). Some air interfaces also allow the use of multiple modulation types, depending on the state of the transmission channel.

- As discussed in chapter 3 , the mobile communication channel is characterized by a low SNR and frequency selective multipath fading. Most of the modulation type classification algorithms found in the literature perform relatively poorly under these hostile conditions.

- Standard modulation type classification algorithms are usually based on the assumption that there exists only one modulated signal of one particular user in the channel at a given moment. This assumption may be appropriate for the air interfaces which are based on the TDMA scheme, where each user is allowed to access the channel for a fraction of time on a periodic basis. However, it does not hold for CDMA systems, where signals from all users overlap both in the time and the frequency domain. In this case, the received signal consists of the sum of all the modulated user signals which, in the worst case scenario, have different amplitudes and delays, and are distorted by different channel impulse functions. Conventional modulation type classification algorithms are unable to extract the modulation type from such a signal mix. Similarly, in the case of OFDM, the symbols from one particular user are transmitted over multiple overlapping carriers in parallel. Hence, the received signal consists of multiple modulated carriers interfering with each other in time and frequency, and the modulation type on particular carriers cannot be classified by conventional methods. Thus, conventional modulation type recognition algorithms cannot be used to recognize CDMA and OFDM based air interfaces, which constitute the majority of the newer generation wireless communication systems.

In our work, we present a different approach to the air interface identification problem. We propose exploiting the cyclostationary properties, which exist in virtually all man made communication signals, as features for air interface recognition. In the following, we are going to show that signals belonging to different air interface standards usually exhibit different cyclostationary properties. The presence and absence of these distinct properties can be exploited for the recognition of the particular system. The proposed method presents a unified approach to the recognition of signals belonging to the all three basic air interface categories discussed in chapter 3: single carrier TDMA systems, OFDM systems and single carrier CDMA systems.

5.2   Continuous Time Cyclostationary Processes

This section provides an overview on continuous time cyclostationary processes [39]. It begins with the introduction of the concept of cyclostationarity along with the formal definitions of conjugate and nonconjugate cyclic autocorrelation functions and spectral correlation density functions. Subsequently, the concept of cycloergodicity is introduced and an alternative interpretations to the cyclostationarity is discussed, which provides a more profound insight to the nature of cyclostationarity. Finally, the motive behind the intention to exploit the cyclostationarity properties of communication signals is discussed.

5.2.1   Periodically Correlated Processes

For a complex zero mean time continuous process $x(t)$, $(t \in \mathbb{R})$, the time varying autocorrelation function (TVAF) is defined as:

$$R_{xx}(t + \tau/2, t - \tau/2) = E\{x(t + \tau/2)x^*(t - \tau/2)\} \tag{5.1}$$

In the continuous time theory of cyclostationarity, it has been found more convenient to use the symmetric version of the TVAF, rather than the asymmetric version, $R_{xx}(t, t - \tau) == E\{x(t)x^*(t - \tau)\}$. However, the results provided in this section can be easily modified for the assymetric case [39].

The random process $x(t)$ is characterized as *periodically correlated*, if the TVAF is periodic in time variable t with a period P, i.e.

$$R_{xx}(t + \tau/2, t - \tau/2) = R_{xx}(t + \tau/2 + mP, t - \tau/2 + mP); \forall m \in \mathbb{Z} \tag{5.2}$$

As a result of this periodicity, the time varying autocorrelation function of $x(t)$ can be represented as a Fourier series:

$$R_{xx}(t + \tau/2, t - \tau/2) = \sum_{\alpha} R_{xx}^{\alpha}(\tau)e^{j2\pi\alpha t} \tag{5.3}$$

where the sum is taken over the integer multiples of the fundamental frequency $\alpha_f = k/P$, $k \in \mathbb{N}$. The Fourier coefficients, which depend on the lag parameter τ are called the *cyclic autocorrelation function* and are given as

[39]:

$$R_{xx}^{\alpha}(\tau) = \frac{1}{P} \int_{-P/2}^{P/2} R_{xx}(t + \tau/2, t - \tau/2)e^{-j2\pi\alpha t}dt \qquad (5.4)$$

For some complex valued signals, the time varying conjugate autocorrelation function (TVCAF) may also be useful, which is defined as

$$R_{xx^*}(t + \tau/2, t - \tau/2) = E\{x(t + \tau/2)x(t - \tau/2)\} \qquad (5.5)$$

Analogous to the nonconjugate case, the complex valued random process $x(t)$ is called conjugate periodically correlated, if the TVCAF is periodic in time:

$$R_{xx^*}(t + \tau/2, t - \tau/2) = R_{xx^*}(t + \tau/2 + mP, t - \tau/2 + mP); \forall m \in \mathbb{Z} \qquad (5.6)$$

and admits a Fourier series representation

$$R_{xx^*}(t + \tau/2, t - \tau/2) = \sum_{\alpha} R_{xx^*}^{\alpha}(\tau)e^{j2\pi\alpha t} \qquad (5.7)$$

As before, the sum is taken over the integer multiples of the fundamental cycle frequency $\alpha_f = k/P$. The Fourier coefficients of the TVCAF are referred to as the conjugate cyclic autocorrelation function and are given as:

$$R_{xx^*}^{\alpha}(\tau) = \frac{1}{P} \int_{-P/2}^{P/2} R_{xx^*}(t + \tau/2, t - \tau/2)e^{-j2\pi\alpha t}dt \qquad (5.8)$$

5.2.2   Polyperodically correlated processes

A complex valued zero mean continuous process $x(t)$ is called (conjugate) polyperiodically correlated , if the TVAF (TVCAF) consists of multiple periodic components with incommensurate periods $P_1, \ldots, P_n$. In this case the TVAF (or TVCAF) admit a Fourier series representation:

$$R_{xx}(t + \tau/2, t - \tau/2) = \sum_{\alpha} R_{xx}^{\alpha}(\tau)e^{j2\pi\alpha t}$$

$$R_{xx^*}(t + \tau/2, t - \tau/2) = \sum_{\alpha} R_{xx^*}^{\alpha}(\tau)e^{j2\pi\alpha t} \qquad (5.9)$$

where the sum is taken over all the incommensurate fundamental frequencies $\alpha \in \{k_1/P_1, \ldots, k_n/P_n\}$ with $k_1, \ldots k_n \in \mathbb{Z}$. Since multiple periodicities with different fundamental frequencies exist, the Fourier coefficients cannot be calculated performing a time averaging operation over one period, as in (5.4) and (5.8), and an infinitely long time interval has to be used instead, in order to suppress the contributions from the signal components exhibiting different periodicities. Thus, the cyclic autocorrelation function for a polyperiodically correlated process can be expressed as

$$R_{xx}^{\alpha}(\tau) = \lim_{T \to \infty} \frac{1}{T} \int_{-T/2}^{T/2} R_{xx}(t + \tau/2, t - \tau/2)e^{-j2\pi\alpha t}dt \tag{5.10}$$

and the conjugate cyclic autocorrelation function for a conjugate polyperiodically correlated process is [39]

$$R_{xx^*}^{\alpha}(\tau) = \lim_{T \to \infty} \frac{1}{T} \int_{-T/2}^{T/2} R_{xx^*}(t + \tau/2, t - \tau/2)e^{-j2\pi\alpha t}dt \tag{5.11}$$

In the following work, the term *cyclostationary* is used to characterize both conjugate and nonconjugate periodically and polyperiodically correlated processes. The terms *conjugate cyclostationary* and *nonconjugate cyclostationary* are employed, wherever it is necessary to explicitly differentiate between the conjugate and nonconjugate cases. Furthermore, the more general definitions from (5.10) and (5.11) are going to be used for the cyclic autocorrelation functions throughout this chapter.

5.2.3 Properties of Cyclic Autocorrelation Functions

The conjugate and nonconjugate cyclic autocorrelation functions are discrete functions of the frequency parameter α and are continuous in the lag parameter τ. For a process which does not exhibit cyclostationarity, $R_{xx}^{\alpha}(\tau) = 0$ and $R_{xx^*}^{\alpha}(\tau) = 0 \, \forall \alpha \neq 0$. It should be noted that, for a purely stationary process, these functions are reduced to conventional autocorrelation functions. Any nonzero value of the frequency parameter α, for which $R_{xx}^{\alpha}(\tau) \neq 0$ or $R_{xx^*}^{\alpha}(\tau) \neq 0$ is called a *cycle frequency*, and the discrete set of the cycle frequencies A_{xx} (corresponding to $R_{xx}^{\alpha}(\tau)$) and A_{xx^*} (corresponding to $R_{xx^*}^{\alpha}(\tau)$) are referred to as the *cycle spectrum* and *conjugate cycle spectrum* respectively. For a cyclostationary signal, the cycle spectra contain harmonics of each of the incommensurate fundamental cycle frequencies. A signal is said to exhibit cyclostationarity (or conjugate cyclostationarity)

with the cycle frequency α_0, if $\alpha_0 \in A_{xx}$ ($\alpha_0 \in A_{xx^*}$). For telecommunication signals, the cycle frequencies are typically related to the symbol rate, spreading code repetiton rate, carrier frequency, frequency hopping rate, chipping rate, etc [40].

5.2.4 Cycloergodicity

The concept of ergodicity in relation to a random process implies that the long term behaviour of time averaged measurements on a sample path of a random process can be calculated from the probabilistic model of the random process using ensemble averages, i.e. expectation operator, and the large sample behaviour of hypothetical ensemble averaged measurements can be predicted from actual time averaged measurements on one sample path of the ensemble.This means that the time and ensemble average operations can be freely exchanged.i.e.

$$E\{x(t)\} = \lim_{T \to \infty} \frac{1}{T} \int_{-T/2}^{T/2} x(t)dt \tag{5.12}$$

which leads to

$$\lim_{T \to \infty} \frac{1}{T} \int_{-T/2}^{T/2} E\{x(t)\}dt = \lim_{T \to \infty} \frac{1}{T} \int_{-T/2}^{T/2} x(t)dt \tag{5.13}$$

since $E\{E\{\cdot\}\} = E\{\cdot\}$. These assumptions , in general, simplify mathematical analysis and experimental design greatly. The property of stationarity is a prerequisit for a random process to exhibit ergodic properties.

The concept of ergodicity can be extented to include cyclostationary processes. This property is referred to as *cycloergodicity* [41]. For a cycloergodic process, the asymptotic sinusoidally weighted sample path averages are equal to the corresponding sinusoidally weighted ensemble averages, i.e.

$$\lim_{T \to \infty} \frac{1}{T} \int_{-T/2}^{T/2} E\{x(t)\}e^{-j2\pi\alpha t}dt = \lim_{T \to \infty} \frac{1}{T} \int_{-T/2}^{T/2} x(t)e^{-j2\pi\alpha t}dt \tag{5.14}$$

With the assumption of cycloergodicity, the expectation operator in the nonconjugate and conjugate cyclic autocorrelation functions can be dropped

[39]:

$$R_{xx}^{\alpha}(\tau) = \lim_{T \to \infty} \frac{1}{T} \int_{-T/2}^{T/2} x(t+\tau/2)x^*(t-\tau/2)e^{-j2\pi\alpha t}dt \qquad (5.15)$$

and

$$R_{xx^*}^{\alpha}(\tau) = \lim_{T \to \infty} \frac{1}{T} \int_{-T/2}^{T/2} x(t+\tau/2)x(t-\tau/2)e^{-j2\pi\alpha t}dt \qquad (5.16)$$

5.2.5   Cyclostationarity as Spectral Correlation

A useful interpretation of the cyclic autocorrelation Function can be obtained by factoring $e^{-j2\pi\alpha t}$ in (5.15):

$$R_{xx}^{\alpha}(\tau) = \lim_{T \to \infty} \frac{1}{T} \int_{-T/2}^{T/2} [x(t+\tau/2)e^{-j\pi\alpha(t+\tau/2)}][x(t-\tau/2)e^{j\pi\alpha(t-\tau/2)}]^* dt (5.17)$$

Thus, $R_{xx}^{\alpha}(\tau)$ can be interpreted as a conventional cross correlation function:

$$R_{xx}^{\alpha}(\tau) = \lim_{T \to \infty} \frac{1}{T} \int_{-T/2}^{T/2} u(t+\tau/2)v(t-\tau/2)^* dt = R_{uv}(\tau) \qquad (5.18)$$

with

$$u(t) = x(t)e^{-j\pi\alpha t} \qquad (5.19)$$

and

$$v(t) = x(t)e^{+j\pi\alpha t}. \qquad (5.20)$$

$u(t)$ and $v(t)$ are frequency translates of $x(t)$ by $+\alpha/2$ and $-\alpha/2$ respectively. It follows from (5.18) that a signal $x(t)$ exhibits cyclostationarity if and only if its spectral components separated by a cycle frequency α are temporally correlated, i.e. $R_{uv}(\tau)$ is nonzero for some τ and for $\alpha \neq 0$ [39]. The conjugate cyclic autocorrelation function can be reexpressed as a cross

correlation function in a similar fashion:

$$R_{xx*}^{\alpha}(\tau) = \lim_{T\to\infty} \frac{1}{T} \int_{-T/2}^{T/2} u(t+\tau/2)w^*(t-\tau/2)dt = R_{uw}(\tau) \qquad (5.21)$$

where

$$w(t) = x^*(t)e^{+j\pi\alpha t}. \qquad (5.22)$$

is the frequency translate of $x^*(t)$

5.2.6   The Spectral Correlation Density Function

The conventional power spectral density function (PSD) is a useful measure employed to localize the average power $E\{|x(t)|^2\} = R_{xx}(0)$ of a stationary random process $x(t)$ in the frequency domain. The PSD can be expressed as:

$$S_{xx}(f) = \lim_{T\to\infty} E\{|\frac{1}{T}X_T(f)|^2\} \qquad (5.23)$$

where

$$X_T(f) = \int_{-T/2}^{T/2} x(u)e^{-j2\pi f u}du \qquad (5.24)$$

is the Fourier Transform of $x(t)$ over the time interval T. It can be shown that $S_{xx}(f)$ is directly related to $R_{xx}(\tau)$ through the Wiener-Khinchin relation:

$$S_{xx}(f) = \int_{-\infty}^{\infty} R_{xx}(\tau)e^{-j2\pi f\tau}d\tau \qquad (5.25)$$

Similarly, for a cyclostationary process, the spectral correlation density function (SCD) provides a measure for the localisation of the correlation between the frequency shifted versions of the signal $x(t)$, i.e. $R_{uv}(0) = R_{xx}^{\alpha}(0)$, in the frequency domain.The spectral correlation density function can be derived starting from the so called instantaneous PSD, in the same manner as the cyclic autocorrelation is derived from the time varying autocorrelation function. The instantaneous PSD of a signal is defined as the Fourier transform of the time varying autocorrelation function with respect to the

lag parameter τ:

$$S_{xx}(t, f) = \int_{-\infty}^{\infty} R_{xx}(t + \tau/2, t - \tau/2)e^{-j2\pi f\tau}d\tau \qquad (5.26)$$

If $x(t)$ exhibits cyclostationarity, this function admits a Fourier series representation

$$S_{xx}(t, f) = \sum_{\alpha} S_{xx}^{\alpha}(f)e^{j2\pi\alpha t} \qquad (5.27)$$

where the Fourier coefficients can be calculated as

$$S_{xx}^{\alpha}(f) = \lim_{T\to\infty} \frac{1}{T} \int_{-T/2}^{T/2} S_{xx}(t, f)e^{-j2\pi\alpha t}dt. \qquad (5.28)$$

$S_{xx}^{\alpha}(f)$ is referred to as the spectral correlation density function. From (5.26) and (5.28), it is easily seen that the spectral correlation density function and the cyclic autocorrelation function are related through the cyclic version of the Wiener-Khinchin relation, i.e:

$$S_{xx}^{\alpha}(f) = \int_{-\infty}^{\infty} R_{xx}^{\alpha}(\tau)e^{-j2\pi f\tau}d\tau \qquad (5.29)$$

Like its nonconjugate counterpart, the conjugate spectral correlation density function can be obtained by Fourier transforming the conjugate cyclic autocorrelation function:

$$S_{xx^*}^{\alpha}(f) = \int_{-\infty}^{\infty} R_{xx^*}^{\alpha}(\tau)e^{-j2\pi f\tau}d\tau \qquad (5.30)$$

Similar to (5.23) it can be shown that the conjugate and nonconjugate spectral correlation density functions can be calculated using the Fourier transform of the signal directly [42]. With the assumption of cycloergodicity

$$S_{xx}^{\alpha}(f) = \lim_{V\to\infty} \lim_{T\to\infty} \frac{1}{V} \int_{-V/2}^{V/2} \frac{1}{T} X_T(t, f + \alpha/2)X_T^*(t, f - \alpha/2)dt \quad (5.31)$$

and

$$S_{xx^*}^{\alpha}(f) = \lim_{V \to \infty} \lim_{T \to \infty} \frac{1}{V} \int_{-V/2}^{V/2} \frac{1}{T} X_T(t, f + \alpha/2) X_T(t, \alpha/2 - f) dt \quad (5.32)$$

with $X_T(t, f) = \int_{t-T/2}^{t+T/2} x(u) e^{-j2\pi f u} du$. Following the same line of thought as in Section 5.2.5, the conjugate and nonconjugate spectral correlation density functions can be interpreted as conventional cross spectral density functions of frequency translated versions of $x(t)$, i.e.

$$S_{xx}^{\alpha}(f) = S_{uv}(f) \quad (5.33)$$

and

$$S_{xx^*}^{\alpha}(f) = S_{uw}(f) \quad (5.34)$$

where $u(t)$, $v(t)$ and $w(t)$ are defined in (5.19) (5.20) and (5.22) respectively.

The existence of temporal correlation between spectral components separated by the cycle frequency α in a cyclostationary signal can be interpreted as spectral redundancy in the information theoretic sense. Signal processing techniques which do not make use of the cyclostationarity ignore the presence of this redundant information in the signal, whereas the methods exploiting cyclostationarity take advantage of this redundancy, in order to increase the performance and robustness of the algorithms used.

When the signal $x(t)$ undergoes a linear time variant filtering operation

$$z(t) = h(t) * x(t) = \int_{-\infty}^{\infty} h(u) x(t - u) du \quad (5.35)$$

the nonconjugate and the conjugate SCD of the output signal $z(t)$ can be calculated as [40]

$$S_{zz}^{\alpha}(f) = H(f + \alpha/2) H^*(f - \alpha/2) S_{xx}^{\alpha}(f) \quad (5.36)$$

and

$$S_{zz^*}^{\alpha}(f) = H(f + \alpha/2) H(\alpha/2 - f) S_{xx^*}^{\alpha}(f) \quad (5.37)$$

respectively, where $H(f)$ is the Fourier transform of $h(t)$. Hence, the linear time invariant filtering operation cannot change the cycle spectra of the signal. However, depending on the shape of the filter spectrum, the filtering operation may lead to a suppression or an enhancement of the cyclostationary characteristics.

5.2.7   Motivation

Exploiting cyclostationarity in air interface recognition for a Software Radio system presents two main advantages, which shall be discussed in this section.

First of all, virtualy all man-made communication signals exhibit cyclostationarity with cycle frequencies related to hidden periodicities underlying the signal, such as the carrier frequency, symbol and/or chip rates, period of the spreading or scrambling codes etc. From this reason, signals from different air interfaces with different transmission schemes, symbol rates etc. exhibit cyclostationarity with different cycle frequencies and for different values of the lag parameter τ. Thus, each air interface signal has its unique cyclic signature. The presence or absence of a particular signature in the received signal is therefore a distinct feature that can be used to recognize a particular air interface.

The second advantage lies in the discriminatory capability that the use of cyclic statistics presents between the signal sources with disparate cycle spectra and the robustness against noise and interference which this signal selectivity provides.

Let $x(t)$ be a noisy observation of the cyclostationary signal of interest $s(t)$

$$x(t) = s(t) + n(t), \qquad (5.38)$$

where $n(t)$ is stationary noise. It can be easily shown that the cyclic autocorrelation function and the spectral correlation density function of $x(t)$ are given by:

$$R_{xx}^{\alpha}(\tau) = R_{ss}^{\alpha}(\tau) \qquad S_{xx}^{\alpha}(f) = S_{ss}^{\alpha}(f); \qquad \alpha \neq 0 \qquad (5.39)$$

In a more general case, where the interfering signal or signals also exhibit cyclostationarity, it is still possible to separate the signal of interest from the interference by choosing a cyclic frequency α_0 which is different from that

of the interfering signals. Let $x(t)$ be a composite signal

$$x(t) = \sum_{l=1}^{L} s_l(t) + n(t),$$ (5.40)

with the zero mean cyclostationary signals $s_l(t)$, all of which are statistically independent of each other and the additive stationary noise $n(t)$, it can easily be shown that:

$$R_{xx}^{\alpha}(\tau) = \sum_{l=1}^{L} R_{s_l s_l}^{\alpha}(\tau) + R_{nn}(\tau)\delta[\alpha]$$ (5.41)

and

$$S_{xx}^{\alpha}(f) = \sum_{l=1}^{L} S_{s_l s_l}^{\alpha}(f) + S_{nn}(f)\delta[\alpha]$$ (5.42)

with the Kroenecker delta function $\delta[\alpha]$. From (5.41) and (5.42), it follows that choosing $\alpha = \alpha_k \neq 0$ so that the only signal with the particular cycle frequency α_k is $s_k(t)$, i.e. $\alpha_k \in A_{s_k s_k}$ and $\alpha_k \notin A_{s_l s_l}$, $\forall l \neq k$, we can write:

$$R_{xx}^{\alpha_k}(\tau) = R_{s_k s_k}^{\alpha_k}(\tau)$$ (5.43)

and

$$S_{xx}^{\alpha_k}(f) = S_{s_k s_k}^{\alpha_k}(f)$$ (5.44)

The same considerations are also valid for the conjugate cyclic autocorrelation and conjugate spectral correlation density functions. Hence, when multiple signals overlap in time and frequency domain, their cyclic autocorrelation and SCD functions do not overlap in the cycle frequency domain, as long as the signals possess distinct cycle frequencies.

However, in practice, this perfect signal selectivity, which the ideal cyclic autocorrelation and the spectral correlation density functions exhibit, suffers from noise and interference. For finite observation lengths, the presence of noise and interference affects the bias and the variance of the estimations of $R_{xx}^{\alpha_0}(\tau)$ and $S_{xx}^{\alpha_0}(f)$ respectively. This effect diminishes with increasing observation length T_o.

5.3 Cyclostationary Properties of Communication Signals

In this section, the cyclostationary properties of communication signals are investigated, which are commonly encountered in practice, starting with basic linear modulated signals, continuing with GMSK modulation, which is a very widely used nonlinear modulation type, especially in TDMA based GSM and DECT systems, as discussed in chapter 3. Subsequently, cyclic autocorrelation functions of signals based on OFDM and CDMA schemes are investigated, which are used in newer generation wireless communications systems.

5.3.1 The Cyclic Autocorrelation of a linear modulated Signal

A digital modulated signal is characterized as linear modulated, if the total waveform of the signal can be expressed as the sum of waveforms of individual symbols. Hence, a linear modulated signal can be expressed as an infinite sum of time shifted impulse functions $g(t)$, weighted by the discrete time modulating sequence a_n, which is a realisation of the discrete time random process $\mathbf{a}$. The impulse functions are separated in time by integer multiples of the symbol duration T_s. Given that the initial timing of the signal is unknown, the linear modulated signal can be expressed as

$$x(t) = \sum_{-\infty}^{\infty} a_n g(t - nT_s - \epsilon) \tag{5.45}$$

with the unknown symbol timing ϵ. In the following, we assume that the symbol sequence is indpendent and identically distributed, i.e. the different states $a^{(i)}$ of the random process $\mathbf{a}$ occur with equal probability, and the occurrence of the states in different symbol intervals are independent of each other, that means for the individual probabilities:

$$P(a_n = a^{(i)}) = \frac{1}{M} \tag{5.46}$$

and

$$P(a_n = a^{(j)} \wedge a_m = a^{(k)}) = P(a_n = a^{(j)}) \cdot P(a_m = a^{(k)}) \tag{5.47}$$

This assumption implies that the data sequence is uncorrelated The time varying autocorrelation function of the linear modulated signal can be calculated as:

$$R_{xx}(t + \tau/2, t - \tau/2) = E\left\{ \sum_{n=-\infty}^{\infty} \sum_{m=-\infty}^{\infty} a_n a_m^* \right.$$

$$\left. g(t - nT_s - \epsilon + \tau/2)g^*(t - mT_s - \epsilon - \tau/2) \right\}.$$

Assuming that $g(t)$ is real valued and the symbol sequence a_n is independent and identically distributed (i.i.d.), $E\{a_n a_m^*\} = \sigma_a^2 \delta[n - m]$, where $\sigma_a^2 = E\{|a_n|^2\}$ is the variance of the emitted symbols, the autocorrelation function can be expressed as an infinite sum of the lag product of the impulse functions

$$R_{xx}(t + \tau/2, t - \tau/2) = \sigma_a^2 \sum_{n=-\infty}^{\infty} g(t - nT_s - \epsilon + \tau/2)$$

$$. \quad g(t - nT_s - \epsilon - \tau/2) \tag{5.48}$$

It is straightforward to see that $R_{xx}(t + \tau/2, t - \tau/2)$ is time-periodic with a period equal to T_s, which means that the linear modulated signal exhibits cyclostationarity with a fundamental cycle frequency $\alpha_f = 1/T_s$ and the cycle spectrum contains the integer multiples of $f_s = 1/T_s$:

$$R_{xx}^\alpha(\tau) = \begin{cases} R_{xx}^{kf_s}(\tau), & \alpha = kf_s; k \in \mathbb{Z} \\ 0, & \text{otherwise} \end{cases} \tag{5.49}$$

If the pulse function $g(t) = g_R(t)$ is a full duty-cycle rectangular pulse given as

$$g_R(t) = \begin{cases} 1, & |t| < T_s/2 \\ 0, & \text{otherwise} \end{cases} \tag{5.50}$$

the cyclic autocorrelation of the linear modulated signal can be expressed as:

$$R_{xx}^{kf_s}(\tau) = \sigma_d^2 \frac{\sin[\pi k f_s(T_s - |\tau|)]}{\pi k} e^{j2\pi k f_s \epsilon} \qquad for |\tau| < T_s \tag{5.51}$$

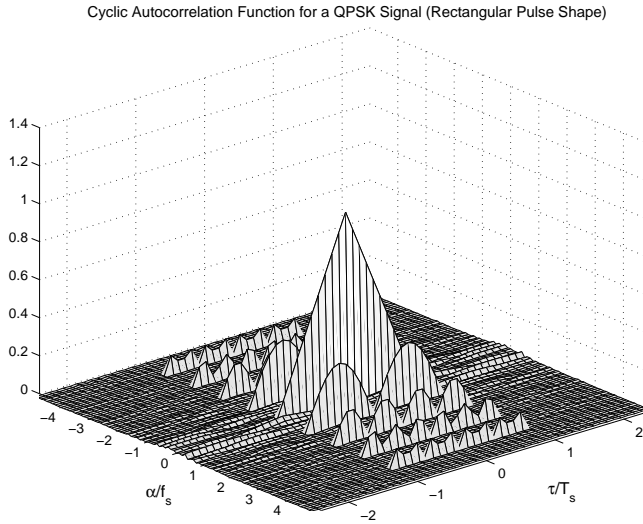Cyclic Autocorrelation Function for a QPSK Signal (Rectangular Pulse Shape)

Fig. 5.1 The magnitude of the nonconjugate cyclic autocorrelation estimate for a QPSK signal with rectangular pulse shape

The magnitude of the cyclic correlation estimate for a QPSK modulated signal with rectangular pulse shape is displayed in Fig. 5.1, where the discrete correlation surfaces for $\alpha = k f_s$ are clearly visible. The maximum value of cyclic correlation occurs for $\alpha = \pm 1/T_s = \pm f_s$ and $\tau = \pm T_s/2$.

The effect of the pulse shape

Since the rectangular pulse shape has a spectrum which decays relatively slowly, i.e. with $1/|f|$ for large f, other pulse shape functions with higher spectral efficiency are usually employed in practical digital communication systems. In the following, we are going to investigate the influence of the spectrum of $g(t)$ on the cyclic autocorrelation function $R_{xx}^{\alpha}(\tau)$ for a linear modulated signal. Expressing the pulse shape $g(t)$ in terms of its Fourier transform

$$g(t) = \int_{-\infty}^{\infty} G(f) e^{j2\pi f t} df \tag{5.52}$$

allows the reexpression of the cyclic autocorrelation function in terms of the pulse spectra. We obtain

$$
\begin{aligned}
R_{xx}^{kf_s}(\tau) \;=\; & \lim_{T\to\infty} \frac{\sigma_a^2}{T} \int_{-T/2}^{T/2} \int_{-\infty}^{\infty} \int_{-\infty}^{\infty} \Big[exp[j2\pi\big(f_1 t - f_1\epsilon \\
& + f_1\tau/2 + f_2 t - f_2\epsilon - f_2\tau/2 - kf_s t)]G(f_1)G(f_2) \\
& \sum_{n=-\infty}^{\infty} e^{-j2\pi n T_s[f_1+f_2]} \Big] df_1 df_2 dt.
\end{aligned}
$$

Expressing the infinite sum of phasors as an infinite sum of impulses we get

$$
\begin{aligned}
R_{xx}^{kf_s}(\tau) \;=\; & \lim_{T\to\infty} \frac{\sigma_a^2}{T} \int_{-T/2}^{T/2} \int_{-\infty}^{\infty} \int_{-\infty}^{\infty} \Big[exp[j2\pi\big(f_1 t - f_1\epsilon + f_1\tau/2 + f_2 t \\
& - f_2\epsilon - f_2\tau/2 - kf_s t)]G(f_1)G(f_2) \\
& \cdot \sum_{i=-\infty}^{\infty} \delta[f_1 + f_2 - if_s] \Big] df_1 df_2 dt. \qquad (5.53)
\end{aligned}
$$

Finally, integrating with respect to f_1 to eliminate the impulses leads to

$$
\begin{aligned}
R_{xx}^{kf_s}(\tau) \;=\; & \frac{\sigma_a^2}{T_s} \int_{-\infty}^{\infty} \Big[e^{-j2\pi f\tau} G(f) \sum_{i=-\infty}^{\infty} G(if_s - f)e^{-j2\pi i f_s(\epsilon-\tau/2)} \\
& \cdot \lim_{T\to\infty} \frac{1}{T} \int_{-T/2}^{T/2} e^{j2\pi f_s t(i-k)} \Big] dt df. \\
\;=\; & \frac{\sigma_a^2}{T_s} \int_{-\infty}^{\infty} e^{-j2\pi[(f\tau + kf_s(\epsilon-\tau/2)]} G(f)G(kf_s - f) df \qquad (5.54)
\end{aligned}
$$

From (5.54), it becomes clear that the amount of cylic correlation in the linear modulated signal depends on the spectral overlapping between the frequency shifted versions of the pulse spectrum, i.e. between $G(f)$ and $G(kf_s - f)$. The amount of this spectral overlapping obviously depends on the shape of the particular signal pulse function.
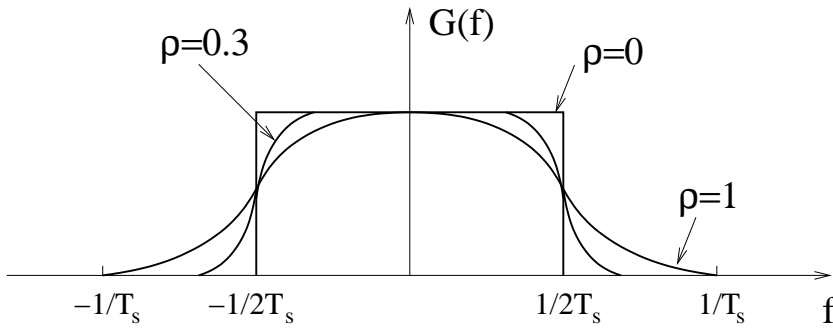
Fig. 5.2 Raised Cosine Spectrum

In digital communications, the signal pulse is usually designed to allow symbol rates comparable to the two sided channel bandwidth B while minimizing the intersymbol interference (ISI) between adjacent symbols in time. The condition for no intersymbol interference is in time domain

$$g(nT_s) = \begin{cases} 1 & (n = 0) \\ 0 & (n \neq 0) \end{cases} \tag{5.55}$$

which, in frequency domain translates to the following condition

$$\sum_{m=-\infty}^{\infty} G(f + m/T_s) = T_s \tag{5.56}$$

which is called the Nyquist pulse shaping criterion, or Nyquist criterion for distortionless baseband communication [14]. For $T_s = 1/B$, this condition can only be satisfied by a rectangular spectrum, which leads to a pulse shape $g(t) = \frac{sin(\pi t/T_s)}{\pi t/T_s}$. However, there are two practical difficulties, that make this pulse shape unsuitable for system design

- This pulse shape is physically unrealizable because of the abrupt transitions at the boundaries.

- $g(t)$ decreases as $1/|t|$ for large $|t|$, resulting in a relatively slow rate of decay. Accordingly, a timing mismatch in the receiver can result in a very high intersymbol interference. Hence this pulse shape allows no margin for error in the sampling times.
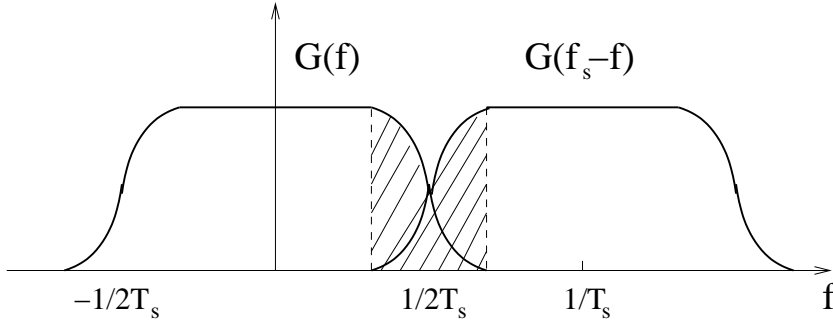
Fig. 5.3 Spectral overlapping between the frequency shifted versions of $G(f)$

A widely used pulse spectrum for this case is the raised cosine spectrum, which consists of a flat portion and a roll-off portion that has a sinusoidal form [14]

$$G_{rc}(f) = \begin{cases} T_s & (0 \le |f| \le \frac{1-\rho}{2T_s}) \\ \frac{T_s}{2}\left\{1 + cos\left[\frac{\pi T_s}{\rho}\left(|f| - \frac{1-\rho}{2T_s}\right)\right]\right\} & (\frac{1-\rho}{2T_s} \le |f| \le \frac{1+\rho}{2T_s}) \quad (5.57) \\ 0 & (|f| \le \frac{1+\rho}{2T_s}) \end{cases}$$

where the parameter ρ is called the roll of factor and takes values in the range $0 \le \rho \le 1$. The roll off factor determines the amount of the so called *excess bandwidth* of the signal, i.e. the bandwidth occupied by the signal beyond the Nyquist bandwidth $W_{Nyq} = 1/T_s$, which is the minimum amount of bandwidth required by the Nyquist theorem. For example, when $\rho = 0.3$, the excess bandwidth is 30%, and when $\rho = 1$, the excess bandwidth is 100%. For $\rho = 0$ it converges to a rectangular spectrum, as shown in Fig 5.2 The pulse $g_{rc}(t)$ having the raised cosine spectrum is given by [14]:

$$g_{rc}(t) = \frac{sin(\pi t/T_s)}{\pi t/T_s}\frac{\pi \rho t/T}{1 - 4\rho^2 t^2/T_s^2} \tag{5.58}$$

Usually, the transmit and receive filters in a telecommunication system are designed so that the total effect of these filters approximate the desired spectrum. In this case, the so called root raised cosine filters are employed.
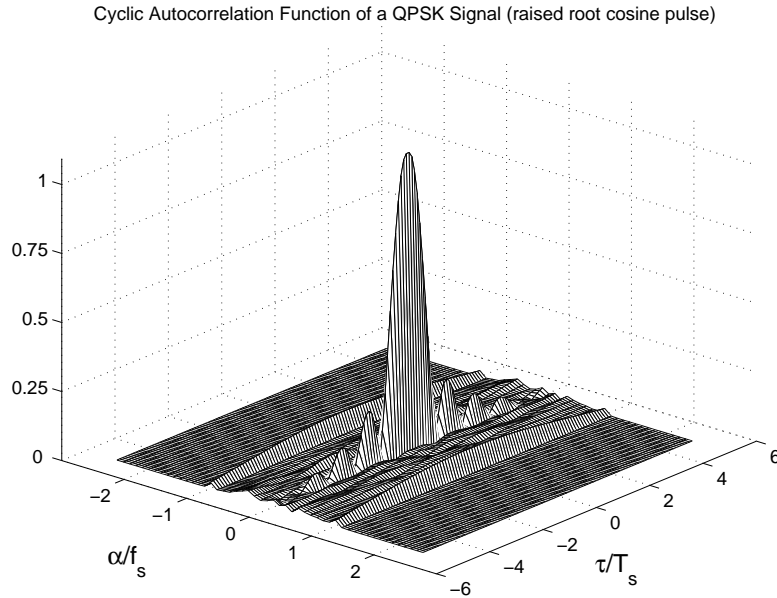
Cyclic Autocorrelation Function of a QPSK Signal (raised root cosine pulse)

Fig. 5.4 The magnitude of the nonconjugate cyclic autocorrelation estimate for a QPSK signal with root raised cosine pulse shape

The root raised cosine spectral characteristic is given by:

$$G_{rrc}(f) = \sqrt{|G_{rc}(f)|} \qquad (5.59)$$

The root raised cosine filter is used in series pairs, so that the total filtering effect is that of a raised cosine filter. The advantage is that if the transmit side filter is stimulated by an impulse, then the receive side filter is forced to filter an input pulse shape that is identical to its own impulse response, thereby setting up a matched filter and maximizing signal to noise ratio while at the same time minimizing intersymbol interference. The pulse having the root raised cosine spectrum is [14]

$$g_{rrc}(t) = \frac{4\rho}{\pi\sqrt{T_s}} \frac{cos(\frac{(1+\rho)\pi t}{T_s}) + \frac{T_s}{4\rho t}sin(\frac{(1-\rho)\pi t}{T_s})}{1 - 4\rho t/T_s} \qquad (5.60)$$

Again, the roll off factor is the parameter determining the excess bandwidth of the signal. UTRA, IS-95, IS-136 and PDC are some of the air interfaces using the root raised cosine spectrum, both at the transmitter and the receiver.

Since the root raised cosine pulse spectrum suppresses the frequency components of the signal for $|f| > \frac{1+\rho}{2T_s} = \frac{1+\rho}{2}f_s$ with $0 \le \rho \le 1$ there exists no spectral overlapping between the frequency translated versions of $G_{rrc}(f)$ for $|k| > 1$, i.e.

$$G_{rrc}(f)G_{rrc}(kf_s - f) = 0; |k| > 1 \qquad (5.61)$$

Thus, for a linear modulated signal with root raised cosine spectrum, we get significant spectral correlation only for $k = \pm 1$. Fig 5.3 illustrates the spectral overlapping for a root raised cosine pulse shape and $k = 1$. The amount of spectral overlapping obviously increases with increasing excess bandwidth or, equivalently, with increasing ρ.

The magnitude of the cyclic autocorrelation function for a QPSK modulated signal employing a root raised cosine spectrum with $\rho = 0.22$ is displayed in Fig. 5.4. As predicted, the cyclic autocorrelation is suppressed for $|k| > 1$. In contrast to the previous case, the cyclic correlation surfaces at $\alpha = \pm f_s$ peak at $\tau = 0$

5.3.2   Cyclostationary Properties of a GMSK signal

The Gaussian minimum shift keying (GMSK),which is employed in GSM and DECT, is a nonlinear modulation type, which makes the theoretical calculation of the cyclic autocorrelation functions quite a difficult task. The analysis provided in this section is based on separating the GMSK signal into its linear and nonlinear components and focusing on the linear part of the signal, which is a permissible approach, since the linear part of the signal contains ca. 99% of the total signal energy [43].

Linearisation of GMSK

GMSK can be interpreted as a 2-level FSK modulation with a modulation index $h = 0.5$. The complex envelope of a GMSK modulated signal is

$$s(t) = exp\Big[j2\pi h \sum_{n=-\infty}^{\infty} d_n \int_{-\infty}^{t} g_f(\tau - nT_s)d\tau\Big] \qquad (5.62)$$

with the symbol sequence $d_n \in \{-1, 1\}$, symbol rate $f_s = 1/T_s$ and $g_f(t)$ a frequency impulse with a time bandwidth product BT_s.

$$g_f(t) = \frac{1}{T_s} rect\left(\frac{t}{T_s}\right) * p_{Gauss}(t) \tag{5.63}$$

where $p_{Gauss}(t)$ is a Gaussian impulse

$$p_{Gauss}(t) = \sqrt{\frac{2\pi}{ln2}} \cdot B \cdot exp\left(-\frac{2(\pi Bt)^2}{ln2}\right) \tag{5.64}$$

For the GSM system, the factor $BT_s = 0.3$ was chosen, whereas in DECT, $BT_s = 0.5$. In practice, the infinite long Gaussian impulse is cut to a length LT_s with $L \geq 3$. In [43], it is shown that a GMSK signal can be represented as the superposition of 2^{L-1} elementary impulse functions $c_K(t)$

$$s(t) = \sum_{n=-\infty}^{\infty} \sum_{K=1}^{2^{L-1}} exp[j\pi h A_{K,n} c_K(t - nT_s)] \tag{5.65}$$

with the statistically dependent modulating sequence $A_{K,n}$, which can be expressed as a function of the data sequence d_n as follows

$$A_{K,n} = \sum_{i=-\infty}^{n} d_i - \sum_{l=1}^{2^{L-1}} d_{k-l} v_{K,l}$$

$$K = \sum_{l=1}^{2^{L-1}} 2^{l-1} v_{K,l}; \qquad v_{K,l} \in 0; 1 \tag{5.66}$$

The bit sequence $v_{K,L-1}, \dots, v_{K,1}$ corresponds to the binary representation of the index K. A very detailed discussion about the derivation of the elementary impulse forms $c_K(t)$ is provided in [44] and [43]. For $L = 4$ which is commonly used in practice, the GMSK signal consists of the superposition of 8 elementary impulse functions:

$$s(t) = \sum_{n=-\infty}^{\infty} exp\big[j\pi h A_{0,n}\big] c_0(t - nT_s)$$

$$+ \sum_{n=-\infty}^{\infty} \sum_{K=1}^{7} exp[j\pi A_{K,n}] c_K(t - nT_s) \tag{5.67}$$

It is easily seen that the first sum can be interpreted as a linear modulation. From this reason, the base-band GMSK signal can be represented as the superposition of a linear and a nonlinear component:

$$s(t) = \sum_{n=-\infty}^{\infty} exp\big[j\pi h \sum_{i=-\infty}^{n} d_i\big] c_0(t - nT_s)$$

$$+ \sum_{n=-\infty}^{\infty} \sum_{K=1}^{7} exp[j\pi A_{K,n}] c_K(t - nT_s)$$

$$= s^{lin}(t) + s^{nl}(t) \tag{5.68}$$

In Fig. 5.5, the first two impulses $c_0(t)$ and $c_1(t)$ are displayed for $BT_s = 0.3$. It can be shown that $c_0(t)$ contains 99% of the signal energy [44], hence the GMSK signal can be approximated by its linear component fairly accurately. For a detailed discussion on this representation and the elementary impulse functions $c_K(t)$, see [43]. The linear part of the signal $s^{lin}(t)$ can be written as

$$s(t) \approx s^{lin}(t) = \sum_{n=-\infty}^{\infty} z_n c_0(t - nT_s) \tag{5.69}$$

with the symbol sequence

$$z_n = exp\big[j\pi h \sum_{i=-\infty}^{n} d_i\big] = exp\big[j\frac{\pi}{2}(d_n + \sum_{i=-\infty}^{n-1} d_i)\big]$$

$$= jd_n z_{n-1} \tag{5.70}$$

It can be shown that the linear approximation of the GMSK signal is more accurate for higher values of BT_s, which is not surprising, since the GMSK
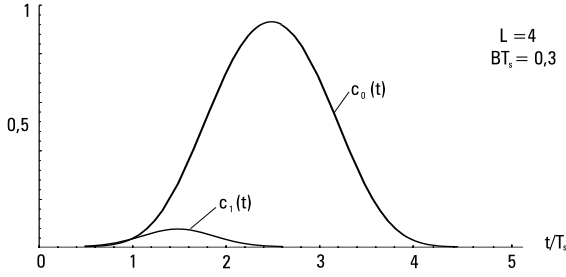
Fig. 5.5 $c_0(t)$ and $c_1(t)$ for $L = 4$, $BT_s = 0.3$

signal converges to a MSK signal for $BT_s \to \infty$, which is a linear modulation type. Since the input signal sequence $d_n \in \{-1, 1\}$, we see that the modulating sequence z_n in $s^{lin}(t)$ consists of alternating real and imaginary symbols. This property leads to a conjugate cyclostationary behaviour in the GMSK modulated signal.

Conjugate Cyclic Autocorrelation Function of a GMSK signal

We start our analysis with the conjugate cyclic autocorrelation $R_{ss^*}^{\alpha}(\tau)$ of a GMSK signal. In light of the discussion above, only the linear part of the signal is considered. Assuming that the timing of the signal is unknown to the receiver, we can express the time varying conjugate autocorrelation function due to the linear component of the signal as follows:

$$R_{ss^*}^{\alpha}(t + \tau/2, t - \tau/2) \cong E\{s^{lin}(t - \epsilon + \tau/2)s^{lin}(t - \epsilon - \tau/2)\}$$

$$= \sum_{n=-\infty}^{+\infty} \sum_{m=-\infty}^{+\infty} E\{z_n z_m\} c_0(t - \epsilon - nT_s + \tau/2)$$

$$\cdot \ c_0(t - \epsilon - mT_s - \tau/2) \tag{5.71}$$

using (5.70) and $E\{d_n d_m\} = E\{d_n d_m^*\} = \delta[n - m]$, we get

$$E\{z_n z_m\} = (-1)^n z_{-\infty}^2 \delta[n - m] \tag{5.72}$$

with the constant $z^2_{-\infty} \in \{-1, 1\}$, which depends on the initial state of the sequence z_n. Thus the the conjugate cyclic autocorrelation function can be written as

$$R^\alpha_{ss^*}(t + \tau/2, t - \tau/2) = \sum_{n=-\infty}^{+\infty} z^2_{-\infty}(-1)^n c_0(t - \epsilon - nT_s + \tau/2)$$

$$\cdot\ c_0(t - \epsilon - mT_s - \tau/2) \tag{5.73}$$

Obviously, $R^\alpha_{ss^*}(t + \tau/2, t - \tau/2)$ is periodic with a period equal to $2T_s$, since the sequence $(-1)^n$ is periodic with a period equal to 2, which leads to a conjugate cyclostationarity with cycle frequencies $\alpha = k/2T_s = kf_s/2$, $k = \pm 1, \pm 2 \ldots$. We can write:

$$R^\alpha_{ss^*}(\tau) = \begin{cases} R^{kf_s/2}_{ss^*}(\tau), & \alpha = kf_s/2 \\ 0, & \text{otherwise} \end{cases} \tag{5.74}$$

The conjugate cyclic autocorrelation function can be calculated as

$$R^{kf_s/2}_{ss^*}(\tau) = z^2_{-\infty} \lim_{T\to\infty} \frac{1}{T} \int_{-T/2}^{T/2} \sum_{n=-\infty}^{\infty} (-1)^n c_0(t - \epsilon - nT_s + \tau/2)$$

$$\cdot\ c_0(t - \epsilon - \tau - nT_s - \tau/2)e^{-jk2\pi(f_s/2)t}dt. \tag{5.75}$$

as in the previous case, expressing the pulse $c_0(t)$ in terms of its Fourier transform

$$c_0(t) = \int_{-\infty}^{\infty} C_0(f)e^{j2\pi ft}df$$

and realizing that $(-1)^n = e^{j\pi n}$ leads to

$$R^{kf_s/2}_{ss^*}(\tau) = z^2_{-\infty} \lim_{T\to\infty} \frac{1}{T} \int_{-T/2}^{T/2} \int_{-\infty}^{\infty} \int_{-\infty}^{\infty} \Big[exp[j2\pi\big(f_1 t - f_1\epsilon + f_1\tau/2$$

$$+f_2 t - f_2\epsilon - f_2\tau/2 - k(f_s/2)t)\big]C_0(f_1)C_0(f_2)$$

$$\cdot \sum_{n=-\infty}^{\infty} e^{-j2\pi nT[f_1+f_2-(f_s/2)]} \Big] df_1 df_2 dt. \tag{5.76}$$

Expressing the infinite sum of phasors as an infinite sum of impulses we get

$$R_{ss^*}^{kf_s/2}(\tau) = \frac{z_{-\infty}^2}{T_s} \lim_{T\to\infty} \frac{1}{T} \int_{-T/2}^{T/2} \int_{-\infty}^{\infty} \int_{-\infty}^{\infty} \Big[exp[j2\pi\big(f_1 t - f_1\epsilon + f_1\tau/2$$

$$+ f_2 t - f_2\epsilon - f_2\tau/2 - k(f_s/2)t)]C_0(f_1)C_0(f_2)$$

$$\cdot \sum_{i=-\infty}^{\infty} \delta[f_1 + f_2 - f_s(i+\frac{1}{2})]\Big] df_1 df_2 dt. \tag{5.77}$$

Integrating with respect to f_1 to eliminate the impulses leads to:

$$R_{ss^*}^{kf_s/2}(\tau) = \frac{z_{-\infty}^2}{T_s} \int_{-\infty}^{\infty} e^{-j2\pi f\tau} C_0(f)$$

$$\cdot \sum_{i=-\infty}^{\infty} C_0(f_s\frac{2i+1}{2} - f)e^{-j2\pi f_s \frac{2i+1}{2}(\epsilon-\tau/2)}$$

$$\cdot \lim_{T\to\infty} \frac{1}{T} \int_{-T/2}^{T/2} e^{j2\pi f_s t\frac{2i+1-k}{2}} dt df.$$

$$= \frac{z_{-\infty}^2}{T_s} \int_{-\infty}^{\infty} e^{-j2\pi(f\tau+\frac{k}{2}f_s(\epsilon-\tau/2))} C_0(f)C_0(k\frac{f_s}{2} - f)df$$

$$\tag{5.78}$$

Nonconjugate Cyclic Autocorrelation Function of a GMSK Signal

Since $s^{lin}(t)$ is a linear modulated signal and $E\{z_n z_m^*\} = \delta_{nm}$, the GMSK signal also exhibits nonconjugate cyclostationarity with a fundamental cycle frequency $\alpha_f = 1/T_s = f_s$. Recalling (5.54), the cyclic autocorrelation
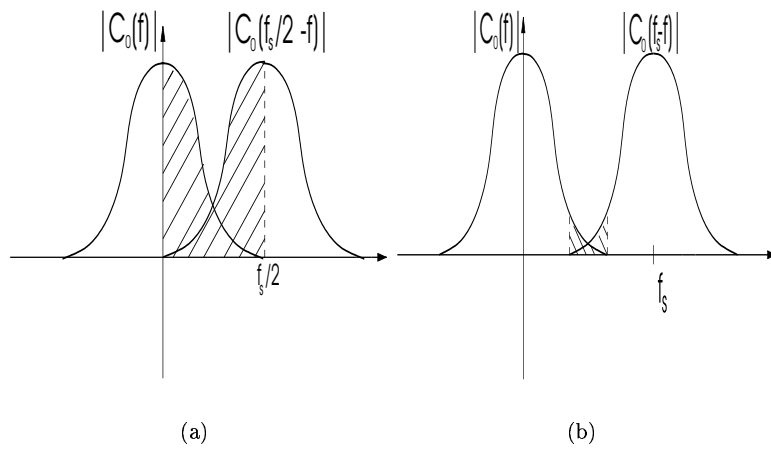
Fig. 5.6 Spectral overlapping for (a) the conjugate and (b) the nonconjugate cyclic autocorrelation functions
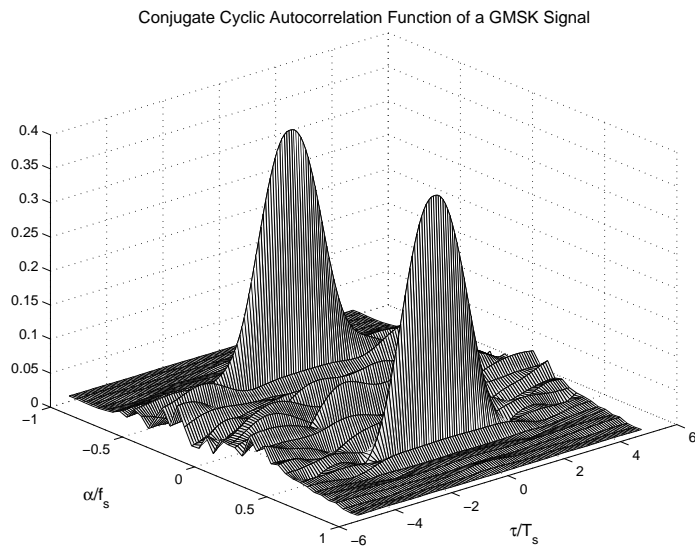

Fig. 5.7 Magnitude of the conjugate Cyclic Autocorrelation Function estimate of a base-band GMSK signal

function for this case can be given as:

$$R_{ss}^{kf_s}(\tau) = \frac{1}{T_s} \int_{-\infty}^{\infty} e^{-j2\pi[(f\tau+kf_s(\epsilon-\tau/2)]} C_0(f) C_0(kf_s - f) df \qquad (5.79)$$

The Effect of the Pulse Shape

Equations (5.78) and (5.79) show that the spectrum of the pulse function $c_0(t)$ determines the shape of both conjugate and nonconjugate autocorrelation functions of the signal. Since spectrum of the pulse, $C_0(f)$, associated with the linear part of the GMSK signal is very narrow, the spectral overlapping between $C_0(f)$ and $C_0(kf_s - f)$ in (5.79), which is illustrated in Fig. 5.6(b) for $k = 1$ is very small, leading to an almost total suppression of the nonconjugate cyclic autocorrelation function. However, the spectral overlapping between $C_0(f)$ and $C_0(kf_s/2 - f)$ which appears in the expression for the conjugate cyclic autocorrelation function, is much larger, as illustrated in Fig. 5.6(a), making the conjugate cyclic statictics of the GMSK signal the logical choice for the purpose of air interface identification.

The magnitude of the conjugate cyclic autocorrelation function $R_{ss*}^{\alpha}(\tau)$ of a GMSK signal with $BT_s = 0.3$ is shown in Fig. 5.7, where the discrete cyclic correlation surfaces of the signal at $\alpha = \pm f_s/2$ are clearly visible. The maximum amount of correlation occurs at $\tau = 0$.

5.3.3 OFDM Signals

In an OFDM system, the PSK or QAM modulated information symbols are transmitted over multiple carriers in parallel. OFDM uses overlapping carriers for the transmission. Therefore the symbol waveforms from one individual user modulated on different carriers overlap with each other in time and frequency. The baseband OFDM signal can be expressed as a sum of single carrier modulated signals

$$s(t) = \sqrt{\frac{1}{N_c}} \sum_{n=-\infty}^{\infty} \sum_{i=0}^{N_c-1} d_{n,i} e^{j2\pi i \Delta f(t-nT_s-\epsilon)} g_R(t-nT_s-\epsilon) e^{-j2\pi \frac{N_c-1}{2} \Delta f t} \quad (5.80)$$

where $d_{n,i}$ is the n'th information symbol modulated on the i'th carrier, N_c is the number of carriers, Δf is the carrier separation, ϵ is the unknown symbol timing and $g_R(t)$ is the rectangular pulse function of length T_s. $T_s = T_u + T_g$ is the symbol length, where $T_u = 1/\Delta f$ is the useful symbol duration and T_g is the length of the guard interval. Assuming that the OFDM
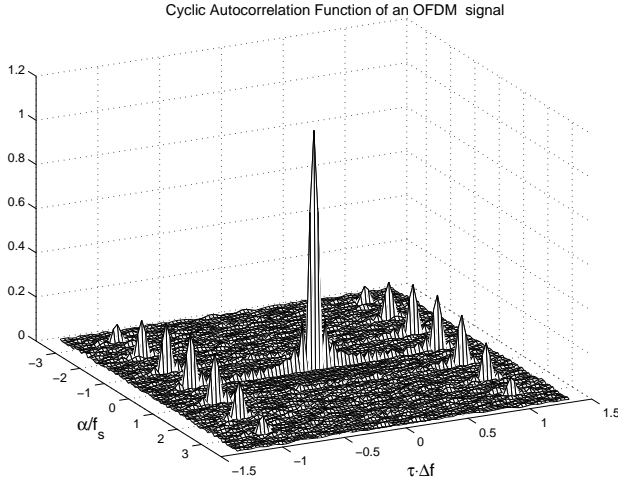
Fig. 5.8 Magnitude of the Cyclic Autocorrelation Estimate of an OFDM signal.

symbol is extended cyclically in the guard interval and that $d_{n,i}$ is centered i.i.d., the time varying autocorrelation of the signal can be expressed as:

$$R_{ss}(t + \tau/2+, t - \tau/2) = A \sum_{n=-\infty}^{\infty} \sum_{i=0}^{N_c-1} e^{j2\pi i \Delta f \tau} e^{-j2\pi \frac{N_c-1}{2} \Delta f \tau}$$

$$g_R(t - nT_s - \epsilon + \tau/2) g_R^*(t - nT_s - \epsilon - \tau/2)$$

with $A = \sigma_d^2/N_c$ and $\sigma_d^2 = E\{d_{n,i} d_{n,i}^*\}$. This expression can be further simplified to:

$$R_{ss}(t + \tau/2, t - \tau/2) = A \frac{\sin(\pi N_c \Delta f \tau)}{\sin(\pi \Delta f \tau)} \tag{5.81}$$

$$\cdot \sum_{n=-\infty}^{\infty} g_R(t - nT_s - \epsilon + \tau/2) g_R^*(t - nT_s - \epsilon - \tau/2)$$

It is easily seen that $R_{ss}(t + \tau/2, t - \tau/2)$ is periodic in t with a period equal to T_s, hence the OFDM signal exhibits nonconjugate cyclostationarity

with a cycle frequency $\alpha = k/T_s = kf_s$. The cyclic autocorrelation function can be calculated as:

$$R_{ss}^{kf_s}(\tau) = A\frac{sin(\pi N_c \Delta f\tau)\sin[\pi kf_s(T_s - |\tau|)]}{\pi k sin(\pi\Delta f\tau)}e^{j2\pi kf_s\epsilon} \tag{5.82}$$

The magnitude of the cyclic autocorrelation function for an OFDM signal with $N_c = 15$, $T_u = 16T_s/21$ is shown in Fig. 5.8, where the discrete cyclic autocorrelation surfaces at the harmonics of the symbol rate $\alpha = k/T_s = kf_s$ are perfectly discernible. The peaks of the cyclic autocorrelation occur at $\tau = \pm T_u = \pm 1/\Delta f$, where the factor $\frac{sin(\pi N_c \Delta f\tau)}{sin(\pi\Delta f\tau)}$ takes its maximum value.

5.3.4 CDMA Signals

In a CDMA system, the received signal consists of the sum of all the individual user signals. In section 5.2.7, we have established the fact that a composite signal which consists of the sum of statistically independent signals has a cyclic autocorrelation function which is the sum of individual cyclic autocorrelation functions. From this reason, the cyclic autocorrelation function of the total CDMA signal is equal to the sum of the cyclic autocorrelation functions of the received user signals, and depends on many factors, which include

- The total number of active users in the system,

- The nature of the user specific spreading codes employed by the individual users,

- Whether additional scrambling is employed or not, and the nature of the scrambling code used,

- The relative amplitudes, with which the individual user signals are received,

- The relative time difference of arrival of user signals.

In the following, we are going to demonstrate that signals of individual users exhibit cyclostationarity with cycle frequencies $f_s = 1/T_s$ and $f_c = 1/T_c$. The signal of the l'th user in a CDMA system can be given as

$$x_l(t) = \sum_{n=-\infty}^{+\infty}\sum_{q=1}^{Q} d_{n,l}c_{l,q}g(t - nT_s - qT_c - \epsilon_l) \tag{5.83}$$

Where $Q = T_s/T_c$ is the spreading sequence length, $d_{n,l}$ the data sequence of the l'th user and $c_{l,q}$ is the code sequence of the l'th user. The time varying autocorrelation function for this signal can be calculated as:

$$R_{x_l x_l}(t + \tau/2, t - \tau/2) = E\Big\{ \sum_{n=-\infty}^{+\infty} \sum_{m=-\infty}^{+\infty} \sum_{q=0}^{Q} \sum_{p=0}^{Q} d_{n,l} c_{l,q} d_{n,l}^* c_{l,p}^*$$

$$\cdot\ g(t - nT_s - qT_c - \epsilon_l + \tau/2)$$

$$\cdot\ g^*(t - mT_s - pT_c - \epsilon_l - \tau/2)\Big\} \qquad (5.84)$$

Which can be simplified to:

$$R_{x_l x_l}(t + \tau/2, t - \tau/2) = \sigma_d^2 \sum_{n=-\infty}^{+\infty} \sum_{q=0}^{Q} \sum_{p=0}^{Q} c_{l,q} c_{l,p}^*$$

$$\cdot\ g(t - nT_s - qT_c - \epsilon_l + \tau/2)$$

$$\cdot\ g^*(t - nT_s - pT_c - \epsilon_l - \tau/2) \qquad (5.85)$$

It can be easily seen that the inner double sum term in (5.85) represents the product of the shifted versions of the code sequence of length T_s. The outer summation term causes the repetition of the lag product with a period of T_s, thus, the signal exhibits nonconjugate cyclostationarity with a cycle frequency $1/T_s = f_s$. However, it is obvious that the cyclic autocorrelation function depends on the particular code sequence of the user:

$$R_{x_l x_l}^{k f_s}(\tau) = \frac{\sigma_d^2}{T_s} \int_{-\infty}^{\infty} e^{-j2\pi[(f\tau + k f_s(\epsilon - \tau/2)]} C_l(f) C_l(k f_s - f) df \qquad (5.86)$$

where $C_l(f)$ is the Fourier transform of the particular code waveform $c_l(t) = \sum_{q=1}^{Q} c_{l,q} g(t - qT_c)$. There are several practical problems associated with using the cyclostationarity with the symbol frequency f_s as a feature for air interface identification.

- Some CDMA systems, for example UTRA -FDD and -TDD allow the use of variable symbol rates, according to the user needs. This is accomplished by using spreading codes with different spreading factors. Hence, the individual user signals may have different symbol rates,

leading to different cycle frequencies for each user.

- In some cases, scrambling may be used in addition to the user specific spreading. Usually, scrambling is performed over multiple symbol periods, destroying the cyclostationarity with the symbol rate and introducing a new cyclostationarity with the reciprocal of the scrambling code length $1/T_{sc}$.

- Since we are in search of a general solution to the recognition problem, the dependence of the cyclic autocorrelation function on the particular code sequences is undesirable.

In the following, it is shown that the time varying autocorrelation function has a periodic component, which does not depend on the spreading code sequence. (5.85) can be rexpressed in the following manner:

$$
\begin{aligned}
R_{x_l x_l}(t + \tau/2, t - \tau/2) \;=\; & \sigma_d^2 \sum_{n=-\infty}^{+\infty} \sum_{q=1}^{Q} \sum_{\substack{p=1 \\ p \neq q}}^{Q} c_{l,q} c_{l,p}^* g(t - nT_s - qT_c - \epsilon_l + \tau/2) \\
& \cdot \; g^*(t - nT_s - pT_c - \epsilon_l - \tau/2) \\
+ \; & \sigma_d^2 \sum_{n=-\infty}^{+\infty} \sum_{q=1}^{Q} |c_{l,q}|^2 g(t - nT_s - qT_c - \epsilon_l + \tau/2) \\
& \cdot \; g^*(t - nT_s - qT_c - \epsilon_l - \tau/2) \qquad\qquad (5.87)
\end{aligned}
$$

Since $|c_{l,q}|^2 = 1$ and $QT_c = T_s$, the second term of (5.87) can be simplified to a simple summation

$$
\sigma_d^2 \sum_{q=-\infty}^{+\infty} g(t - qT_c - \epsilon_l + \tau/2) g^*(t - qT_c - \epsilon_l - \tau/2) \qquad\qquad (5.88)
$$

Note that this term is periodic with a period of T_c and does not depend on the particular user code, and it is actually the same term that appears in the time varying autocorrelation function of a linear modulated signal, as in (5.48). In other words, a single user signal always exhibits cyclostationarity with the chip rate $f_c = 1/T_c$, as a result of the impulse shaping, regardless of the structure or the length of the particular code employed. Thus, the cyclic autocorrelation function of a single CDMA signal consists of a code dependent component, which is nonzero for $\alpha = kf_s$ and a code
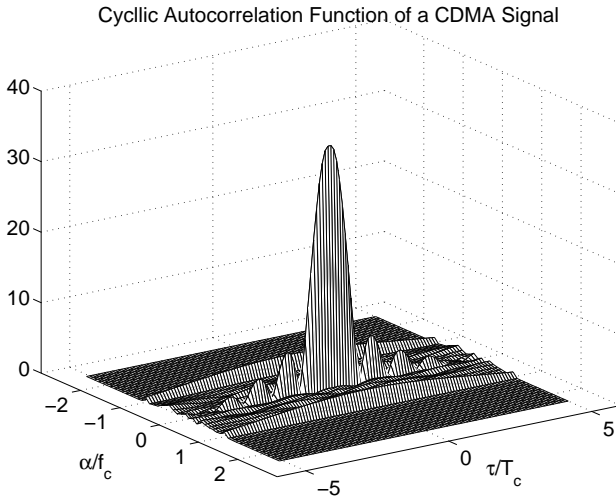
Cycllic Autocorrelation Function of a CDMA Signal

Fig. 5.9 Magnitude of the Cyclic Autocorrelation Estimate of a CDMA signal.

independent component, which is nonzero for $\alpha = k/T_c = kf_c$. It should also be noted that the chip rate $f_c = Qf_s$ itself is also an integer multiple of the symbol rate. From this reason, the total cyclic autocorrelation function at the cycle frequency $\alpha = k/T_c = kf_c$ has both a code dependent and a code independent component. However, it can be shown that the contribution from the code dependent term in (5.87) diminishes, as the aperiodic autocorrelation function [20] of the code sequence approaches the ideal delta function, which is desirable for CDMA code sequences, since codes with such autocorrelation properties are more robust against the effects of multipath propagation.

The code independent component in the cyclic autocorrelation function of the user signal remains unchanged even if scrambling is carried out. As a matter of fact, scrambling usually improves the autocorrelation characteristics of the user signals, further decreasing the code dependency. Since every user signal exhibits cyclostationarity with the chip rate of the system, the total received signal also exhibits cylostationarity with f_c. Therefore, exploiting the chip rate cyclostationarity is the logical choice for the purpose of air interface identification for a CDMA signal.

Fig. 5.9 displays the magnitude of the cyclic autocorrelation function of a synchronous CDMA signal, based on UTRA-FDD downlink specifications.

The number of users $L = 16$ and the spreading code length is $Q = 16$, the scrambling code length is $Q_{sc} = 38400$. The individual users employ QPSK modulation with root raised cosine pulse shape, using a roll-off factor $\rho = 0.22$. The cyclic autocorrelation surfaces at $\alpha = \pm f_c$ are clearly visible. The cyclostationarity caused by the scrambling sequence do not appear in this estimate, since the observation length of the estimator is shorter than the scrambling code period $T_{sc} = 38400 T_c$.

5.3.5   Spectral line generation

A signal $y(t)$ contains a finite strength additive sine wave component with frequency f_0, say $Ae^{j2\pi(f_0 t+\theta)}$ if the Fourier coefficient

$$b_{f_0} = \lim_{T\to\infty} \frac{1}{T} \int_{-T/2}^{T/2} y(t)e^{-j2\pi f_0 t}dt \tag{5.89}$$

is nonzero and is equal to $b_{f_0} = Ae^{j2\pi\theta}$. In this case, the power spectral density of $y(t)$ includes a spectral line at $f = f_0$. That is, the PSD contains the additive term

$$|b_{f_0}|^2\delta(f-f_0) \tag{5.90}$$

with the dirac delta function $\delta(\cdot)$

From the cycloergodic definitions of the cyclic autocorrelation functions given in (5.15) and (5.16), it is obvious that additive sine wave components can be regenerated from cyclostationary signals using so called delay-and-multiply (DM) nonlinearities, as illustrated in Fig. 5.10, where the optional complex conjugation operation has been denoted by $(*)$ and the delay parameter is denoted as T_d. The Fourier coefficients corresponding to the regenerated spectral lines can be expressed as:

$$b_{f_0} = \lim_{T\to\infty} \frac{1}{T} \int_{-T/2}^{T/2} x(t)x^*(t-T_d)e^{-j2\pi f_0 t}dt = R_{xx}^{f_0}(T_d)e^{-j2\pi f_0 T_d/2} \tag{5.91}$$

for the DM nonlinearity with complex conjugation and,

$$\tilde{b}_{f_0} = \lim_{T\to\infty} \frac{1}{T} \int_{-T/2}^{T/2} x(t)x(t-T_d)e^{-j2\pi f_0 t}dt = R_{xx^*}^{f_0}(T_d)e^{-j2\pi f_0 T_d/2} \tag{5.92}$$
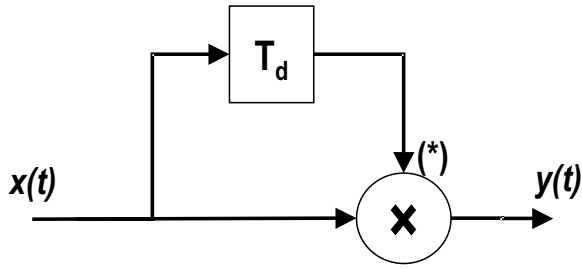
Fig. 5.10 The Delay-and- Multiply nonlinearity

for the DM device without complex conjugation operation respectively. Thus, the intensity of the spectral line regenerated by a delay-and-multiply device is actually equal to the magnitude of the corresponding (conjugate or non-conjugate) cyclic autocorrelation function at $\alpha = f_0$ and $\tau = T_d$. Therefore, in order to regenerate the spectral line with maximum possible intensity at the frequency f_0, the delay parameter T_d has to be chosen such that it samples the corresponding cyclic autocorrelation surface at is maximum value. This interpretation also clarifies the reason, why, traditionally, the delay parameter is chosen as $T_d = T_s/2$ for regenerating symbol rate spectral lines for linear modulated signals: From Fig. 5.1 it is obvious that for linear modulated signals with rectangular pulse shapes, the cyclic autocorrelation surface corresponding to $\alpha = 1/T_s$ exhibits maxima at $\tau = \pm T_s/2$, and it has a zero at $\tau = 0$. However, if a pulse shape with root raised cosine spectrum is used, the optimum value of the delay parameter is $T_d = 0$, which can be seen in Fig. 5.4.

GMSK-specific spectral lines

Since the GMSK signal exhibits both conjugate and nonconjugate cyclostationarity, both versions of the DM device can be employed for the spectral line generation.

Figs. 5.11 and 5.12 display the spectral lines regenerated from a GMSK signal with $BT_s = 0.3$ by a DM device with complex conjugation operation, which corresponds to the nonconjugate cyclic autocorrelation function, and by a DM nonlinearity without complex conjugation, which corresponds to the conjugate cyclic autocorrelation function respectively. For both cases, the delay is chosen as $T_d = 0$ in order to regenerate the optimum spectral lines. As discussed in section 5.3.2, the GMSK signal exhibits nonconjugate cyclostationarity with a cycle frequency $\alpha = 1/T_s = f_s$, however $R_{xx}^{f_s}(\tau)$
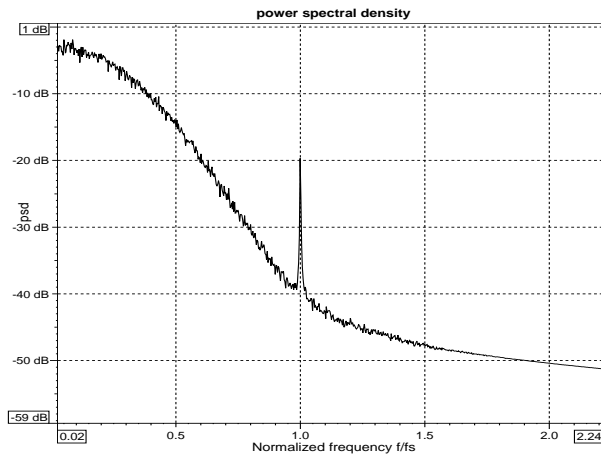
Fig. 5.11 PSD of the DM output for a GMSK signal (with complex conjugation)
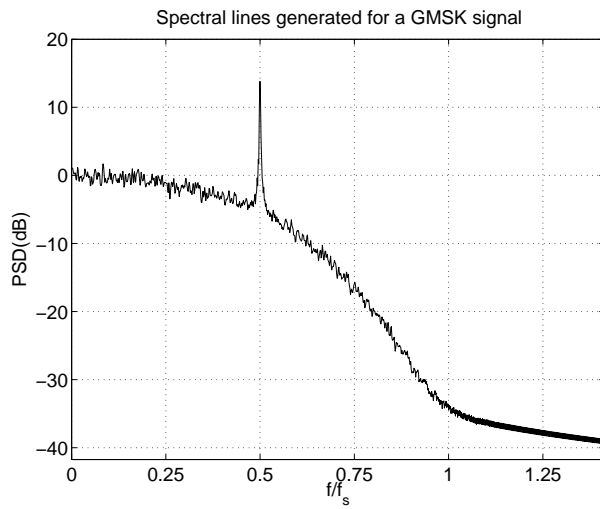
Fig. 5.12 PSD of the DM output for a GMSK signal (without complex conjugation)
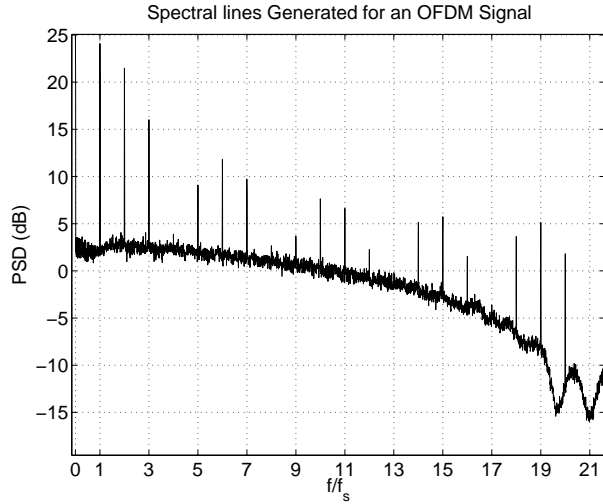
Fig. 5.13 PSD of the DM output for an OFDM signal (with complex conjugation)

is very weak because of the pulse shape involved. Therefore, the spectral line at $f = f_s$ in Fig. 5.11 is also very weak and difficult to detect under noise. Nonetheless, as expected, the spectral line at $f = f_s/2$ in Fig. 5.12 corresponding to $R_{xx^*}^{f_s/2}(T_d)$ is fairly strong and much easier to detect.

OFDM-specific spectral lines

The OFDM signal exhibits only nonconjugate cyclostationarity, hence a DM with complex conjugation has to be used for spectral line regeneration. The PSD of the DM output for the OFDM signal of section 5.3.3 is displayed in Fig. 5.13, where the spectral lines corresponding to discrete cyclic autocorrelation surfaces at harmonics of $1/T_s$ are perfectly visible. The delay parameter is chosen as $T_d = 1/\Delta f$, where the cyclic autocorrelation exhibits sharp peaks.

CDMA-specific spectral lines

Finally, the DM output for the CDMA signal described in section 5.3.4 is displayed in Fig. 5.14. $T_d = 0$ was chosen to obtain the spectral line at $f = 1/T_c = f_c$ with the maximum possible intensity.
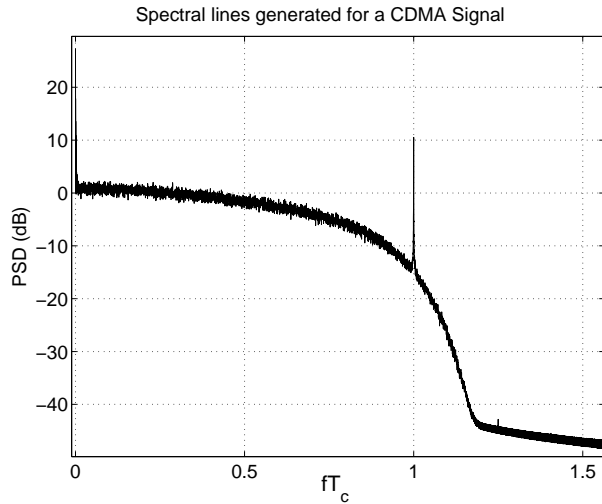
Fig. 5.14 PSD of the DM output for a CDMA signal (with complex conjugation)

Regeneration of spectral lines using a delay and multiply device has been used in the literature for presence detection of DS/SS signals under noise in [45] and [46], for the detection of the channel allocation information in a spectrum pooling system in [47], for modulation type classification of PSK and MSK signals in [48] or for synchronization purposes in [49]. However, this papers have analysed the spectral line regeneration without any mention of the concept of cyclostationarity.

5.3.6   Summary

The cyclostationary signal analysis provided in this section shows that signals from different air interfaces exhibit different kinds of cyclostationarity for different values of the parameters α and τ. Each of the investigated signal types has shown conjugate and/or nonconjugate cyclostationary behaviour with cycle frequencies and delays related to the symbol or chip rates of the particular system. Table 5.1 summarizes the results of the analysis from this section, where τ_0 denotes the value of the lag parameter, for which the cyclic autocorrelation surfaces take their maximum value.

Assuming that the Software Radio receiver knows the particular cyclostationary behavior of each air interface signal to be recognized, which is

Signal Type	Nonconjugate cyclostationarity	Conjugate cyclostationarity	τ_0
Linear modulated with rectangular pulse	$\alpha_0 = 1/T_s$	N/A	$T_s/2$
Linear modulated with rrc pulse	$\alpha_0 = 1/T_s$	N/A	0
GMSK	$\alpha_0 = 1/T_s$	$\alpha_0 = 1/2T_s$	0 for both
OFDM	$\alpha_0 = 1/T_s$	N/A	$1/\Delta f$
CDMA with rrc pulse	$\alpha_0 = 1/T_c$	N/A	0

Tab. 5.1 Cyclostationary behaviour of different signal types

in concurrence with the SR structure displayed in Fig. 1.1, the problem of air interface recognition reduces itself to the detection of the presence of a particular cyclic signature, i.e. to the detection of cyclostationary behaviour in the received signal for certain values of α and τ. The next section investigates an asymptotically constant false alarm rate (CFAR) test, which is devised exactly for this purpose.

5.4   A CFAR Test for Detection of Cyclostationary Behaviour

This section provides a method for detecting the presence of cyclostationarity in a given signal employing the statistical test for the presence of conjugate cyclostationarity, which has been developed by Dandawate in [50] for discrete time processes which exhibit conjugate cyclostationarity, on the oversampled received signal $x[i] = x(iT_{sample})$ and show that it can be extended to detect nonconjugate cyclostationarity also.

The test provided in this section checks for a given cycle frequency $\alpha = \alpha_0$, the presence of the conjugate cyclostationarity from a data segment of length T_o. The discrete time version of the estimation of the conjugate cyclic autocorrelation function is given as [50]:

$$\hat{R}_{xx^*}^\alpha(v) = \frac{1}{T_o} \sum_{i=0}^{T_o-1} x[i]x[i+v]e^{-j2\pi\alpha i} \tag{5.93}$$

with v the discrete version of the lag parameter τ. Here, the assymetric definition of the conjugate cyclic autocorrelation function is used, since $v/2$ does not exist for odd values of v in the discrete lag domain.

The conjugate cyclic autocorrelation estimate can be written as the sum of the actual value and the estimation error $\Delta_{xx^*}^{\alpha}(v)$

$$\hat{R}_{xx^*}^{\alpha}(\nu) = R_{xx^*}^{\alpha}(v) + \Delta_{xx^*}^{\alpha}(v) \tag{5.94}$$

Considering the general case, where presence of cycles has to be checked for a set of lags v, rather than a single one, a $1 \times 2N$ row vector consisting of conjugate cyclic autocorrelation estimates at the cycle frequency $\alpha = \alpha_0$ can be defined as follows:

$$\begin{aligned}
\hat{\mathbf{r}}_{\mathbf{xx}^*} &= \left[Re\left\{\hat{R}_{xx^*}^{\alpha_0}(v_1)\right\}, ..., Re\left\{\hat{R}_{xx^*}^{\alpha_0}(v_N)\right\} \right. \\
&\quad \left. , Im\left\{\hat{R}_{xx^*}^{\alpha_0}(v_1)\right\}, ..., Im\left\{\hat{R}_{xx^*}^{\alpha_0}(v_N)\right\} \right]
\end{aligned} \tag{5.95}$$

with the fixed lags $v_1, ..., v_N$. The row vector of the true values of the conjugate cyclic autocorrelation $\mathbf{r}_{\mathbf{xx}^*}$ is defined similarly as:

$$\begin{aligned}
\mathbf{r}_{\mathbf{xx}^*} &= \left[Re\left\{R_{xx^*}^{\alpha_0}(v_1)\right\}, ..., Re\left\{R_{xx^*}^{\alpha_0}(v_N)\right\} \right. \\
&\quad \left. , Im\left\{R_{xx^*}^{\alpha_0}(v_1)\right\}, ..., Im\left\{R_{xx^*}^{\alpha_0}(v_N)\right\} \right]
\end{aligned} \tag{5.96}$$

and the estimation error vector $\boldsymbol{\Delta}_{\mathbf{xx}^*}$

$$\begin{aligned}
\boldsymbol{\Delta}_{\mathbf{xx}^*} &= \left[Re\left\{\Delta_{xx^*}^{\alpha_0}(v_1)\right\}, ..., Re\left\{\Delta_{xx^*}^{\alpha_0}(v_N)\right\} \right. \\
&\quad \left. , Im\left\{\Delta_{xx^*}^{\alpha_0}(v_1)\right\}, ..., Im\left\{\Delta_{xx^*}^{\alpha_0}(v_N)\right\} \right]
\end{aligned} \tag{5.97}$$

so that we can write

$$\hat{\mathbf{r}}_{\mathbf{xx}^*} = \mathbf{r}_{\mathbf{xx}^*} + \boldsymbol{\Delta}_{\mathbf{xx}^*} \tag{5.98}$$

Using this vector-matrix notation, the detection of the presence of conjugate cyclostationarity can be formulated in terms of a binary hypothesis testing problem. Given that the hypothesis H_0 represents the case where $x(t)$ does not exhibit conjugate cyclostationarity with the cycle frequency α_0 and the hypothesis H_1 represents the case where $x(t)$ does exhibit conjugate cyclostationarity, the following binary hypothesis testing problem can be formulated:

$H_0 : \alpha_0$ is not a cycle frequency $\forall v \in \{v_n\}_{n=1}^N \Rightarrow \hat{\mathbf{r}}_{\mathbf{xx}^*} = \mathbf{\Delta}_{\mathbf{xx}^*}$
$H_1 : \alpha_0$ is a cycle frequency for some $v \in \{v_n\}_{n=1}^N \Rightarrow \hat{\mathbf{r}}_{\mathbf{xx}^*} = \mathbf{r}_{\mathbf{xx}^*} + \mathbf{\Delta}_{\mathbf{xx}^*}$

Since $\mathbf{r}_{\mathbf{xx}^*}$ is nonrandom, the distribution of $\hat{\mathbf{r}}_{\mathbf{xx}^*}$ under H_0 and H_1 differs only in mean.

Devising a decision strategy for this binary hypothesis testing problem requires the knowledge of the distribution of $\mathbf{\Delta}_{\mathbf{xx}^*}$, which is unknown, because the distribution of the data is not known to the air interface recognition subsystem of the software radio under the hypothesis H_0. Therefore, in [50], it has been proposed to exploit the asymptotic properties of the cyclic autocorrelation estimators to infer the asymptotic properties of the estimation error vector $\mathbf{\Delta}_{\mathbf{xx}^*}$.

5.4.1 Asymptotic Statistics of the Conjugate Cyclic Autocorrelation Estimators

It is easily seen that $\hat{R}_{xx^*}^\alpha(v)$ is an unbiased estimate of $R_{xx^*}^\alpha(v)$. Hence, the estimation error $\Delta_{xx^*}^\alpha(v)$ vanishes as $T_0 \to \infty$. In his work, Dandawate has shown that it is also a consistent estimate and the quantity $\sqrt{T_o}\hat{R}_{xx^*}^\alpha(v)$ is asymptotically complex normal distributed, provided that $x(t)$ fullfils a so called *mixing condition* (See appendix A for details). The complex normality has been proven by showing that cumulants of orders ≥ 3 of $\sqrt{T_o}\hat{R}_{xx^*}^\alpha(v)$ vanish asymptotically, i.e. as $T_o \to \infty$, which is a direct result of the abovementioned mixing condition [50]. Furthermore, in the same paper, he has demonstrated that its covariance can be expressed in terms of the conjugate and nonconjugate cross spectral correlation density functions of the lag products $f_v[i] = x[i]x[i+v]$.

$$\lim_{T_o \to \infty} T_o cov(\hat{R}_{xx^*}^\alpha(v), \hat{R}_{xx^*}^\beta(\rho)) = S_{f_v f_\rho^*}^{\alpha+\beta}(\beta)$$

$$\lim_{T_o \to \infty} T_o cov(\hat{R}_{xx^*}^\alpha(v), (\hat{R}_{xx^*}^\beta(\rho))^*) = S_{f_v f_\rho}^{\alpha-\beta}(-\beta) \tag{5.99}$$

Where the cross spectral density functions are defined as:

$$S_{f_v f_\rho^*}^\alpha(f) = \lim_{T_o \to \infty} \frac{1}{T_o} \sum_{i=0}^{T_o-1} \sum_{\xi=-\infty}^{\infty} cov(f_v[i], f_\rho[i+\xi]) e^{-j2\pi f\xi} e^{-j2\pi \alpha t} \tag{5.100}$$

and

$$S^{\alpha}_{f_v f_\rho}(f) = \lim_{T_o \to \infty} \frac{1}{T_o} \sum_{i=0}^{T_o-1} \sum_{\xi=-\infty}^{\infty} cov(f_v[i], f_\rho^*[i+\xi]) e^{-j2\pi f\xi} e^{-j2\pi\alpha t} \quad (5.101)$$

From these results, it can be concluded that the distribution of the estimation error vector converges asymptotically to a normal distribution:

$$\lim_{T_o \to \infty} \sqrt{T_o} \boldsymbol{\Delta}_{\mathbf{xx^*}} \overset{D}{=} \mathcal{N}(\mathbf{0}, \boldsymbol{\Sigma}_{\mathbf{xx^*}}) \qquad (5.102)$$

where $\overset{D}{=}$ denotes the convergence in distribution and $\mathcal{N}(\mathbf{0}, \boldsymbol{\Sigma}_{\mathbf{xx^*}})$ is a multivariate normal distribution with mean 0 and covariance matrix $\boldsymbol{\Sigma}_{\mathbf{xx^*}}$, which depends on the particular signal. Using (5.99), the covariance matrix can be expressed as:

$$\boldsymbol{\Sigma}_{\mathbf{xx^*}} = \begin{bmatrix} \mathbf{Re}\left\{\frac{\mathbf{Q}^{(*)}+\mathbf{Q}}{2}\right\} & \mathbf{Im}\left\{\frac{\mathbf{Q}^{(*)}-\mathbf{Q}}{2}\right\} \\ \mathbf{Im}\left\{\frac{\mathbf{Q}^{(*)}+\mathbf{Q}}{2}\right\} & \mathbf{Re}\left\{\frac{\mathbf{Q}-\mathbf{Q}^{(*)}}{2}\right\} \end{bmatrix} \qquad (5.103)$$

The (l, m)th entries of the complex covariance matrices $\mathbf{Q}^{(*)}$ and $\mathbf{Q}$ are given as

$$\mathbf{Q}^{(*)}(l, m) = S^{2\alpha_0}_{f_{v_l} f^*_{v_m}}(\alpha_0)$$

$$\mathbf{Q}(l, m) = S^{0}_{f_{v_l} f_{v_m}}(-\alpha_0) \qquad (5.104)$$

Since the asymptotic statistics of the estimation error is known, the generalized likelihood principle can be employed to generate a suitable decision statistics for the binary hypothesis test.

5.4.2   The Generalized Likelihood Principle

One of the most celebrated methods in the statistics is the so called likelihood ratio test. It provides a powerful tool, which is used in many applications in communication theory, especially in hypothesis testing problems, such as detection. Consider the binary hypothesis testing problem, where the hypotheses H_0 and H_1 have the a-priori probabilities $P(H_1) = 1 - P(H_0)$, and a decision has to be made based on the observation r. The maximum a

posteriori decision rule leads to a decision for H_1 if

$$P(H_1|r) > P(H_0|r) \tag{5.105}$$

and for H_0 otherwise. The conditional probability density functions of the random variable r are called the likelihood functions and are defined as:

$$p(r|H_0) = p_0(r)$$

$$p(r|H_1) = p_1(r) \tag{5.106}$$

and using Bayes' rule, the maximum a posteriori decision can be rexpressed as

$$\frac{p_1(r)}{p_0(r)} > \frac{(1 - P(H_1))}{P(H_1)} \tag{5.107}$$

The ratio $\lambda(r) = \frac{p_0(r)}{p_1(r)}$ is referred to as the likelihood ratio, and a test based on $\lambda(r)$ is called a likelihood ratio test. Generally, it is more convenient to use the natural logarithm of the likelihood ratio, which is referred to as the log likelihood ratio $\ln(\lambda(r))$, which is a permissible approach, since the natural logarithm is a monotonic increasing function [51]. The likelihood ratio is also encountered in detection problems with different optimality criteria, in which cases only the term on the right-hand side of the inequality changes. If the both hypotheses are equiprobable, we get the so called maximum likelihood detection. For known signals under AWGN, this test leads to the well known matched filter receiver.

For detecting signals with unkown or random parameters, an a-priori probability density function for these parameters can be assumed, and an averaged likelihood ratio can be generated using these probability density functions. i.e.

$$\lambda(r) = \frac{\int_{\{\theta\}} p_1(r|\theta)w(\theta)d\theta}{\int_{\{\phi\}} p_0(r|\phi)v(\phi)d\phi} \tag{5.108}$$

where θ and ϕ are the unknown random parameters, and $w(\theta)$and $v(\phi)$ are the probability density functions of these parameters (known or assumed). If no knowledge about the distribution of the parameters exits and it is not appropriate to assume any such distribution, the so called *generalized*

likelihood principle can be applied [51].

$$\lambda(r) = \frac{max_{\{\theta\}} p_1(r|\theta)}{max_{\{\phi\}} p_0(r|\phi)} \tag{5.109}$$

That is, the values of θ and ϕ are used, which maximize the likelihood functions. It should be noted that this is an inituitive solution to this problem, and may not necessarily lead to optimum detection in the sense of maximizing the detection probabilities or minimizing the error rates, however, it provides a useful tool for certain detection problems. The values of θ and ϕ, that maximize $p_1(r|\theta)$ and $p_0(r|\phi)$ are the so caled maximum likelihood estimates of these parameters, and are denoted as $\hat{\theta}$ and $\hat{\phi}$. Thus, the generalized likelihood principle can be summarized as follows:

- From the received data, form the maximum likelihood estimates of the unknown parameters.

- Use these estimates in the likelihood ratio, as if they were the true values of the parameters.

Actually, this detector is the same as the maximum likelihood receiver for completely known signals, the only difference being that the estimated values of the parameters are used instead of the true but unknown parameters.

In the following, the detection problem of unknown but nonrandom signals under noise in the context of generalized likelihood ratio test is investigated. Consider the binary hypothesis testing problem:

$$H_1 : \mathbf{r} = \mathbf{Hs} + \mathbf{n}$$

$$H_0 : \mathbf{r} = \mathbf{n} \tag{5.110}$$

where $\mathbf{n}$ is a zero mean multivariate Gaussian distribution and $\mathbf{s}$ is a nonrandom but unknown signal. The probability density functions of $\mathbf{r}$ under both hypotheses differ only in mean, hence the likelihood functions for this hypothesis test can be expressed as:

$$p_0(\mathbf{r}) = \frac{1}{(2\pi)^{n/2}|\mathbf{\Sigma}|^{1/2}} exp\Big(\frac{-\mathbf{r^T\Sigma^{-1}r}}{2}\Big) \tag{5.111}$$

and

$$p_1(\mathbf{r}|\mathbf{s}) = \frac{1}{(2\pi)^{n/2}|\mathbf{\Sigma}|^{1/2}} exp\Big(\frac{-(\mathbf{r} - \mathbf{Hs})^{\mathbf{T}}\mathbf{\Sigma}^{-1}(\mathbf{r} - \mathbf{Hs})}{2}\Big) \qquad (5.112)$$

where $\mathbf{\Sigma}$ is the covariance matrix of $\mathbf{n}$. If $\mathbf{s}$ were completely known, the log likelihood ratio would be calculated as:

$$ln(\lambda(\mathbf{r})) = \ln\Big(\frac{\mathbf{p_1(r)}}{\mathbf{p_0(r)}}\Big) = \mathbf{r}^{\mathbf{T}}\mathbf{\Sigma}^{-1}\mathbf{Hs} - \frac{1}{2}\mathbf{s}^{\mathbf{T}}\mathbf{H}^{\mathbf{T}}\mathbf{\Sigma}^{-1}\mathbf{Hs} \qquad (5.113)$$

In this case, the first term would be used as decision statistic, since the second term does not depend on $\mathbf{r}$. Since $\mathbf{s}$ is an unknown nonrandom signal, we can use the generalized likelihood principle from (5.109), substituting $\mathbf{s}$ with its maximum likelihood estimate $\hat{\mathbf{s}}$, which is given as [51]:

$$\hat{\mathbf{s}} = (\mathbf{H}^{\mathbf{T}}\mathbf{\Sigma}^{-1}\mathbf{H})^{-1}\mathbf{H}^{\mathbf{T}}\mathbf{\Sigma}^{-1}\mathbf{r}, \qquad (5.114)$$

provided that $(\mathbf{H}^{\mathbf{T}}\mathbf{\Sigma}^{-1}\mathbf{H})$ is not singular. Hence, the generalized likelihood decision statistics for this binary Hypothesis testing problem is

$$Z = \mathbf{r}^{\mathbf{T}}\mathbf{\Sigma}^{-1}\mathbf{H}(\mathbf{H}^{\mathbf{T}}\mathbf{\Sigma}^{-1}\mathbf{H})^{-1}\mathbf{H}^{\mathbf{T}}\mathbf{\Sigma}^{-1}\mathbf{r} = \mathbf{r}^{\mathbf{T}}\mathbf{\Sigma}^{-1}\mathbf{r} \qquad (5.115)$$

The decision statistic Z has a quadratic form and can be viewed as a weighted energy detector. In the special case, where $\mathbf{n}$ is uncorrelated, Z would be proportional to $\mathbf{r}^{\mathbf{T}}\mathbf{r} = \sum \mathbf{r_i^2}$ which is the energy of the received signal $\mathbf{r}$.

5.4.3   The Decision Statistics

Because of the asymptotic normality of $\sqrt{T_o}\mathbf{\Delta_{xx^*}}$, the test statistics from (5.115) can be directly applied to the binary hypothesis test at hand, with $\mathbf{H} = \mathbf{I}$:

$$Z_{xx^*} = T_o\hat{\mathbf{r}}_{\mathbf{xx^*}}\hat{\mathbf{\Sigma}}_{\mathbf{xx^*}}^{-1}\hat{\mathbf{r}}_{\mathbf{xx^*}}^{\mathbf{T}} \qquad (5.116)$$

where $\hat{\mathbf{\Sigma}}_{\mathbf{xx^*}}$ is the estimated covariance matrix.

It can be shown that, under H_0, the distribution of Z_{xx^*} converges asymptotically to a central χ^2 distribution with $2N$ degrees of freedom, irrespective of the distribution of the input data (see [50], also Appendix A). Hence, for a given threshold, the false alarm probabilities can be analy-

tically calculated for sufficiently large observation lengths T_o , regardless of the particular signal, leading to an asymptotically constant false alarm rate (CFAR) test. One can write, under H_0:

$$\lim_{T_o \to \infty} Z_{xx^*} \overset{D}{=} \chi^2_{2N} \tag{5.117}$$

where the pdf of the χ^2_{2N} distribution is given as

$$p_Y(y) = \frac{1}{2^N (N-1)!} y^{N-1} e^{-y/2} \tag{5.118}$$

On the other hand, under H_1, the distribution of the test statistics Z_{xx^*} converges approximately to a normal distribution [50], :

$$\lim_{T_o \to \infty} Z_{xx^*} \overset{D}{\approx} \mathcal{N}(T_o \mathbf{r_{xx^*}} \mathbf{\Sigma_{xx^*}^{-1}} \mathbf{r_{xx^*}^T}, 4T_o \mathbf{r_{xx^*}} \mathbf{\Sigma_{xx^*}^{-1}} \mathbf{r_{xx^*}^T}) \tag{5.119}$$

The test from (5.116) allows the detection of the cyclic signature of signals exhibiting conjugate cyclostationarity, such as the GSM and DECT signals. To be able to recognize signals exhibiting nonconjugate cyclostationarity, such as the CDMA and OFDM signals, this test has to be modified. Following the same line of reasoning as in [50], using the mixing condition of (A.4), a similar test can be derived for the presence of nonconjugate cyclostationarity, which has the same asymptotic characteristics as (5.116). Defining the discrete time estimate of the nonconjugate cyclic autocorrelation function as

$$\hat{R}_{xx}^\alpha(v) = \frac{1}{T_o} \sum_{i=0}^{T_o-1} x[i]x^*[i+v]e^{-j2\pi\alpha i} = R_{xx}^\alpha(v) + \Delta_{xx}^\alpha(v)$$

and the vectors $\mathbf{r_{xx}}$, $\mathbf{\hat{r}_{xx}}$, $\mathbf{\Delta_{xx}}$ similar to (5.95), the decision statistics for this case can be given as:

$$Z_{xx} = T_o \mathbf{\hat{r}_{xx}} \mathbf{\hat{\Sigma}_{xx}^{-1}} \mathbf{\hat{r}_{xx}^T} \tag{5.120}$$

The calculation of the entries of the covariance matrix $\mathbf{\hat{\Sigma}_{xx}}$ is performed in a similar fashion as in the previous case (see (5.104)), this time using the cross spectral correlation density functions of the conjugate lag products $\tilde{f}_v[i] = x[i]x^*[i+v]$ instead of $f_v[i]$.
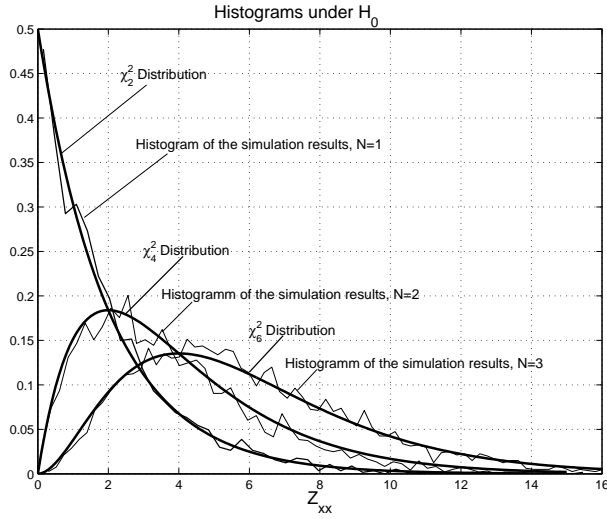
Fig. 5.15 The histograms of Z_{xx} under H_0

As discussed above, the variance normalization which is carried out in the generation of the test statistics makes the thresholding required for a certain false alarm rate P_f independent from the particular signal at hand, since the distribution of the decision statistics approaches a χ^2_{2N} distribution for sufficiently large observation intervals. Figure 5.15 displays the histogram of the simulation results for the decision statistic Z_{xx} for various values of N under H_0 with 3000 detection runs. The decision statistics is generated by searching for nonconjugate cyclostationarity in an OFDM signal with symbol rate f_s at a cycle frequency $\alpha = 1.3125 f_s$. The signal is further contaminated by AWGN with SNR=10dB. As seen in Fig. 5.15, the simulation results and the theoretical χ^2_{2N} distributions agree very well, supporting the theoretical results.

In our investigations, we have observed that using $N > 1$ decreases the detection performance, which can be attributed to two main reasons

- The mean and variance of the decision statistics under H_0 increases linearly with N, requiring a higher threshold for the same false alarm rate [14].

- As long as one of the v's is chosen such that $\hat{R}^\alpha_{xx^*}(v)$ corresponds to the maximum value of the cyclic autocorrelation function under H_1,
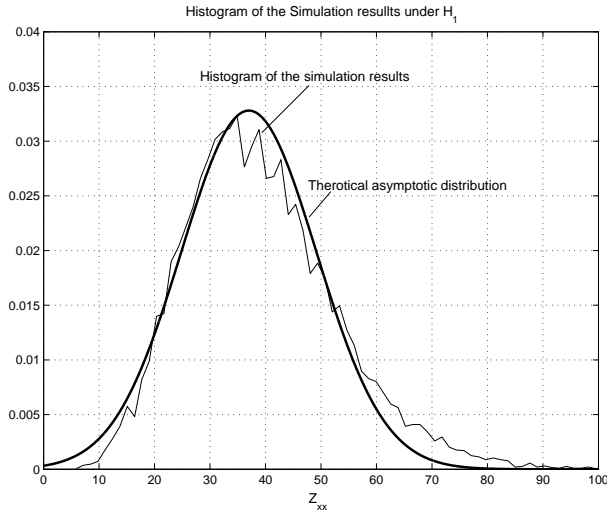
Fig. 5.16 The histogram of Z_{xx} under H_1, QPSK signal plus 3dB Noise

> using additional estimates at other values of the lag parameter ob-
> viously contributes more measurement noise to the detection statistic,
> increasing the variance and decreasing the detection performance.

In light of the discussion above, in all the following simulations, N is cho-
sen as $N = 1$ and the lag parameter v is chosen such that it samples the
corresponding cyclic Autocorrelation function at its maximum. Fig. 5.16
compares the histogram of the simulation results for the detection statistics
under H_1 for a QPSK signal with rectangular pulse shape under AWGN with
SNR=3dB and 6000 detection runs with the theoretical asymptotic distribu-
tion from (5.119). The theoretical and simulated curves agree for the most
part, except at the tails.

5.4.4 Implementation Issues

The test statistics from (5.116) and (5.120) can be generated in practice
by using computationally efficient FFT based algortihms, since entries of
the $\hat{\mathbf{r}}_{\mathbf{xx}}$ and $\hat{\mathbf{r}}_{\mathbf{xx}^*}$ are basically the Fourier transforms of the lag products
$\tilde{f}_v[i]$ and $f_v[i]$ respectively, at a fixed frequency α_0. Sample rate coversion
techniques may be required to place α_0 exactly at the center of an FFT bin,
since using an ADC with a fixed master clock rate is more practicable [52].

In the estimation of the entries of the covariance matrices $\hat{\mathbf{\Sigma}}_{\mathbf{xx}}$ and $\hat{\mathbf{\Sigma}}_{\mathbf{xx}^*}$ FFT based frequency smoothing methods can be used[50]. In the following simulations, a frequency smoothing technique with a Kaiser Window of parameter $\beta_K = 10$ has been employed.

5.4.5   Simulation Results

This section provides simulation results for the performance of the statistical tests from (5.116) and (5.120) in detecting the cyclic signatures of four different air interface signals described in previous sections, under realistic multipath conditions.

The GSM Signal

For the GSM signal described in the previous sections, Z_{xx^*} is used as the detection statistic, in order to detect the presence of the conjugate cyclostationarity in the received signal for $\alpha_0 = f_s/2$ and $\tau = 0$. Fig 5.17 displays the detection probability P_d vs. SNR for several values of T_o and $P_f = 0.05$, both for AWGN and multipath cases. The effects of multipath propagation are modeled using the typical urban channel model [53] with user speeds of 15m/s. As seen in Fig. 5.17 frequency selective multipath fading channel decreases the detection performance greatly. However, satisfactory detection results can be achieved for moderate detection intervals and SNR $\geq$ 6dB. Fig. 5.18 displays the receiver operation characteristics (i.e. P_d vs. P_f) of the detector for a fixed SNR of 3dB. Figures 5.17 and 5.18 indicate that increasing the observation length T_o improves the detection perfomance, however, a saturation effect takes place as T_o grows.

The DECT Signal

For the DECT signal, Z_{xx^*} is used as the detection statistic, in order to detect the presence of the conjugate cyclostationarity in the received signal with $\alpha_0 = f_s/2$ and $\tau = 0$. The Indoor B model [54] with user speeds of 5m/s is used for modelling the radio propagation channel. Fig 5.19 displays P_d vs. SNR for several values of T_o and $P_f = 0.05$. Comparing the AWGN curves from Figs. 5.19 and 5.17, we see that the detection performance for the DECT signal is significanty better than for GSM, which comes from the fact that the DECT signal, with a BT_s product of 0.5, has a wider pulse spectrum than the GSM signal with $BT_s = 0.3$. Fig. 5.20 displays the receiver operation characteristics (ROC) of the detector for a fixed SNR of 3dB.
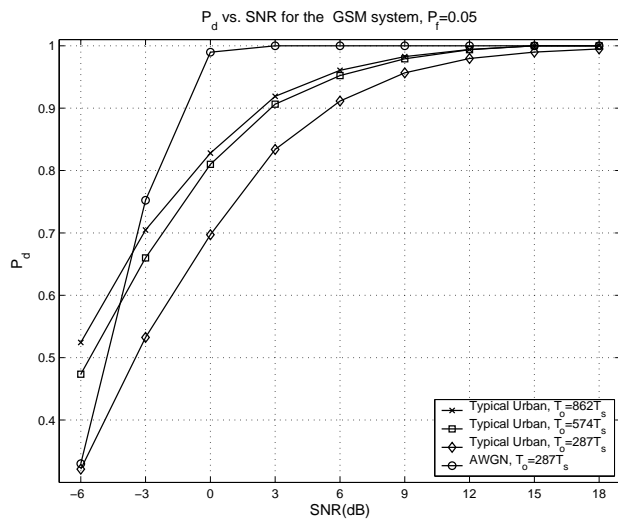
Fig. 5.17 P_d vs SNR for $P_f = 0.05$ for the GSM signal.

Fig. 5.18 The Receiver Operating Characteristics for the GSM Signal
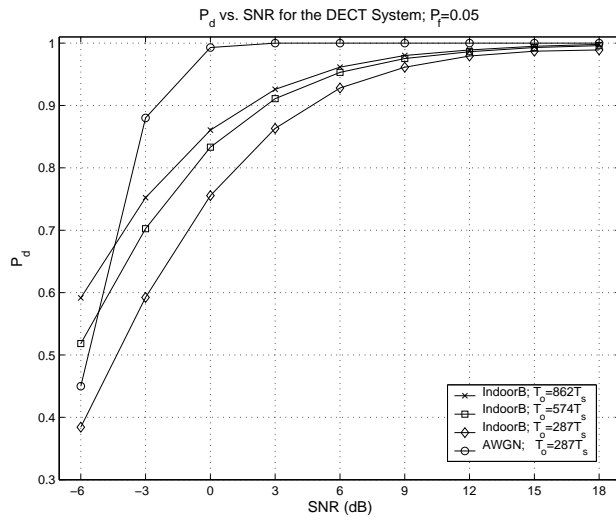
Fig. 5.19 P_d vs SNR for $P_f = 0.05$ for the DECT system.

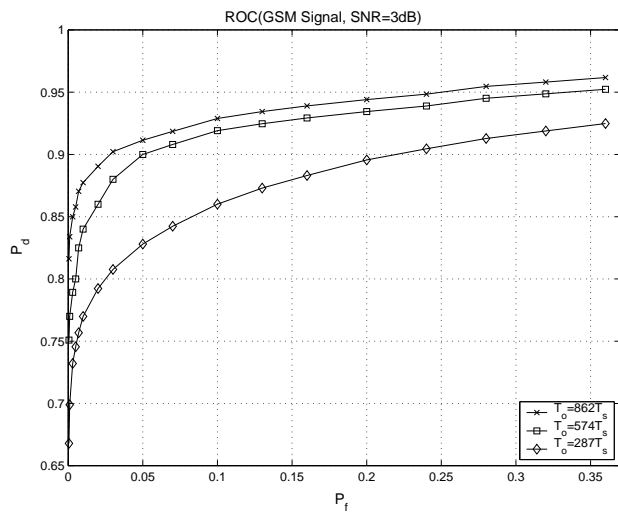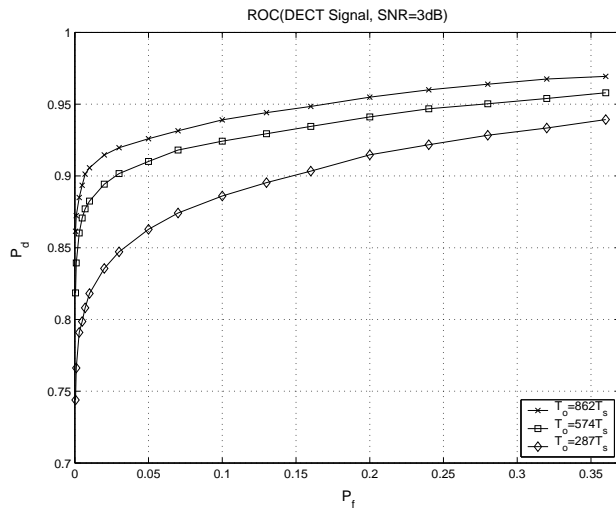**Fig. 5.20** The Receiver Operating Characteristics for the DECT Signal
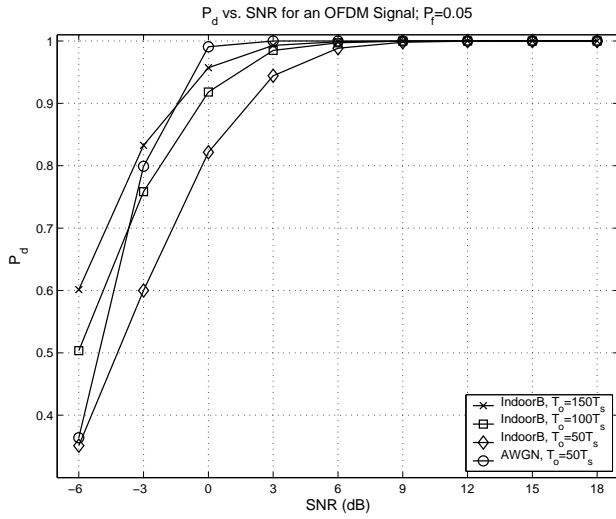
Fig. 5.21 P_d vs SNR for $P_f = 0.05$ for the OFDM system.
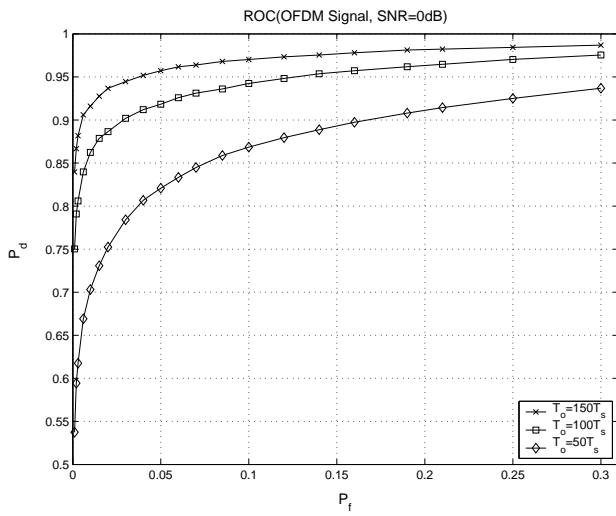
Fig. 5.22 The Receiver Operating Characteristics for the OFDM Signal

The OFDM Signal

For the OFDM Signal described in section 5.3.3, Z_{xx} is used as the detection statistic, in order to detect the presence of the nonconjugate cyclostationarity
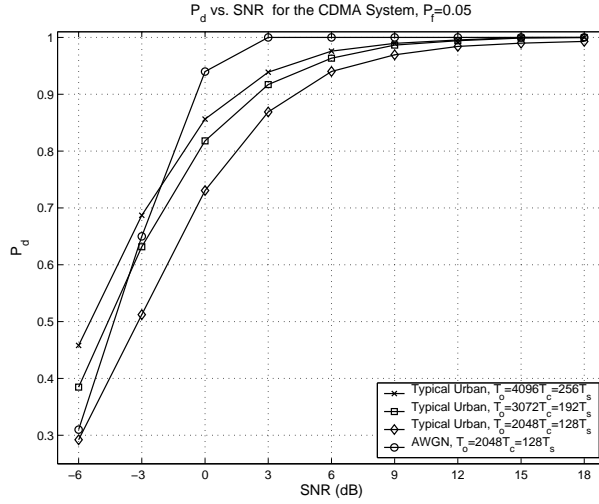
Fig. 5.23 P_d vs SNR for $P_f = 0.05$ for the CDMA system.

in the received signal with $\alpha_0 = 1/T_s$ and $\tau = 1/\Delta f$. The detection results for $P_f = 0.05$ and the ROC for SNR= 0dB are displayed in Figs. 5.21 and 5.22 respectively. Once again, the IndoorB channel model is used for simulating the effects of the wireless channel, with user speeds of 5 m/s.

The CDMA Signal

For the CDMA Signal described in section 5.3.4, Z_{xx} is used as the detection statistic, in order to detect the presence of the nonconjugate cyclostationarity in the received signal with $\alpha_0 = 1/T_c$ and $\tau = 0$. The detection results for $P_f = 0.05$ and the ROC for SNR=3dB are displayed in Figs. 5.23 and 5.24 respectively. Typical Urban channel model with 15m/s user speeds is used for simulating the effects of the mobile propagation channel.

5.4.6   Summary

The simulation results indicate that the statistical test for the presence of cyclostationarity introduced in this section is indeed a powerful tool for detecting the cyclic signature of signals. This test has the advantage of being a CFAR test in the sense that the threshold guaranteeing a particular P_f does not depend on the particular received signal, and can be calculated
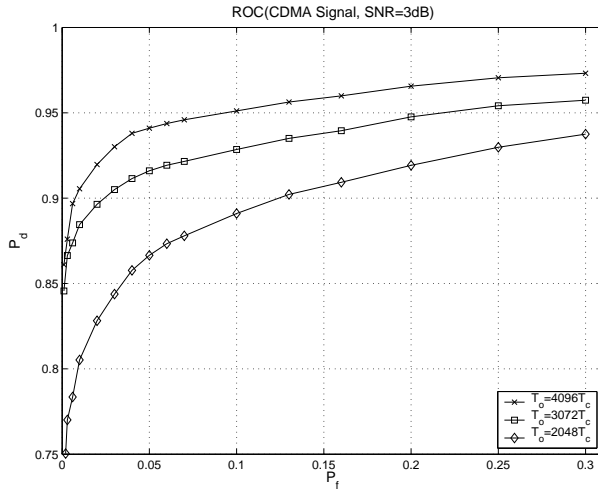
Fig. 5.24 The Receiver Operating Characteristics for the CDMA Signal

analytically or by using look-up tables for χ^2 distributions. This property makes it possible to dispense with the use of confusion matrices as a measure of performace of the air interface identification system, since the false alarm rate for every type of input signal is the same due to the variance normalization. The results show that a satisfactory detection performance can be attained for moderate observation interval lengths T_o, and relatively low SNR values, for SNR≥6dB in the case of GSM, DECT and CDMA signals, and for SNR≥3dB for the OFDM signal, allowing the recognition of signals, which are received with enough power to permit communication with acceptable bit error rates. Parts of the results presented in this section have been published in [55] and in [56].

5.5 Effects of the Carrier Frequency Estimation Errors

The air interface recognition technique presented in this chapter is based on the assumption that the baseband signal from the air interface to be recognized is available at the Software Radio receiver. This, however, requires a perfect knowledge of the carrier frequency of the signal of interest, which, in practice, is estimated by the channel segmentation stage prior to the iden-

tification. The estimated carrier frequency, obviously, may be contaminated by estimation errors. This section investigates the effects of this estimation errors on the proposed method. Denoting the carrier frequency estimation error as δ_{f_c}, we can write the contaminated baseband signal of interest as:

$$\tilde{x}(t) = x(t)e^{-j2\pi\delta_{f_c}t} \tag{5.121}$$

The nonconjugate cyclic autocorrelation function of $\tilde{x}(t)$ can be written as:

$$R_{\tilde{x}\tilde{x}}^{\alpha}(\tau) = e^{-j2\pi\delta_{f_c}\tau}R_{xx}^{\alpha}(\tau) \tag{5.122}$$

Thus, the carrier offset has no effect on the nonconjugate cyclic autocorrelation function, other than a linear phase term, and does not have any influence on the cycle frequencies of the signal of interest, which makes the proposed method very robust against this kind of estimation error, if the signal of interest exhibits nonconjugate cyclostationarity.

However, things look differently for the conjugate cyclic autocorrelation function, which can be calculated as:

$$R_{\tilde{x}\tilde{x}^*}^{\alpha}(\tau) = R_{xx^*}^{\alpha+2\delta_{f_c}}(\tau) \tag{5.123}$$

In this case, the carrier offset leads to a shift in the conjugate cyclic autocorrelation function in the α direction. Thus, every cycle frequency is shifted by an amount of $2\delta_{f_c}$, which, at the first sight, seems to make the recognition impossible, unless δ_{f_c} is precisely known.

Nevertheless, it can be easily shown that the conjugate cycle spectrum of communication signals shows a symmetry, that is, if α_0 is a cycle frequency, then $-\alpha_0$ is also a cycle frequency of the signal (see Fig. 5.7). Since the whole conjugate cyclic autocorrelation function is shifted by the same amount, the distance between two cyclic autocorrelation surfaces remains the same, i.e. $2\alpha_0$. Hence, the recognition can be carried out by conducting a search for the presence of two cycle frequencies in the conjugate cyclic autocorrelation function of $\tilde{x}(t)$ which have a frequency separation of $2\alpha_0$, eliminating the need of knowing the offset δ_{f_c}. The detection of such a cycle frequency pair in $\tilde{x}(t)$ is a clear indication for the presence of conjugate cyclostationarity in $x(t)$ with a frequency of α_0.

Thus, in case of a carrier frequency estimation error for signals exhibiting conjugate cyclostationarity (such as GSM or DECT), the CFAR test proposed in section 5.4 has to be applied multiple times for different pairs of α, which results in a considerable increase in the computational complexity

of the recognition algorithm. However, if the order of magnitude of the frequency offset relative to the cycle frequency α_0 is approximately known a priori, (i.e. the error statistics of the segmentation algorithm) the search can be limited on a small frequency interval, making the use of this approach computationally feasible.

6 Conclusion

In this work, a method for air interface identification in a Software Radio system has been developed and investigated. Air interface identification is a key function supporting the environmental awareness of a SR, which is required for an adaptive and efficient use of the spectral resources and to make an optimum use of the multi standard capability, which is a crucial part of the Software Radio concept. Air interface identification allows a Software Radio terminal to classify the different air interface standards in its environment and to connect to the particular air interface, which can deliver the required service in the most efficient manner. Additionally, it provides the SR with an alternative mode monitoring capability, allowing the SR to perform interstandard handovers if necessary.

The proposed air interface identification method is based on three fundamental assumptions:

1. The air interface identification has to be performed in an environment with a fully dynamic frequency allocation scheme, i.e. each transmission standard can be operated on any frequency band, according to the user demands and traffic considerations. Although today's mobile communication networks are usually based on fixed frequency allocation schemes, there have been tremendous research efforts in the area of dynamic, demand oriented frequency allocation methods in the last decade, indicating a clear global trend towards more efficient and flexible resource allocation methods and more interoperability between different standards, making the above assumption quite reasonable for a future Software Radio system.

2. The air interface identification has to be performed blindly, i.e. without help from the network.

3. The Software Radio terminal has knowledge about all the relevant parameters of every air interface standard it is capable of using in its database, which reduces the identification problem to a recognition problem, i.e. the identification stage has to recognize the signal of interest as one of the known air interface standards, or reject it as unknown.

The first assumption implies that information about the bandwidths and carrier frequencies of the air interface signals of interest are not available to the Software Radio terminal prior to the identification. Therefore, an automatic channel segmentation stage has to precede the identification stage, locating and isolating the individual signals in the environment. A channel segmentation method based on cluster analysis has been developed in chapter four, which, as the simulation results indicate, is capable of detecting and isolating even signals only a couple of dB above the noise level, in channels occupied by multiple users with different bandwidths and transmission powers.

The air interface identification stage presented in the fifth chapter of this work is based on cyclostationary signal analysis, and presents a unified approach to the air interface identification problem for all major signal types encountered in today's mobile communication environment. This approach exploits the uniqueness of the cyclostationary signature of different air interface signals as a feature for recognition, providing a simple and efficient identification strategy, which is applicable to various different signal structures. It has been shown, by means of simulations, that the proposed method is able to provide an excellent detection performance, even under realistic frequency selective multipath fading conditions, and for relatively low SNR values, wich makes it superior to its counterparts based on a modulation type classification approach, which has been widely used in the literature. Additionally, this approach is capable of identifying OFDM and CDMA type signals, which can not be identified using conventional modulation type classification methods due to their complicated signal structures. Other possible applications of the proposed cyclostationary method have been discussed in [57], [58] and [59].

Appendix A

The mixing conditions

The time varying k'th order moment $m_{kx}(i, \mathbf{v})$ of a complex random process $x[i]$ with $\mathbf{v} = [v_1, v_2, \ldots, v_k]$, $v_1 = 0$ is given as

$$m_{kx}(i, \mathbf{v}) = E\{x[i]x[i + v_1] \ldots x[i + v_{k-1}]\} \qquad \text{(A.1)}$$

let ν_j be some nonempty subset of the set of indices $\nu = \{0, 1, \ldots, k\}$, define the order of the subset $n_j = |\nu_j|$ and $m_{n_j x}(i, \mathbf{v}_{\nu_j})$ is the moment of n_j variables with corresponding subscripts in the subset,i.e. $\{x[i + v_m]\}_{m \in \nu_j}$

The k'th order time varying cumulant $c_{kx}(i, \mathbf{v})$ of $x[i]$ can be expressed in terms of the moment functions as

$$c_{kx}(i, \mathbf{v}) = \sum_{P_k} (-1)^{p-1}(p - 1)! \prod_{j=1}^{p} m_{n_j x}(i, \mathbf{v}_{\nu_\mathbf{j}}) \qquad \text{(A.2)}$$

where the summation on is carried out over the distinct partitions P_k of the index set $\{\nu = 1, \ldots, k\}$, which is defined as the collection of p subsets of $\nu, \{\nu_l\}_{l=1}^{p}$, having the following properties:

$$\nu = \bigcup_{l=1}^{p} \nu_l$$

$$\nu_j \bigcap \nu_k = \emptyset \quad \text{for} \quad j \neq k. \qquad \text{(A.3)}$$

.

Note that the more general time variant cumulant, accomodating every combination of complex conjugated and nonjugated signal terms

$$c_{kx_s}(i, \mathbf{v}) = c_{x_{s_1} \ldots x_{s_k}}(i, \mathbf{v})$$

with $x_{s_q} \in \{x[i], x^*[i]\}$, $q = 1, \ldots, k$ can be expressed similarly, using the moment functions with appropriate conjugate-nonconjugate combinations.

The mixing condition used in [50] to derive the asymptotic properties of the cyclic autocorrelation estimates (i.e consistency and asymptotically complex normal distribution) can be given as

$$\sum_{\mathbf{v}=-\infty}^{\infty} \sup_t |v_l c_{kx_s}(t, \mathbf{v})| < \infty \tag{A.4}$$

This assumption requires the absolute summability of the cumulants of $x[i]$, which, inituitively, implies that samples of $x[i]$ which are well separated in time are approximately independent [60], which is obviously fulfilled by all communication signals.

The asymptotic distribution of Z_{xx^*}

The asymptotic distribution of Z_{xx^*} under H_0 can be shown by applying the following theorem, which has been proven in [61]:

THEOREM:

1. If the $1 \times M$ vector $\hat{\boldsymbol{\Psi}}$ is an asymptotically Gaussian estimator of $\boldsymbol{\Psi}$ using T_o data samples,i.e.

    $$\lim_{T_o \to \infty} \sqrt{T_o}(\hat{\boldsymbol{\Psi}} - \boldsymbol{\Psi}) \overset{D}{=} \mathcal{N}(\mathbf{0}, \boldsymbol{\Sigma}_{\boldsymbol{\Psi}}) \tag{A.5}$$

    and $\boldsymbol{\Psi} \neq 0$, then

    $$\lim_{T_o \to \infty} \sqrt{T_o}(\hat{\boldsymbol{\Psi}}\hat{\boldsymbol{\Psi}}^{\mathbf{H}} - \boldsymbol{\Psi}\boldsymbol{\Psi}^{\mathbf{H}}) \overset{D}{=} \mathcal{N}(\mathbf{0}, 4\boldsymbol{\Psi}\boldsymbol{\Sigma}_{\boldsymbol{\Psi}}\boldsymbol{\Psi}^{\mathbf{H}}) \tag{A.6}$$

    but if $\boldsymbol{\Psi} = 0$ and $\boldsymbol{\Sigma}_{\boldsymbol{\Psi}} = \mathbf{I}$, then

    $$\lim_{T_o \to \infty} \sqrt{T_o}(\hat{\boldsymbol{\Psi}}\hat{\boldsymbol{\Psi}}^{\mathbf{H}} - \boldsymbol{\Psi}\boldsymbol{\Psi}^{\mathbf{H}}) \overset{D}{=} \chi_M^2 \tag{A.7}$$

2. If $\lim_{T_o \to \infty}(\hat{\boldsymbol{\Psi}}) = \boldsymbol{\Psi}$ and $\lim_{T_o \to \infty}(\hat{\mathbf{G}}) \overset{m.s.s}{=} \mathbf{G}$, which is an $M \times M$ matrix, then

    $$\lim_{T_o \to \infty} \sqrt{T_o}(\hat{\boldsymbol{\Psi}}\hat{\mathbf{G}}) \overset{D}{=} \boldsymbol{\Psi}\mathbf{G} \tag{A.8}$$

Choosing $\hat{\mathbf{\Psi}} = \hat{\mathbf{r}}_{\mathbf{xx}^*} \mathbf{\Sigma}_{\mathbf{xx}^*}^{-1/2}$ and $M = 2N$, realizing that $\mathbf{\Sigma}_{\mathbf{xx}^*}^{-1/2}$ is a consistent estimate and using theorem 2, $\hat{\mathbf{\Psi}}$ can be shown to be asymptotically normal, since $lim_{T_o \to \infty} \sqrt{T_o} \hat{\mathbf{r}}_{\mathbf{xx}^*}$ is asymptotically normal, as shown in [50]. Therefore using theorems 2 and 1, the asymptotic distribution of Z_{xx^*} under H_0 is given as

$$\lim_{T_o \to \infty} Z_{xx^*} \overset{D}{=} \chi_{2N}^2 \tag{A.9}$$

and under H_1

$$\lim_{T_o \to \infty} Z_{xx^*} \overset{D}{\approx} \mathcal{N}(T_o \mathbf{r}_{\mathbf{xx}^*} \mathbf{\Sigma}_{\mathbf{xx}^*}^{-1} \mathbf{r}_{\mathbf{xx}^*}^{\mathbf{T}}, 4T_o \mathbf{r}_{\mathbf{xx}^*} \mathbf{\Sigma}_{\mathbf{xx}^*}^{-1} \mathbf{r}_{\mathbf{xx}^*}^{\mathbf{T}}) \tag{A.10}$$

Acronyms, Notations and Symbols

Acronyms

ADC	Analog to digital converter
AWGN	Additive white Gaussian noise
BPSK	Binary phase shift keying
CAF	Cyclic autocorrelation function
CCAF	Conjugate cyclic autocorrelation function
CDMA	Code division multiple access
DAB	Digital audio broadcasting
DFT	Discrete Fourier transform
DVB-T	Digital Video Broadcasting-Terrestrial
FE	Front end
FFT	Fast Fourier transform
DECT	Digital European Cordless Telephony
DS/SS	Direct sequence spread-spectrum
IS95	Interim Standard 95
GSM	Global System for Mobile Communications
GMSK	Gaussian minimum shift keying
LAN	Local area network
LSB	Least significant bit
ML	Maximum-likelihood
MSK	Minimum shift keying
NL	Noise level
OFDM	Orthogonal frequency division multiplex
PSD	Power spectral density
PSK	Phase shift keying
SSCL	Self splitting competitive learning
SDR	Software Defined Radio
SR	Software Radio
SNR	Signal to noise ratio
TDMA	Time division multiple access
UMTS	Universal Mobile Telecommunication System
UTRA	UMTS Terrestrial Radio Access
WLAN	Wireless local area network

WSSUS   Wide-sense stationary uncorrelated scattering

Notations

x	Variable
$\hat{x}$	Estimation
$\bar{x}$	Average
$x(t)$	Continuous time signal
$x[n]$	Discrete time signal
$X(f)$	Fourier Transform of $x(t)$
$X(z)$	Z-Transform of $x[n]$
$\mathbf{x}$	Vector (general)
$\vec{X}$	Vector (in the feature space)
$\mathbf{X}$	Matrix
$\|\mathbf{x}\|$	Norm
$\mathrm{Re}\{x\}$	Real part
$\mathrm{Im}\{x\}$	Imaginary part
$\mathrm{E}\{x\}$	Expectation
$cov(x,y)$	Covariance
$x^{lin}(t)$	Linear part of $x(t)$
$x_l(t)$	Low pass equivalent signal to $x(t)$
$R_{xx}^{\alpha}(\tau)$	Nonconjugate cyclic autocorrelation function of $x(t)$
$R_{xx^*}^{\alpha}(\tau)$	Conjugate cyclic autocorrelation function of $x(t)$
$S_{xx}^{\alpha}(f)$	Nonconjugate spectral correlation density function of $x(t)$
$S_{xx^*}^{\alpha}(f)$	Conjugate spectral correlation density function of $x(t)$

Symbols

A_{xx}	Cycle spectrum of $x(t)$
A_{xx^*}	Conjugate cycle spectrum of $x(t)$
$\vec{A}_k$	Asymptotic property vector

B	Bandwidth
b_{f_0}	Fourier Coefficient at frequency f_0
c	Speed of light
$c_k(t)$	Spreading code sequence of the k'th user (CDMA)
$c_K(t)$	Elementary Impulse functions in the linear approximation of GMSK
$\vec{C}_k$	Center property vector
D	Dynamic Range
d_k	Information sequence
$d_{n,i}$	n'th information symbol modulated on the k'th carrier(OFDM), n'th information symbol of the i'th user (CDMA)
e_n	Quantization error
E_s	Energy of a symbol
f	Frequency
f_c	Chip rate
f_C	Carrier frequency
f_D	Doppler Shift
f_{Dmax}	Maximum Doppler Shift
$f_h(\rho)$	Distribution of the fading coefficient
f_{max}	Maximum freqency component contained in a signal
f_s	Symbol rate
f_{sample}	Sampling rate
$f_v[i]$	Lag product
$\tilde{f}_v[i]$	Conjugate lag product
$g(t)$	Impulse Shape
$g_f(t)$	Shape of the frequency pulse (GMSK)
$g_{rc}(t)$	Raised cosine pulse
$g_{rrc}(t)$	Root raised cosine pulse
$g_R(t)$	Rectangular pulse
$G(f)$	Fourier Transform of $g(t)$
$G_{rc}(f)$	Raised cosine pulse spectrum
$G_{rrc}(f)$	Root raised cosine pulse spectrum
$h(t,\nu)$	Time varying channel impulse response

$h_n(t)$	Time varying channel coefficient
H_k	Hypothesis k
$I_0(\cdot)$	Modified Bessel function of order zero
$\mathbf{I}$	Identity Matrix
$J_{K-means}$	K-means cost function
J_{EA}	Edge adaptive K-means cost function
K	Number of clusters (clustering)
	Number of users (CDMA)
$n(t)$	AWGN
$n_{\vec{u}}$	Winning counter of $\vec{u}$
N_C	Number of carriers
N_0	Noise power
N_o	ADC Resolution
$p_{Gauss}(t)$	Gaussian impulse function
$\vec{P}_k$	Cluster prototype
P_d	Probability of detection
P_f	False alarm rate
$p_k(r)$	Likelihood function for the hypothesis k
Q	Spreading code length
Q_0	Number of quantization levels
Q_{sc}	Scrambling code length
$r(t)$	Received signal
$\mathbf{r_{xx}}$	Nonconjugate cylic autocorrelation vector
$\mathbf{r_{xx^*}}$	Conjugate cyclic autocorrelation vector
$R_{xx}^{\alpha}(\tau)$	Nonconjugate cyclic autocorrelation function of $x(t)$
$R_{xx^*}^{\alpha}(\tau)$	Conjugate cyclic autocorrelation function of $x(t)$
$\vec{R}_k$	Distant property vector
$S_{xx}(f)$	PSD of $x(t)$
$S_{xx}^{\alpha}(f)$	Nonconjugate spectral correlation density function of $x(t)$

$S_{xx^*}^{\alpha}(f)$	Conjugate spectral correlation density function of $x(t)$
SNR_Q	Signal to noise ratio due to the quantization error
T_c	Chip duration
T_d	Delay parameter
T_g	Guard time
T_o	Length of the observation interval
T_s	Symbol duration
T_{sample}	Sampling interval
T_u	Useful time
$T(t, f)$	Time varying channel transfer function
v	Discrete lag parameter
V	Maximum Quantization level
$x(t)$	Signal
$x_l(t)$	Low pass equivalent signal to $x(t)$
$\vec{X}_j$	Input pattern vector
z_{jk}	Indicator function
α	Cycle frequency
α_f	Fundamental cycle frequency
β_k	Kaiser window parameter
γ	Angle of arrival of the incident wave
$\delta(\cdot)$	Dirac delta function
$\delta[\cdot]$	Kroenecker delta function
δ_k	Learning rate for $\vec{A}_k$
Δ	Least significant bit
$\Delta_{xx}^{\alpha}(v)$	Estimation error in the nonconjugate cyclic autocorrelation function
$\Delta_{xx^*}^{\alpha}(v)$	Estimation error in the conjugate cyclic autocorrelation function
$\mathbf{\Delta_{xx}}$	Estimation error vector
Δf	Carrier separation

ϵ	Symbol timing error
κ_k	Learning rate for $\vec{R}_k$
η_k	Adaptive learning rate of $\vec{P}_k$
ζ	The SSCL threshold parameter
σ^2	Variance
σ_x^2	Variance of $x(t)$
σ_{aj}^2	Variance of the aperture jitter noise
σ_B^2	Variance of the bandwidth estimate
σ_e^2	Quantization error variance
$\sigma_{e(ib)}^2$	In band quantization noise power
$\sigma_{f_c}^2$	Variance of the carrier frequency estimate
$\mathbf{\Sigma_{xx}}$	Covariance matrix of the nonconjugate cyclic autocorrelation estimate
$\mathbf{\Sigma_{xx^*}}$	Covariance matrix of the conjugate cyclic autocorrelation estimate
$\Delta\tau_0$	Time delay between the shortest and longest multipath
ξ_k	Bias factor
τ	Lag parameter
τ_a	RMS aperture jitter
τ_0	Local Maximum of the CAF
$\Theta(\vec{u}, \vec{v}, \vec{w})$	Neighborhood indication function
χ_{2N}^2	Chi suqare distribution with 2N degrees of freedom
$\Phi(f)$	Doppler spectrum
∇	Gradient operator
Ω	Data domain

Bibliography

[1] J. Mitola, "The software radio achitecture," *IEEE Communications Magazine*, vol. 33, no. 5, pp. 26–38, May 1995.

[2] Dillinger, Medani, and Alonistioti, Eds., *Software Defined Radio: Architectures,Systems and Functions*, John Wiley and Sons, Ltd, 2002.

[3] F. Capar and F. Jondral, "Resource allocation in a spectrum pooling system for packet radio networks using ofdm/tdma," in *IST Mobile and Wireless Telecommunications Summit 2002*, June 2002, pp. 489–493.

[4] J. Mitola, *Cognitive Radio, An integrated Agent Architecture for software Defined Radio*, Ph.D. thesis, Department of Teleinformatics, Royal Institute of Stockholm, 2000.

[5] G. Vardoulias, "Blind radio access technology discovery and monitoring for software defined radio communication systems: problems and techniques," in *Second International Conference on 3G Mobile Communication Technologies*, 26-28 March 2001, pp. 306–310.

[6] M. Burrachini, "The software radio concept," *IEEE Communications Magazine*, vol. 98, no. 9, September 2000.

[7] F. Jondral, *Funksignalanalyse*, Teubner, 1991.

[8] R.H. Walden, "Analog to digital converter survey and analysis," *IEEE Journal on Selected areas in Telecommunications*, vol. 17, no. 4, pp. 539–550, 1999.

[9] P. Aziz, H. Sorensen, and J.Spiegel, "An overview on sigma-delta converters," *IEEE Signal Procssing Magazine*, vol. 13, no. 1, pp. 61–84, Jan 1996.

[10] W. Tuttlebee, *Software Defined Radio: Enabling Technologies*, John Wiley and Sons, 2002.

[11] B. Fleury and P. Leuthold, "Radiowave propagation in mobile radio channels: an overview of european research," *IEEE Communications Magazine*, vol. 34, pp. 70–81, 1996.

[12] M. Paetzold, *Mobilfunkkanäle*, Vieweg Verlag, 1999.

[13] A.F. Molisch, *Wideband Wireless Digital Communications*, Prentice Hall, 2001.

[14] J.Proakis, *Digital Communications*, Mc Graw Hill, 1995.

[15] P.Bello, "Characterization of randomly time variant linear channels," *IEEE Transactions on Communications*, vol. 11, no. 4, pp. 360–393, Dec. 1963.

[16] R. Steele, *Mobile Radio Communications*, Wiley, NY, 1992.

[17] ETSI, "Digital european cordless telecommunications (dect) common interface ets 300171-1 to 175-9," .

[18] S.Verdu, *Multiuser Detection*, Cambridge University Press, 1998.

[19] 3gpp, "Technical specification group radio access network:spreading and modulation (fdd) 3g ts 25.213," Tech. Rep., 3gpp, March 2002.

[20] R. Machauer, *Multicode Detektion im UMTS*, Ph.D. thesis, Universität Karlsruhe (TH), 2002.

[21] S. Weinstein and P.Ebert, "Data transmission by frequency-domain multiplexing using the discrete fourier transform," *IEEE Trans. on Commun. Tech.*, vol. 19, no. 5, pp. 628–634, October 1971.

[22] U. Reimers, *Digitale Fernsehtechnik*, Springer Verlag, 2nd ed., 2001.

[23] Agilent Inc., "Swept and fft analysis: Agilent psa performance spectrum analyzer series, product note," .

[24] M. Engelson, *Modern Spectrum Analyzer Theory and Applications*, Artech House INC, 1984.

[25] K.D. Kammayer and K. Kroschel, *Digitale Signalverarbeitung*, Teubner Studienbücher, 1998.

[26] A. Jain, *Fundamentals of Digital Image Processing*, Prentice Hall, 1989.

[27] F. Raps, K.Kölmann, and H Zeidler, "Hf band emitter detection and segmentation based on image processing," in *Military Communications Conference, Milcom 2001*. IEEE, 28-31 Oct 2001, pp. 131–135.

[28] H. Timm, *Fuzzy Clusteranalyse: Methoden zur Exploration von Daten mit fehlenden Werten sowie klassifizierten Daten*, Ph.D. thesis, Universität Magdeburg, 2002.

[29] Ya-Jun Zhang and Zhi-Qiang Liu, "Self-splitting competitive learning: a new on-line clustering paradigm," *Neural Networks, IEEE Transactions on*, vol. 13, no. 2, pp. 369–380, March 2002.

[30] J.C. Bezdek, J. Keller, R. Krishnapuram, and N.R. Pal, *Fuzzy Models and Algorithms for Pattern Recognition and Image Processing*, Kluwer, Boston, 1999.

[31] R. Duda and P. Hart, *Pattern Classification and Scene Analysis*, Wiley, NY, 1973.

[32] D.L. Pham, "Edge-adaptive clustering for unsupervised image segmentation," in *2000 International Conference on Image Processing*, 10-13 Sep 2000, pp. 816–819.

[33] C.Y.Huang and A. Polydoros, "Likelihood methods for mpsk modulation classification," *IEEE Trans. on Communications*, vol. 43, no. 2/3/4, February,March, April 1995.

[34] Y.C. Lin and C.C.J. Kuo, "Modulation classification using wavelet transform," in *SPIE 1995*, July 1995, pp. 492–503.

[35] C. Schreyögg, "Modulation classification of qam schemes using the dft of phase histogram combined with modulus information," in *MILCOM 97*, November 1997.

[36] K.C.Ho, W. Prokopiw, and Y.T. Chan, "Modulation identificatio by the wavelet transformn," in *MILCOM 95*.

[37] F.F. Liedtke, "Benutzung von histogrammen zur signalklassifikation," in *4ter Aachener Kolloquium Theorie und Anwendung der Signalverarbeitung*, 1981, pp. 269,272.

[38] E.E. Azzouz and A.K.Nandi, "Automatic identification of digital modulation types," *Signal Processing*, vol. 47, no. 1, pp. 55–69, November 1995.

[39] W.A. Gardner, *Cyclostationarity in Communications and Signal Processing*, IEEE Press, 1994.

[40] W.A. Gardner, *Statistical Spectral Analysis: A Nonprobabilistic Theory*, Prentice Hall, NJ, 1987.

[41] R. Boyles and W.A. Gardner, "Cycloergodic properties of discrete-parameter nonstationary stochastic processes," *IEEE Transactions on Information Theory*, pp. 105 – 114, 1983.

[42] P.Rostaing, *Detection des signaux modules en exploitant leurs proprietes cyclostationnaires: Application aux signaux sonar*, Ph.D. thesis, Universite de Nice-Sophia Antipolis, 1997.

[43] A. Wiesler, *Parametergesteuertes Software Radio für Mobilfunksysteme*, Ph.D. thesis, Universität Karlsruhe (TH), 2001.

[44] P. Jung, "Laurent's representation of binary digital continuous phase modulated signals with modulation index 1/2 revisited," *IEEE Transactions on Communications*, 1994.

[45] J.F. Kuehls and E. Geraniotis, "Presence detection of binary phase shift keyed and direct sequence spread spectrum signals using a prefilter delay and multiply device," *IEEE Journal on Selected Areas in Communications*, vol. 8, no. 5, pp. 915–933, 1990.

[46] M.A. Wickert, K.D. Rhead, and D.E. Reed, "Practical limitations in limiting the rate-line detectability of spread spectrum lpi signals," in *MILCOM '90 Conference Record, 'A New Era'.*, 30 Sept, vol. 3.

[47] F.Jondral M. Öner, "Extracting the channel allocation information in a spectrum pooling system using a prefilter delay and multiply non-lineraity," in *2003 IEEE Workshop on Statistical Signal Processing*, September 2003, pp. 46–49.

[48] J. Reichert, *Ein Verfahren zur Klassifikation von Modulationssignalen auf der Basis Ihrer Momente höherer Ordnung*, Ph.D. thesis, TH Darmstadt, 1993.

[49] J.C. Imbeaux, "Performances of the delay-line multiplier circuit for clock and carrier synchronization in digital satellite communications," *IEEE Journal on Selected Areas in Communications*, vol. 1, no. 1, pp. 82–95, Jan 1983.

[50] A.V. Dandawate and G.B. Giannakis, "Statistical tests for presence of cyclostationarity," *IEEE Transactions on Signal Processing*, vol. 42, no. 9, pp. 2355 – 2369, Sept 1994.

[51] A.D. Whalen, *Detection of Signals in Noise*, Academic Press, NY, 1971.

[52] T. Hentschel and G. Fettweiss, "Sample rate conversion for software radio," *IEEE Communications Magazine*, vol. 98, no. 8, pp. 142–150, August 2000.

[53] "Commision of ec : Cost 207, digital land mobile radio communication," 1988.

[54] "Umts 30.03 annex b: Test environments and deployment models;tr 101 1112, v.3.2.0," Apr 1998.

[55] M. Öner and F. Jondral, "Air interface recognition in a software radio system exploiting cyclostationarity," in *15th IEEE Symposium on Personal Indoor Mobile Radio Communcations, PIMRC 2004*, Barcelona, Spain, 5-8 September 2004.

[56] M. Öner and F. Jondral, "Cyclostationary based air interface recognition for software radio systems," in *IEEE Radio and Wireless Conference, RAWCON 2004*, Atlanta, USA, 19-22 September 2004.

[57] M. Öner and F. Jondral, "Extracting the channel allocation information in a spectrum pooling system using cyclic feature detection," in *12th European Signal Processing Conference, EUSIPCO 2004*, Vienna, Austria, 6-10 September 2004.

[58] M. Öner and F. Jondral, "Extracting the channel allocation information in a spectrum pooling system exploiting cyclostationarity," in *15th IEEE Symposium on Personal Indoor Mobile Radio Communcations, PIMRC 2004*, Barcelona, Spain, 5-8 September 2004.

[59] M. Öner and F. Jondral, "Cyclostationary based methods for the extraction of the channel allocation information in a spectrum pooling system," in *IEEE Radio and Wireless Conference, RAWCON 2004*, Atlanta, USA, 19-22 September 2004.

[60] P. Ciblat and E. Serpedin, "A fine blind frequency offset estimator for ofdm/oqam systems," *IEEE Transactions on Signal Processing*, vol. 52, no. 1, pp. 291 – 296, January 2004.

[61] E. L. Lehmann, *Theory of Point Estimation*, Wiley, 1973.

Curriculum Vitae

Personal Data

Name	Mustafa Mengüc Öner
Date of Birth	01.02.1977
Place of Birth	Antalya, Turkey
Nationality	turkish

Education

1983-1987	Primary School in Istanbul
1987-1994	High School Istanbul Lisesi in Istanbul
1994-1998	Bachelor of Science in Electrical Engineering at the Bogazici University, Istanbul
1998-2001	Dipl.-Ing at Universität Karlsruhe, Fakultät für Elektrotechnik und Informationstechnik
2001-2004	PhD. Studies at Institut für Nachrichtentechnik, Universität Karlsruhe